THE UNIVERSITY OF KANSAS CENTER FOR RESEARCH, INC.
2291 Irving Hill Drive—Campus West
Lawrence, Kansas 66045

Progress Report for

A RESEARCH PROGRAM TO REDUCE INTERIOR NOISE IN GENERAL AVIATION AIRPLANES

NASA GRANT NSG 1301

THE EFFECT OF OBLIQUE ANGLE OF SOUND INCIDENCE, REALISTIC EDGE CONDITIONS, CURVATURE AND IN-PLANE PANEL STRESSES ON THE NOISE REDUCTION CHARACTERISTICS OF GENERAL AVIATION TYPE PANELS

KU-FRL-417-10

Prepared by: Ferd Grosveld, Project Manager
Jaap Laméris
David Dunn

Approved by. Jan Roskam,
Principal Investigator

July 1979

SUMMARY

This report describes the work carried out to investigate the influence of an oblique angle of sound incidence, realistic edge conditions, curvature and in-plane panel stresses on the noise reduction characteristics of general aviation type panels. A theoretical study was conducted to predict the noise reduction of inclined and curved panels. These predictions are compared to the experimental results. This analysis shows reasonable agreement between theory and experiment for panels under an oblique angle of sound incidence.

Theoretical as well as experimental results indicate a big increase in noise reduction when a flat test panel is curved. Further curving the panel slightly decreases the noise reduction. Riveted flat panels are shown to give a higher noise reduction in the stiffness-controlled frequency region, while bonded panels are superior in this region when the test panel is curved.

Experimentally measured noise reduction characteristics of flat aluminum panels with uniaxial in-plane stresses are presented and discussed. These test results indicate an important improvement in the noise reduction of these panels in the frequency range below the fundamental panel/cavity frequency.

TABLE OF CONTENTS

TABLE OF CONTENTS (continued)

LIST OF SYMBOLS

Symbol	Definition	Dimension
A	See Equation (36).	[kgs/m]
A_1	amplitude of motion of the incident pressure wave	[m]
A_2	amplitude of motion of the transmitted pressure wave	[m]
a	See Equation (a.1).	[kg/m^3]
a	panel width	[m]
B	See Equation (37).	[kgs/m]
B_1	amplitude of motion of the reflected pressure wave	[m]
b	See Equation (a.2).	[1/rad]
b	panel height	[m]
c	speed of sound in air	[m/s]
c_f	speed of sound in fiberglass	[m/s]
D	flexural rigidity	[Nm]
D	differential	[-]
E	Young's modulus	[N/m^2]
d	vector displacement	[m]
d	See Equation (a.3).	[rad]
f	frequency	[Hz]
h	fiberglass thickness	[m]
ı	$\sqrt{-1}$	[-]
Kp	panel stiffness per unit area	[N/m^3]
k	wave number	[rad/m]
ℓ	cavity length	[m]
M	mass per unit area	[kg/m^2]

LIST OF SYMBOLS (continued)

Symbol	Definition	Dimension
m	panel or cavity mode number (=1,2,3,...)	[m]
m	See Equation (a.7).	[-]
n	See Equation (a.6).	[-]
n	panel or cavity mode number (=1,2,3,...)	[-]
P_f	fiberglass porosity	[-]
p	acoustic pressure	[N/m^2]
p	See Equation (a.11).	[-]
q	See Equation (a.12).	[-]
R	radius of panel curvature	[m]
R_f	flow resistivity of fiberglass	[rayls/m]
r	See Equation (a.13).	[-]
t	time	[s]
t	panel thickness	[m]
u	acoustic particle velocity in x-direction	[m/s]
v	acoustic particle velocity in y-direction	[m/s]
W	panel displacement	[m]
w	acoustic particle velocity in z-direction	[m/s]
x	coordinate in longitudinal direction of the cavity (Figure 2.1)	[m]
y	coordinate in vertical direction, parallel to speaker baffle (Figure 2.1)	[m]
Z_c	cavity impedance at x = 0	[rayls]
Z_ℓ	fiberglass impedance	[rayls]
Z_p	panel impedance	[kgs/m]
z	coordinate in horizontal direction, parallel to speaker baffle (Figure 2.1)	[m]

LIST OF SYMBOLS (continued)

Greek Symbol	Definition	Dimension
∂	particle differential	[-]
ξ	acoustic particle displacement	[m]
ζ	panel damping ratio	[-]
θ	angle between sound incidence and x-axis	[degrees]
λ	wavelength	[m]
η	loss factor	[-]
ν	Poisson's ratio	[-]
ρ	density of air	[kg/m^3]
ρ_f	effective density of air in fiberglass	[kg/m^3]
θ	angle between sound incidence and panel surface	[degrees]
ω	angular frequency	[rad/s]
ω_n	angular natural frequency of panel	[rad/s]
∇	Laplacian operator $(\frac{\partial}{\partial x} + \frac{\partial}{\partial y} + \frac{\partial}{\partial z})$	[-]

Subscripts

c	critical	r	reflected
c	cavity	t	transmitted
f	fiberglass	x	x-direction
i	incident	y	y-direction
		z	z-direction
m	modal number		
		0	initial condition
n	modal number		
		1	source side
p	panel		
		1,1	fundamental resonance mode
q	modal number		
R	ring	2	receiver side

LIST OF SYMBOLS (continued)

Abbreviations	Definition
FRL	Flight Research Laboratory
KU	University of Kansas
NR	Noise Reduction

LIST OF FIGURES

LIST OF FIGURES (continued)

LIST OF FIGURES (continued)

LIST OF FIGURES (continued)

LIST OF FIGURES (continued)

LIST OF TABLES

LIST OF TABLES (continued)

CHAPTER 1

INTRODUCTION

Experiments have been conducted in the KU-FRL* acoustic test facility to investigate the effect of an oblique angle of sound incidence, realistic edge conditions, curvature and in-plane panel stresses on the noise reduction characteristics of General Aviation type panels. A theoretical analysis of the effect of an oblique angle of sound incidence is given in the first section of Chapter 2, while in the second section this analysis is compared to the experimental results. The design and construction of special test devices are described in Chapter 3. These special test devices are used to determine the effect of curvature and riveted or bonded edge conditions, which is discussed in Chapter 4. In this chapter the curvature effect on the noise reduction is analyzed theoretically and the experimental results are compared. The design and construction of a tension device is covered in Chapter 5. Using this tension device, uniaxial and biaxial stresses can be applied to a test panel. Initial noise reduction results for a panel under uniaxial stress are discussed in Chapter 6. Finally, the main conclusions and recommendations conclude this report in Chapter 7.

In this report the terms "frequency-controlled region," "mass-controlled region" and "fundamental resonance frequency" will be mentioned. Figure 1 1 gives an example of a typical noise reduction curve of a General-Aviation-type specimen. The fundamental resonance

---

* University of Kansas Flight Research Laboratory

frequency of the panel/cavity separates the two regions in which the stiffness and the mass, respectively, control the noise reduction characteristics of that panel. At this frequency the largest panel deflections occur. The fundamental panel/cavity resonance frequency is higher than that of a free vibrating panel that is not backed by a cavity. It appears that a cavity acts as a stiffener to the panel. An increase in stiffness raises the fundamental resonance frequency, while adding mass causes the reverse effect. These considerations are the basis for the analysis given in this report.

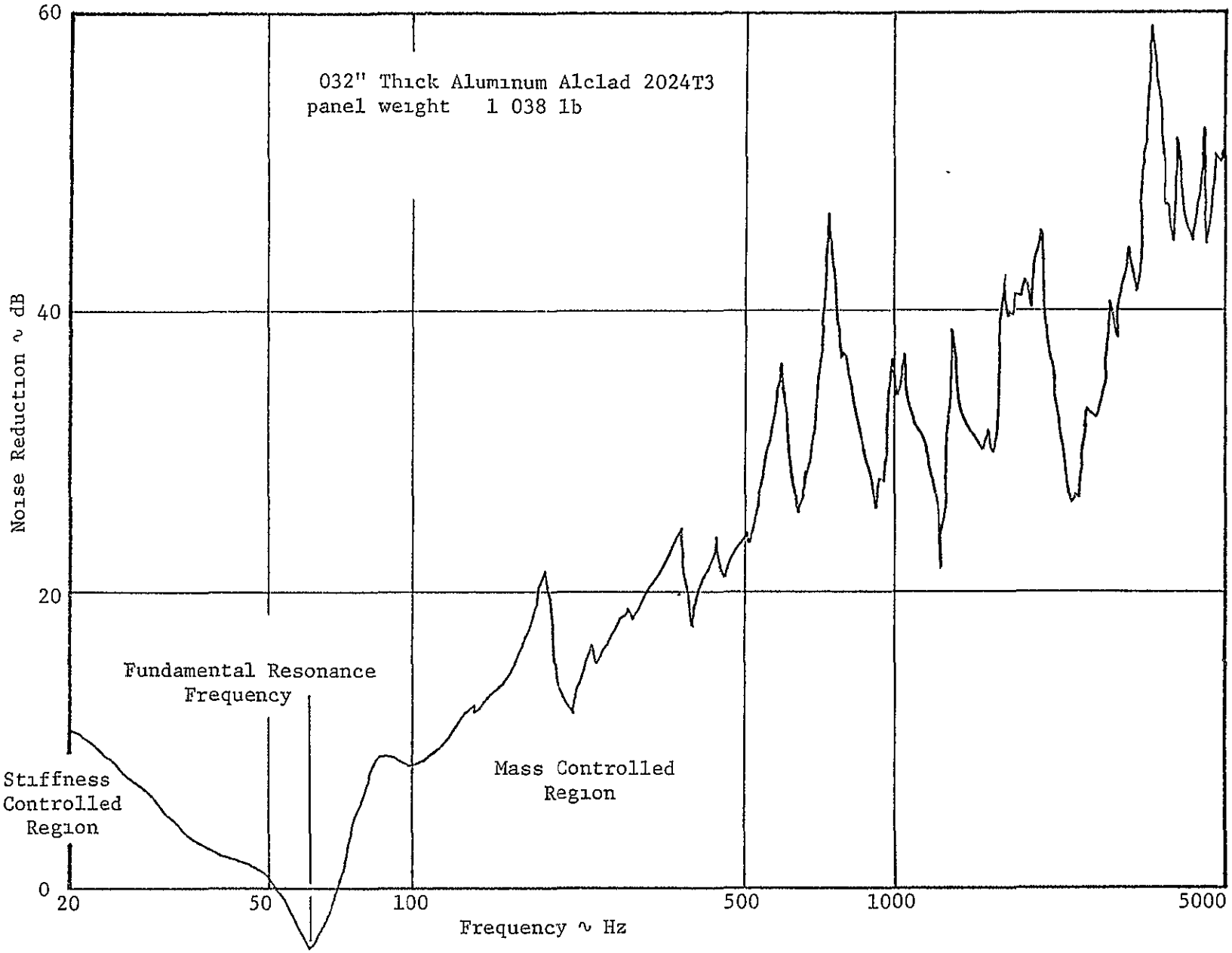

Figure 1.1 Typical Noise Reduction Curve for a General Aviation Type Aluminum Panel

CHAPTER 2

EFFECT OF AN OBLIQUE ANGLE OF SOUND INCIDENCE ON THE NOISE REDUCTION OF AN ALUMINUM PANEL

In the first section of this chapter, a theoretical contemplation is given to determine the theoretical effect of an oblique angle of sound incidence on the noise reduction of an aluminum panel. This will be compared to the experimental noise reduction results, which are presented in the second section.

2.1 Theoretical Analysis

A theoretical prediction of the effect of an oblique angle of sound incidence on the noise reduction of an infinite panel is derived based on the method of Koval (Reference 1).

A plane pressure wave is incident to a hypothetical infinite panel at an oblique angle of incidence ϕ (Figure 2.1). The acoustic media on both sides of the panel are supposed to be the same with air density ρ and velocity of sound c.

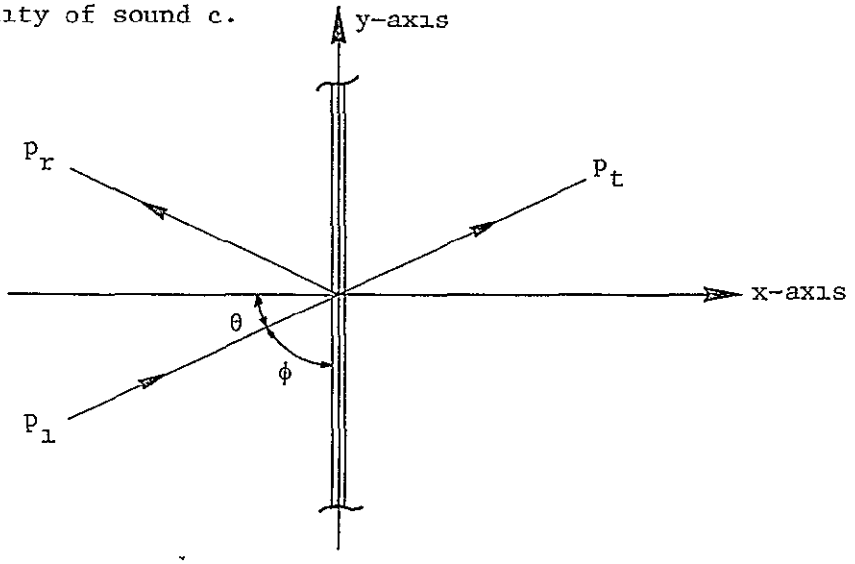

Figure 2.1 Geometry of Pressure Waves Incident to a Hypothetical Infinite Panel

The incident, reflected and transmitted pressures are written as (Reference 2):

$$p_i = A_1 e^{i(\omega t - k\, x \cos\theta - k\, y \sin\theta)} \tag{1}$$

$$p_r = B_1 e^{i(\omega t + k\, x \cos\theta - k\, y \sin\theta)} \tag{2}$$

$$p_t = A_2 e^{i(\omega t - k\, x \cos\theta - k\, y \sin\theta)} \tag{3}$$

where ω is the angular frequency and k the wavelength constant

$$k = \frac{\omega}{c} = \frac{2\pi}{\lambda} \quad (4), \text{ where } \lambda \text{ denotes the wavelength.}$$

Assuming an acoustic particle displacement ξ and a particle velocity u at the panel, the pressure gradient $\partial p/\partial x$ is related to the acceleration in x-direction by:

$$-\frac{\partial p}{\partial x} = \rho_o \frac{D^2\xi}{Dt^2} \tag{5}$$

in y-direction by

$$-\frac{\partial p}{\partial y} = \rho_o \frac{D^2\eta}{Dt^2} \tag{6}$$

and in z-direction by·

$$-\frac{\partial p}{\partial z} = \rho_o \frac{D^2\zeta}{Dt^2} \tag{7}$$

If the first of these equations is differentiated partially with respect to x, the second one to y, the third with respect to z, and then all are added together, the result is·

$$-\left(\frac{\partial^2 p}{\partial x^2} + \frac{\partial^2 p}{\partial^2 y} + \frac{\partial^2 p}{\partial z^2}\right) = \rho_o \frac{D^2}{Dt^2}\left(\frac{\partial \xi}{\partial x} + \frac{\partial \eta}{\partial y} + \frac{\partial \zeta}{\partial z}\right) \tag{8}$$

Equation (8) can be expressed in vector form as

$$-\nabla^2 p = \rho_o \frac{D^2(\nabla \cdot d)}{Dt^2} \tag{9}$$

where $\nabla^2 = (\frac{\partial^2}{\partial x^2} + \frac{\partial^2}{\partial y^2} + \frac{\partial^2}{\partial z^2})$

and $\nabla \cdot d = (\frac{\partial \xi}{\partial x} + \frac{\partial \eta}{\partial y} + \frac{\partial \xi}{\partial z})$ represents the divergence.

Relating acoustic pressure and condensation:

$$p = -\rho c^2 (\frac{\partial \xi}{\partial x} + \frac{\partial \eta}{\partial y} + \frac{\partial \xi}{\partial z}) \tag{10}$$

or

$$p = -\rho c^2 (\nabla \cdot d) \tag{11}$$

which expresses certain elastic properties of a fluid.

If $(\nabla \cdot d)$ is eliminated between Equations (9) and (11), the general acoustic wave equation is obtained:

$$\frac{\partial^2 p}{\partial t^2} = c^2 \nabla^2 p \tag{12}$$

Two boundary conditions must be satisfied at the panel

1 Continuity of displacements normal to the wall

Substituting $p = p_1 + p_r$ in Equation (5), for $x = 0$ at the source side of the panel

$$\left\{\frac{D^2\xi}{Dt^2}\right\}_{x=0} = \left\{\frac{Du}{Dt}\right\}_{x=0} = -\frac{1}{\rho}\left\{\frac{\partial(p_1 + p_r)}{\partial x}\right\}_{x=0} \tag{13}$$

With Equations (1) and (2):

$$\left\{\frac{D^2\xi}{Dt^2}\right\}_{x=0} = -\frac{1}{\rho}\{-A_1 ik \cos\theta + B_1 ik \cos\theta\} e^{i(\omega t - ky \sin\theta)}$$

$$= \frac{i\omega \cos\theta}{c\rho}(A_1 - B_1) e^{i(\omega t - ky \sin\theta)} \tag{14}$$

Solving Equation (14) for ξ

$$\xi = -\frac{i \cos\theta}{\omega c \rho}(A_1 - B_1) e^{i(\omega t - ky \sin\theta)} \tag{15}$$

For x = 0 at the receiver side of the panel:

$$\left\{\frac{D^2\xi}{Dt^2}\right\}_{x=0} = -\frac{1}{\rho}\left\{\frac{\partial p_t}{\partial x}\right\}_{x=0} \tag{16}$$

and

$$\left\{\frac{D^2\xi}{Dt^2}\right\}_{x=0} = -\frac{1}{\rho}\,(-A_2\, i\, k\cos\theta)\, e^{i(\omega t - kg\sin\theta)} \tag{17}$$

Solving Equation (17) for ξ.

$$\xi = -\frac{i\, A_2\cos\theta}{\omega c\rho}\, e^{i(\omega t - ky\sin\theta)} \tag{18}$$

Continuity of displacement gives with Equations (15) and (18).

$$A_1 - B_1 = A_2 \tag{19}$$

The panel displacement at y = 0 is given in the form

$$W = W_o\, e^{i(\omega t - k_t x)} \tag{20}$$

at x = 0, y = 0, the panel displacement equals the particle displacement

$$W_o = \frac{-i\, A_2\cos\theta}{\omega c\rho} \tag{21}$$

or

$$A_2 = \frac{i\omega\, W_o\, c\,\rho}{\cos\theta} \tag{22}$$

2. <u>The relation between acoustic pressures excited on wall and the wall response</u>

The pressure difference across the panel gives at x = 0 and y = 0:

$$(p_i + p_r - p_t)_{\substack{x=0\\y=0}} = (Z_p + Z_c)\, i\,\omega\, W_o\, e^{i\omega t} \tag{23}$$

where Z_p is the panel impedance to the propagating pressure wave and Z_c is the cavity impedance at x = 0.

Then

$$A_1 + B_1 - A_2 = (Z_p + Z_c)\, i\,\omega\, W_o \tag{24}$$

or

$$\frac{A_1 + B_1}{A_2} = \frac{(Z_p + Z_c)\, i\,\omega\, W_o}{A_2} + 1 \tag{25}$$

Substituting Equation (22) into Equation (25):

$$\frac{A_1 + B_1}{A_2} = \frac{(Z_p + Z_c)}{\rho c} \cos \theta + 1 \quad ^2 \tag{26}$$

The noise reduction of a panel is defined as

$$NR = 10 \log \left\{ \frac{(p_i + p_r)^2}{p_t^2} \right\} \tag{27}$$

or

$$NR = 10 \log \left\{ \frac{A_1 + B_1}{A_2} \right\}^2 \tag{28}$$

With Equation (25) this results in:

$$NR = 10 \log \left\{ \frac{(Z_p + Z_c) \cos\theta}{\rho c} + 1 \right\}^2 \tag{29}$$

In case of an infinite flat panel, the impedance Z_p for a single degree of freedom system is given by Reference 3)

$$Z_p = 2 \zeta \omega_n M + i (\omega M - \frac{K_p}{\omega}) \tag{30}$$

where M is the mass per unit area, ω the angular frequency and ω_n the fundamental angular frequency of the panel The panel damping coefficient is denoted by ζ, while the panel stiffness coefficient per unit area K_p may be determined from:

$$K_p = \omega_n^2 M \tag{31}$$

Reference 3 gives for the cavity impedance

$$Z_c = \rho c \frac{Z_\ell + i\rho c \tan k \ell}{\rho c + i Z_\ell \tan k \ell} \tag{32}$$

where Z_ℓ is the fiberglass impedance.

References 3 and 4 define the fiberglass impedance by

$$Z_\ell = \frac{\rho_f}{\sqrt{P_f}} \left(1 - \imath \frac{R_f}{\rho_f \omega}\right)^{1/2} \coth \left[\imath \frac{\omega\sqrt{P_g}}{c_f} \left(1 - \imath \frac{R_f}{\rho_f \omega}\right)^{1/2} h\right] \quad (33)$$

Equation (33) was derived for the normal acoustic impedance of isotropic porous materials with thickness h and backed by a rigid wall. R_f is the flow resistivity and the fiberglass porosity is denoted by P_f. The subscript f indicates that those parameters are related to fiberglass. Separating the real and the imaginary part of Equation (33) as found in Appendix A:

$$Z_\ell = \frac{a}{rd} (pm - qn) - \imath \left\{\frac{a}{rd} (qm + pn)\right\} \quad (34)$$

where:

$$a = \frac{\rho_f}{\sqrt{P_f}} \quad (a.1)$$

$$b = \frac{R_f}{\rho_f \omega} \quad (a.2)$$

$$d = \frac{h \omega \sqrt{P_f}}{c_f} \quad (a\ 3)$$

$$m = d \left\{1 + (1 + b^2)^{1/2}\right\}^{1/2} \quad (a.7)$$

$$n = d \left\{-1 + (1 + b^2)^{1/2}\right\}^{1/2} \quad (a\ 6)$$

$$p = e^{4n} - 1 \quad (a.11)$$

$$q = 2e^{2n} \sin 2m \quad (a.12)$$

$$r = \left\{(e^{2n} \cos 2m - 1)^2 - (e^{2n} \sin 2m)^2\right\} \quad (a.13)$$

Equation (34) substituted in (32) gives for the cavity impedance Z_c

$$Z_c = \frac{\rho c \left[\left[A\rho c (1 - \tan^2 k\ell) - \imath\left[\{A^2 + B^2 - (\rho c)^2\} \tan k\ell + B\rho c (\tan^2 k\ell - 1)\right]\right]\right.}{(\rho c + B \tan k\ell)^2 + (A \tan k\ell)^2} \quad (35)$$

where. $$A = \frac{a}{rd}\,(pm - qn) \tag{36}$$

and $$B = \frac{a}{rd}\,(qm + pn) \tag{37}$$

Substituting Equations (30), (31) and (35) into Equation (29) results in the noise reduction equation for an infinite panel under oblique angle of sound incidence, backed by a closed cavity filled with fiberglass:

$$NR = 10 \log \left[\left\{\frac{2\zeta\omega_n M \cos\theta}{\rho c} + \frac{A\rho c\,(1 - \tan^2 k\ell)\cos\theta}{(\rho c + B\tan k\ell)^2 + (A\tan k\ell)^2} + 1\right\}^2 + \right.$$

$$\left. + \left\{\frac{(\omega_n^2 - \omega^2)\,M\cos\theta}{\omega\rho c} + \frac{\{A^2 + B^2 - (\rho c)^2\}\tan k\ell\cos\theta + B\rho c\,(\tan^2 k\ell - 1)\cos\theta}{(\rho c + B\tan k\ell)^2 + (A\tan k\ell)^2}\right\}^2\right] \tag{38}$$

Tables 2.1, 2.2 and 2.3 contain the data to calculate the noise reduction from Equation (38) for various thicknesses and angles of sound incidence as related to frequency. All calculations were obtained by using a programmable hand calculator and are summarized in Table 2.4.

2.2 Experimental Results

Noise reduction tests have been conducted for aluminum panels of four different thicknesses (.016", .025", .032" and .040") and for four oblique angles of sound incidence (θ = 15°, 30°, 40° and 60° from the x-axis normal to the panel plane [Figure 2.1]). Four different test sections, in combination with an extension tube (Figure 2.2), have been used to investigate the effect of a changing angle of sound incidence. Figure 2.3 shows the configuration of this acoustic test facility. Initially both extension tube and special test sections were lined with fiberglass wedges to minimize reflections from their walls and

Table 2.1 Summary of Data for the Calculation of the Characteristic Impedance of Fiberglass in a Cavity Backed by a Rigid Wall

$\rho_f = \rho = 1\ 226\ [kg/m^3]$	
$\sqrt{P_f} = .949$	(Ref. 4)
$R_f = 20{,}000$ [mks rayls/m]	(Ref. 5)
fiberglass density = 3 [lbs/ft^3]$\sim$49[kg/m^3]	(product data)
$c_f = c/1.18 = 288.4$ [m/s]	(Ref. 4)
h = 2 73 [m]	(measured)
$a = \frac{\rho_f}{\sqrt{P_f}} = 1.292\ [kg/m^3]$	(calculated)
$b = \frac{R_f}{\rho_f 2\pi f} = \frac{2596.33}{f}$ [1/rad]	(calculated)
$d = \frac{h2\pi f\sqrt{P_f}}{c_f} = .0564*f$ [rad]	(calculated)

Table 2.2 Summary of Data for the Calculation of the Characteristic Impedance of an Aluminum Panel

$\zeta = .02$	(estimated)
$M = \rho*t = 2700t$ [kg/m^2]	
t = .016*0 0254[m], .020*0.0254[m]; .025*0.0254[m]; .032*0.0254[m]; .040*0.0254[m]	
ω_n [rad/s]	(experimental)
$\theta = 0°$, 15°, 30°, 40°; and 60°	

Table 2.3 Values for the Parameters A and B as Defined in Equation (36) and Equation (37), Respectively

frequency f· [H_z]	A	B
16	-30.61	-30.43
20	16.54	16.49
32	-13.69	-13.53
63	-26.45	-25.81
125	6.31	6.01
250	-7.32	-6.65
500	898.3	741.8
1000	$-\infty$	$-\infty$
2000	$-\infty$	$-\infty$
4000	$-\infty$	$-\infty$
5000	$-\infty$	$-\infty$

Table 2.4 Calculation of the Noise Reduction for Flat Aluminum Panels of Various Thickness Under an Oblique Angle of Sound Incidence

frequency f [Hz] ↓	thickness t [inch]→	016				025				032				040			
	$f_{1,1}$* [Hz]→	24	25	26	20	33	33	34	33	41	38	35	34	36	46	38	36
	θ** [degrees]→	15	30	40	60	15	30	40	60	15	30	40	60	15	30	40	60
16		14	07	24	- 21	4 36	3 77	3 54	1 60	9 65	7 49	5 32	2 73	8 96	12 65	8 03	4 37
32		07	01	- 02	02	025	021	017	009	1 67	69	20	07	68	4 06	86	25
63		2 11	1 70	1 32	87	3 44	2 93	2 43	1 17	3 60	3 54	3 34	1 79	5 78	3 22	4 09	2 42
125		7 12	6 36	5 55	3 32	10 08	10 02	8 26	5 37	11 60	10 85	10 0	6 89	13 58	12 22	11 6	8 4
250		12 53	11 64	10 65	7 45	16 1	15 2	14 1	10 6	18 0	17 1	16 1	12 6	19 9	18 9	17 9	14 3
500		17 10	16 22	15 24	11 97	21 6	20 6	19 6	16 0	24 1	22 3	21 3	17 7	25 3	24 3	23 3	19 7
1000		23 66	22 71	21 64	17 96	27 5	26 5	25 4	21 7	29 7	28 7	27 6	23 9	31 7	30 7	29 6	25 9
2000		30 27	29 35	28 32	24 80	33 9	32 9	31 9	28 2	36 0	35 1	34 0	30 3	38 0	37 0	35 9	32 2
4000		35 88	34 92	33 84	30 14	39 9	39 0	37 9	34 2	42 1	41 1	40 1	36 4	44 0	43 1	42 0	38 3
5000		37 96	37 01	35 95	32 24	41 8	40 8	39 7	36 0	43 9	43 0	41 9	38 2	45 9	44 9	43 8	40 1

* fundamental panel/cavity resonance frequency

** angle of sound incidence

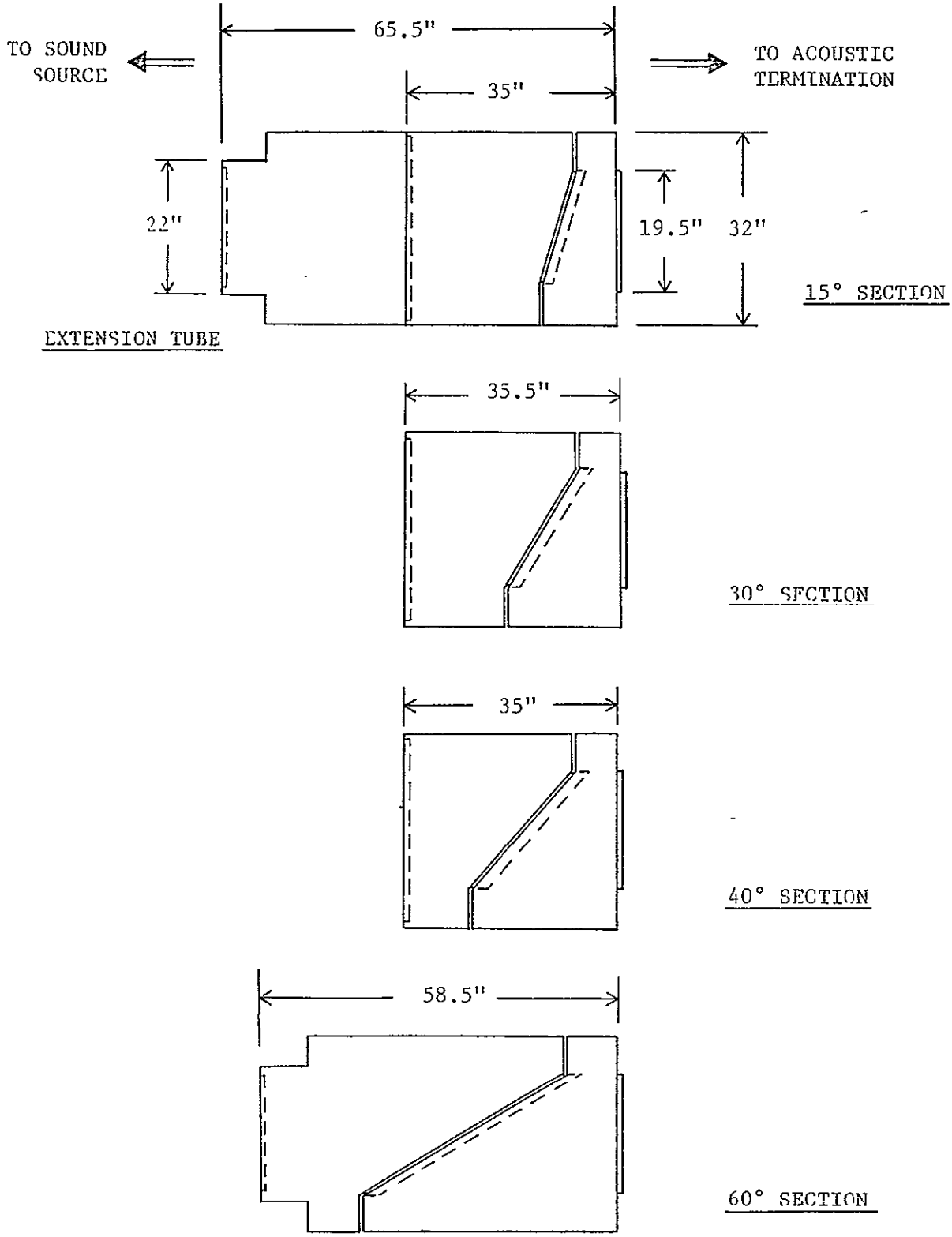

Figure 2.2 Top Views of the Special Test Sections

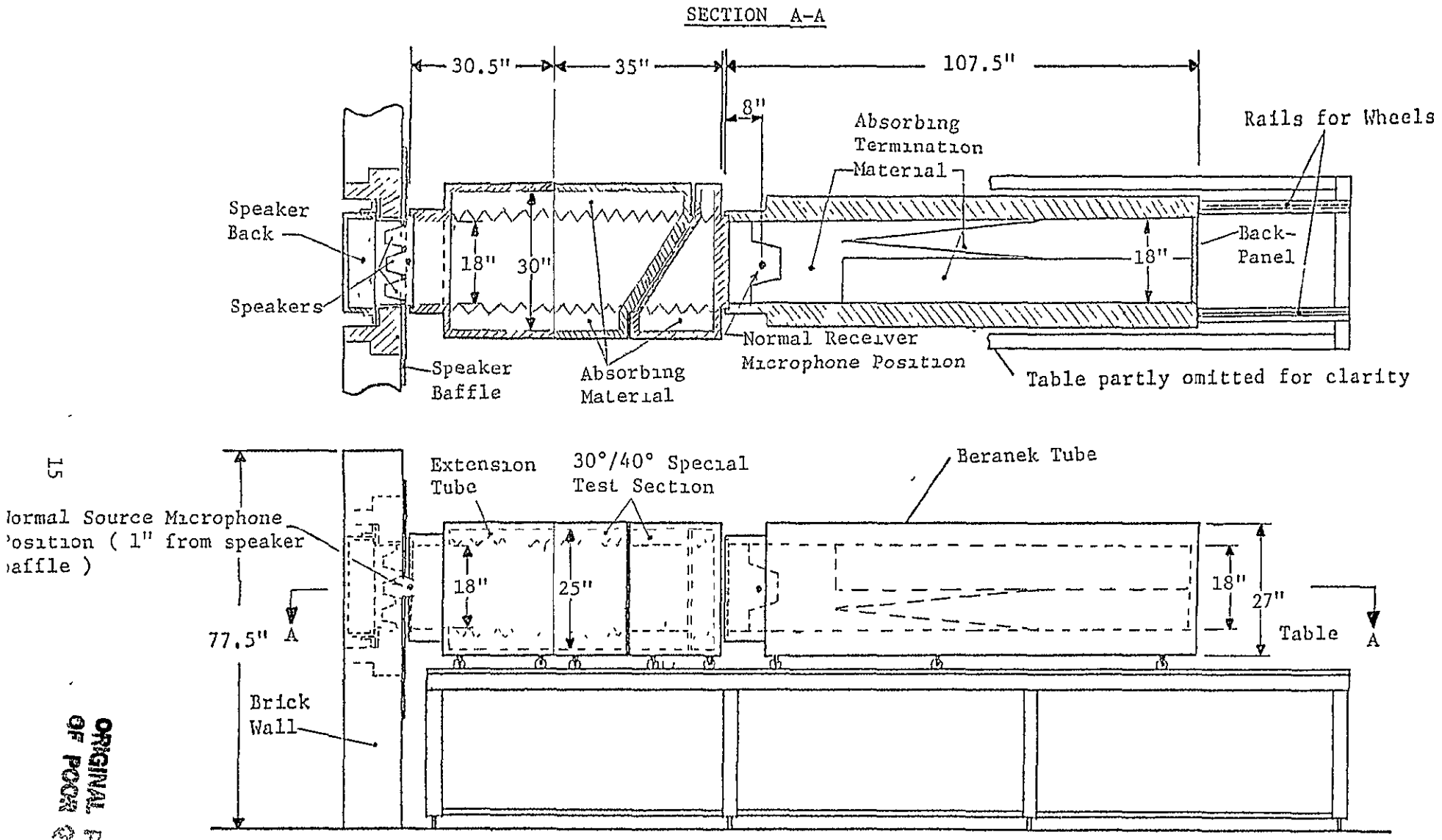

Figure 2.3 KU-FRL Acoustic Panel Test Facility Showing Extension Tube and 30°/40° Special Test Section

to minimize standing waves in between these walls. As they absorbed much of the sound generated by the loudspeakers, the sound at the receiver side of the test panel was too weak to be accurately measured. Four hard wooden walls have been installed in the extension tube, that cover the fiberglass wedges and prevent the absorption of sound by the lining. This leaves a cross-sectional area of 18 x 18 inches in the extension tube. The distance between the hard walls in the special test section is 25 inches and 30 inches respectively in two perpendicular directions. These walls, however, are still covered by fiberglass wedges, leaving a sound passage of 18 x 18 inches (Figure 2.3). The fiberglass wedges reduce reflection from the hard walls, but standing waves between the walls, the speaker box and panel, and between panel and cavity back wall can not be avoided.

The following parameters have to be considered to compare the results

- distance from microphone to speaker box
- distance from microphone to panel surface
- cavities at the source and receiver side of the panel
- characteristics of fiberglass lining the special test sections
- nonidentical properties of panels with the same dimensions and of the same material
- exposed test panel area
- edge conditions of the test panels
- coupling of panel and cavity modes
- properties of each special test section

It is not possible to correct the noise reduction results for each single parameter. For comparison of the experimental results with each of the four test sections, the specific characteristics of the acoustic test facility including these special test sections have to be eliminated. This has been done by measuring the noise reduction between the source and the receiver microphone without a test panel installed, using the configuration depicted in Figure 2.3. This noise reduction then is subtracted from the noise reduction measured after the installation of the test panel. This sequence has been repeated for all tests in all four special test sections. In this way the variation in noise reduction characteristics of the test panel, due to the use of a different test section, is minimized. The experimental results, obtained in the KU-FRL acoustic test facility, are presented in Figures 2.4 to 2.19. Four aluminum panels of different thicknesses (t = .016", .025", .032" and 040") have been tested for four oblique angles of sound incidence (θ = 15°, 30°, 40° and 60°). The theoretical results from Table 2.4 are drawn in these graphs to compare the theoretical analysis with the experimental tests. The theory predicts the trend of the noise reduction as a function of the frequency reasonably well. The lower noise reduction than theoretically predicted in the frequency region between 300 Hz and 1500 Hz is primarily caused by the correction for the special test section sound characteristics without a panel installed and is not a property of the test panel. The peaks and dips in the experimental noise reduction curves can be explained as panel and cavity modes.

Table 2.5 presents the most important hard wall cavity modes of the receiver chamber in the frequency range below 2000 Hz. Re-

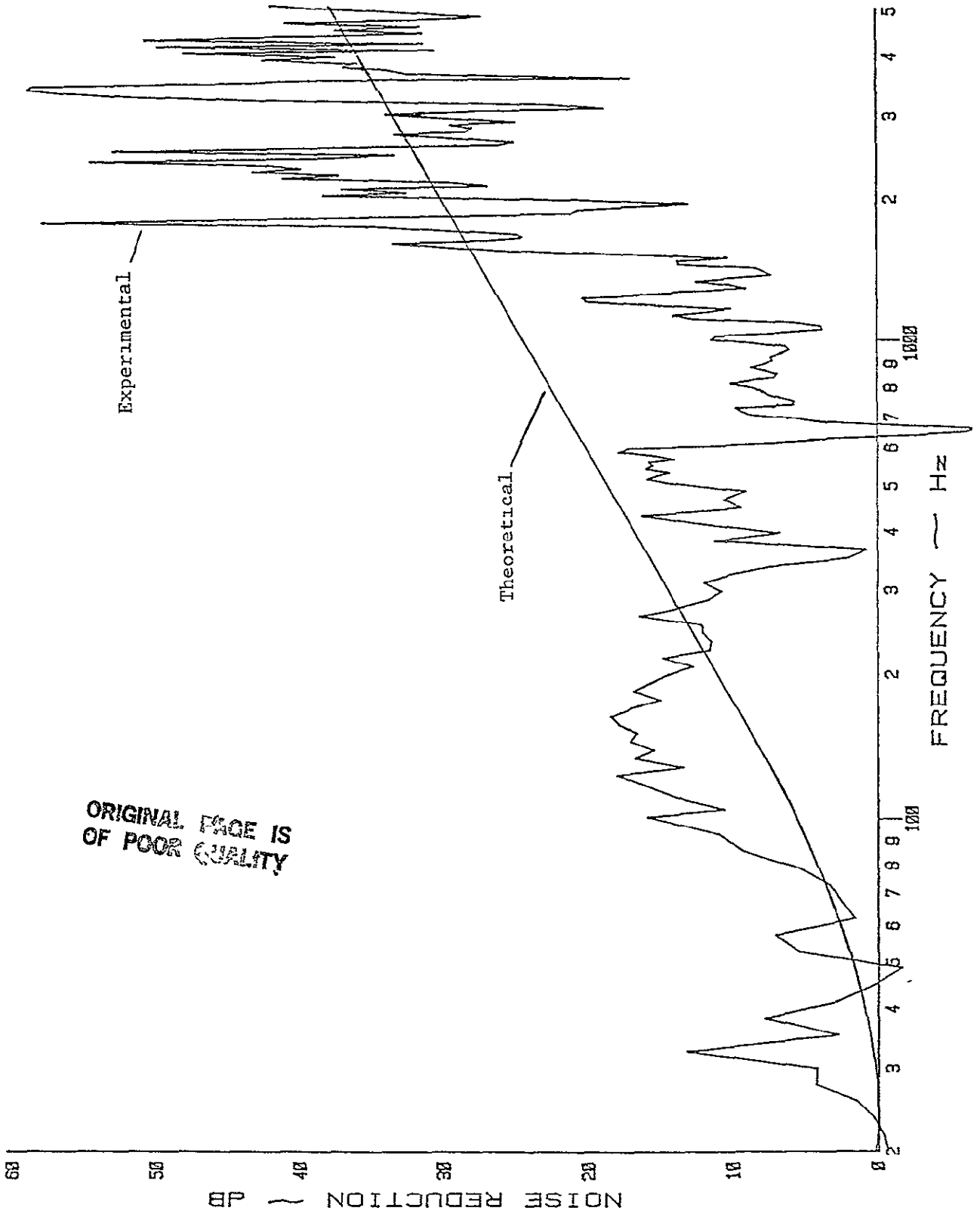

Figure 2 4 Experimental and Theoretical Noise Reduction Characteristics of a .016 Inch Thick Aluminum Panel Under 15° Angle of Sound Incidence.

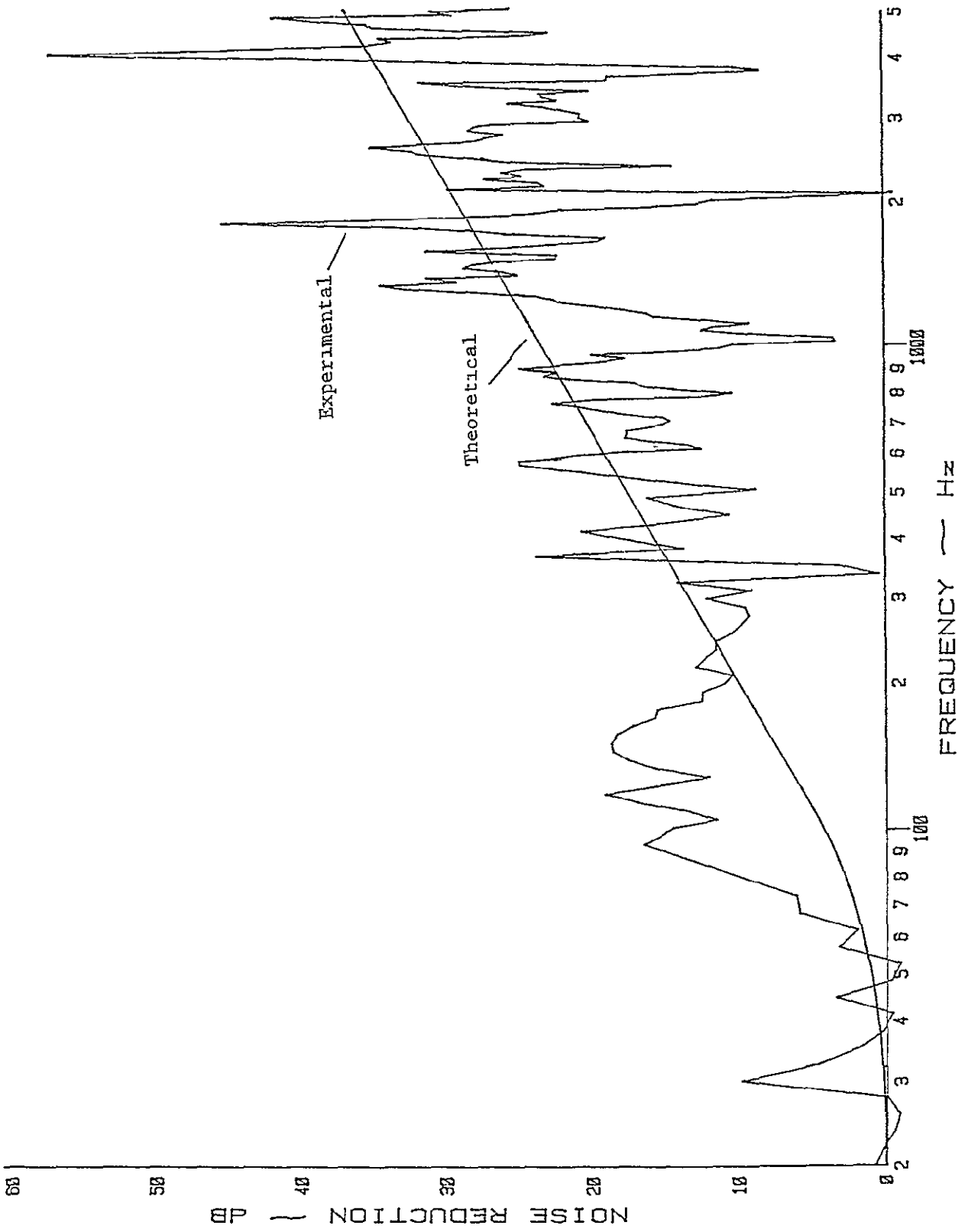

Figure 2.5 Experimental and Theoretical Noise Reduction Characteristics of a 016 Inch Thick Aluminum Panel Under 30° Angle of Sound Incidence.

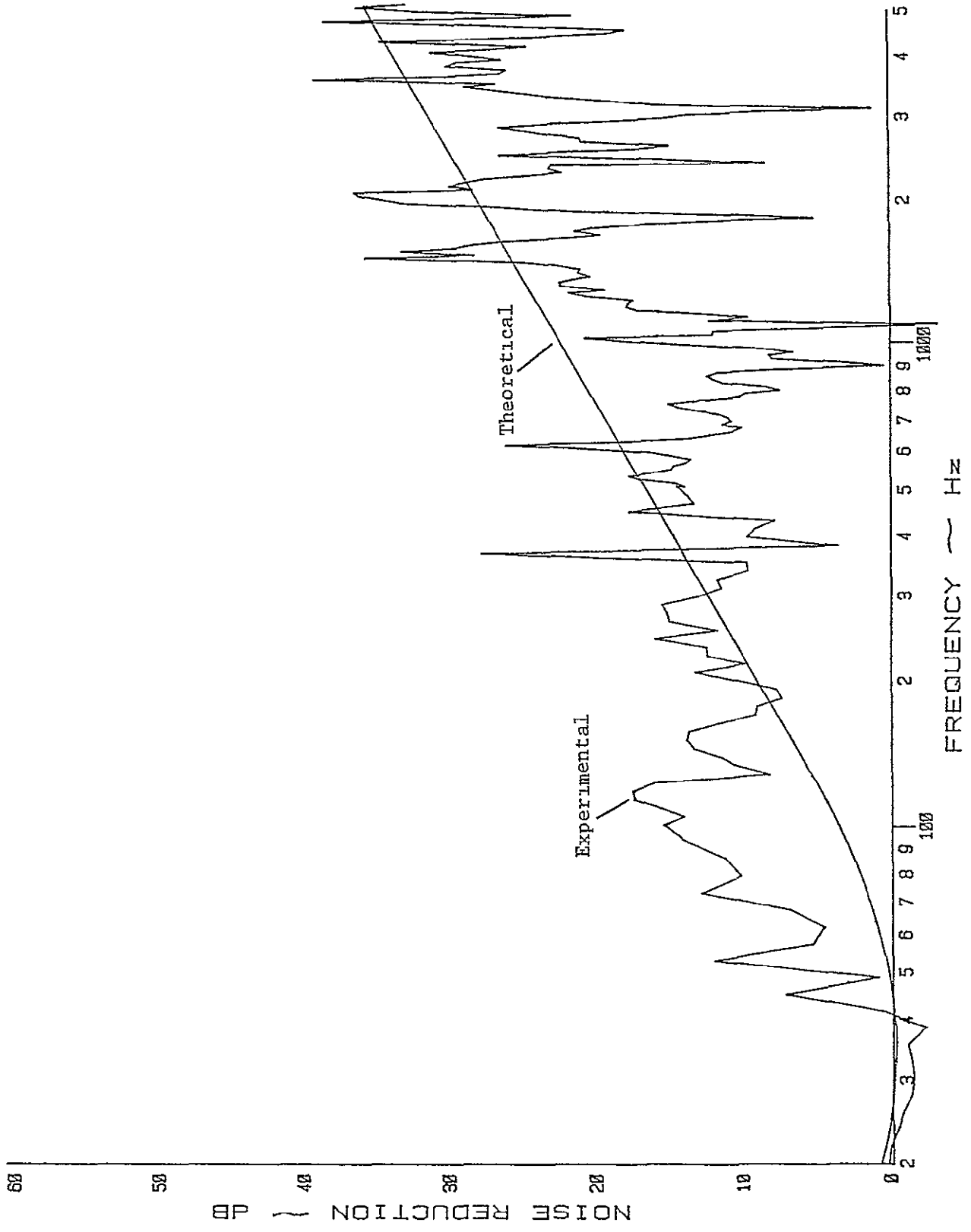

Figure 2.6: Experimental and Theoretical Noise Reduction Characteristics of a .016 Inch Thick Aluminum Panel Under 40° Angle of Sound Incidence.

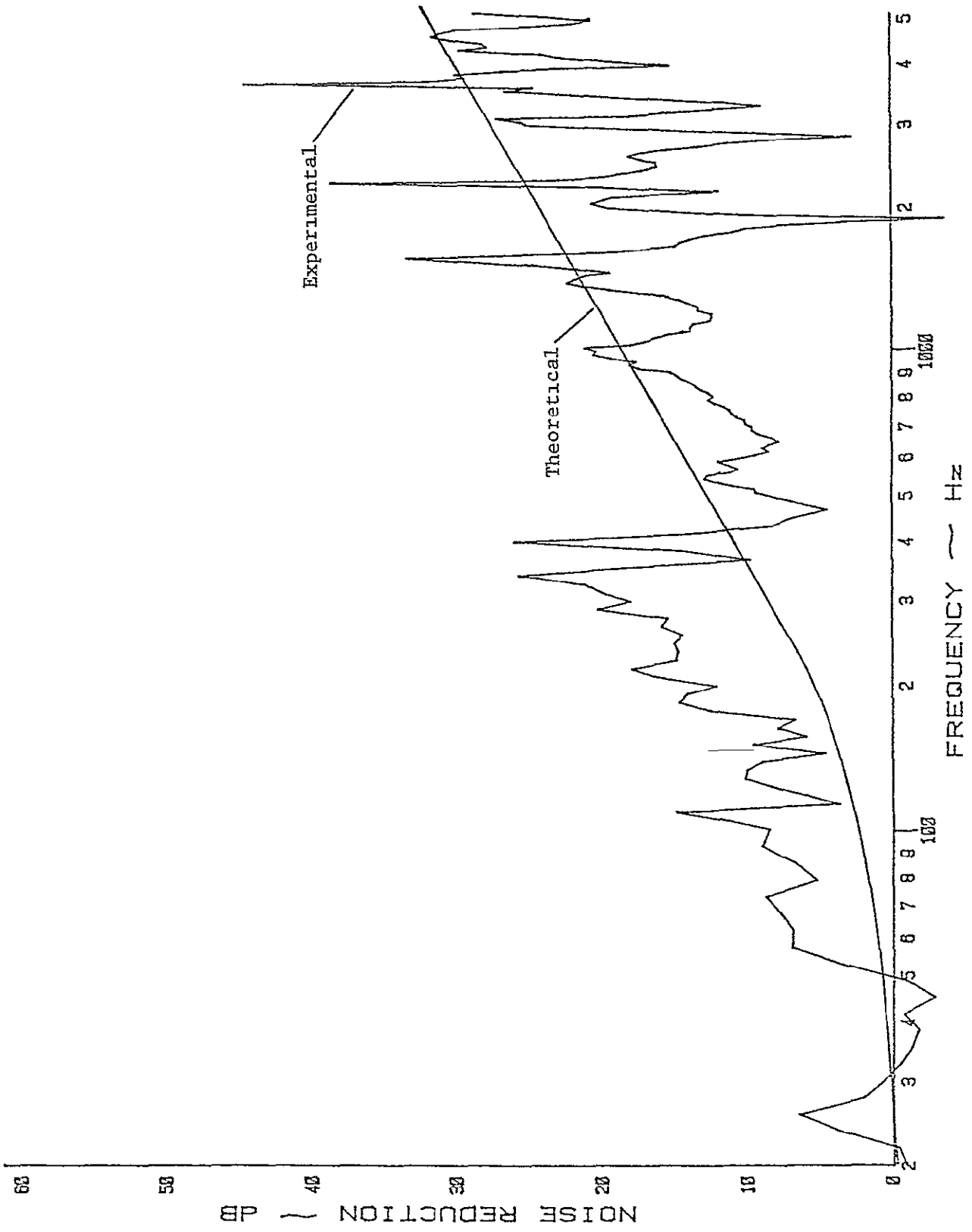

Figure 2.7 Experimental and Theoretical Noise Reduction Characteristics of a .016 Inch Thick Aluminum Panel Under 60° Angle of Sound Incidence.

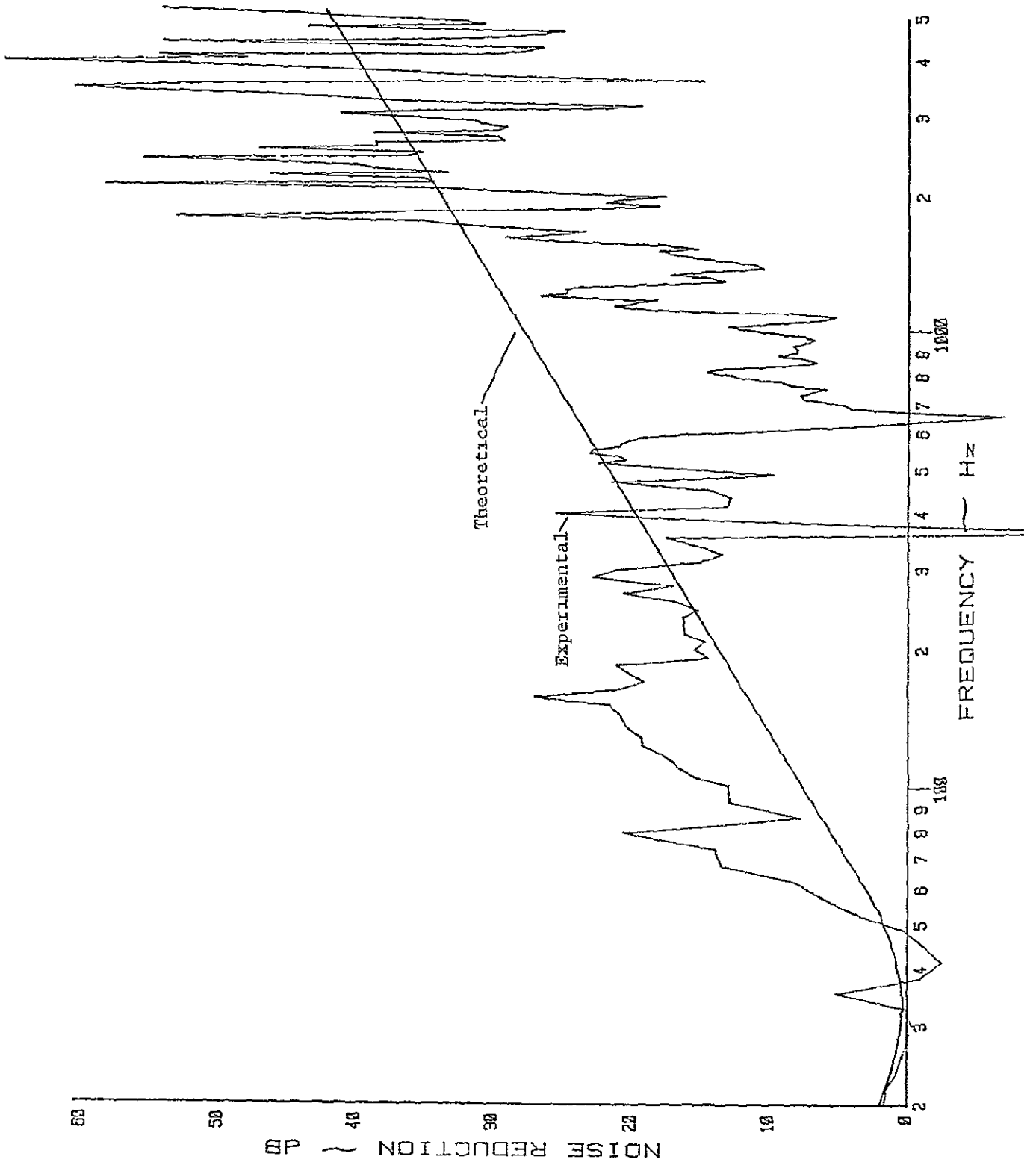

Figure 2.8. Experimental and Theoretical Noise Reduction Characteristics of a .025 Inch Thick Aluminum Panel Under 15° Angle of Sound Incidence.

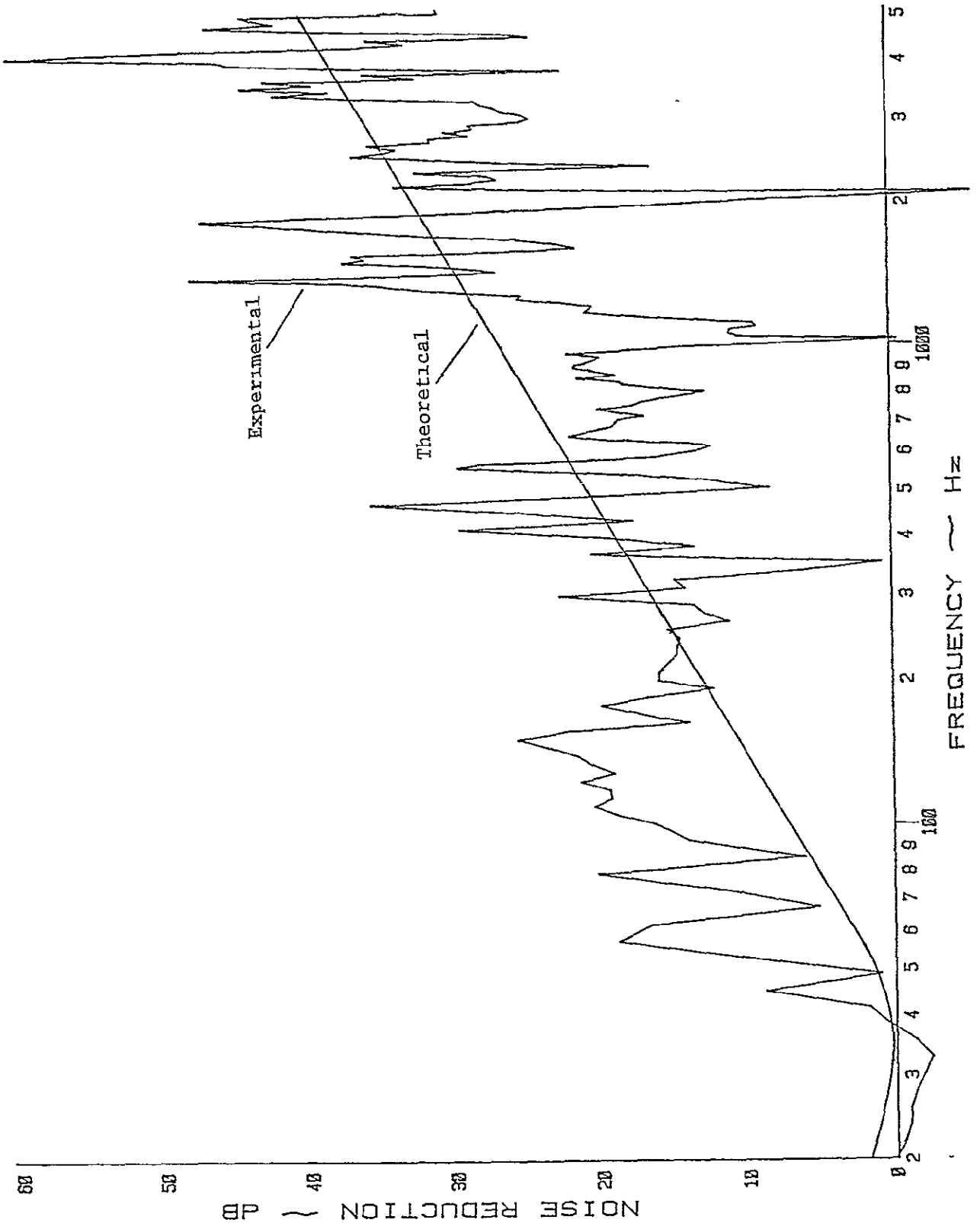

Figure 2.9 Experimental and Theoretical Noise Reduction Characteristics of a .025 Inch Thick Aluminum Panel Under 30° Angle of Sound Incidence.

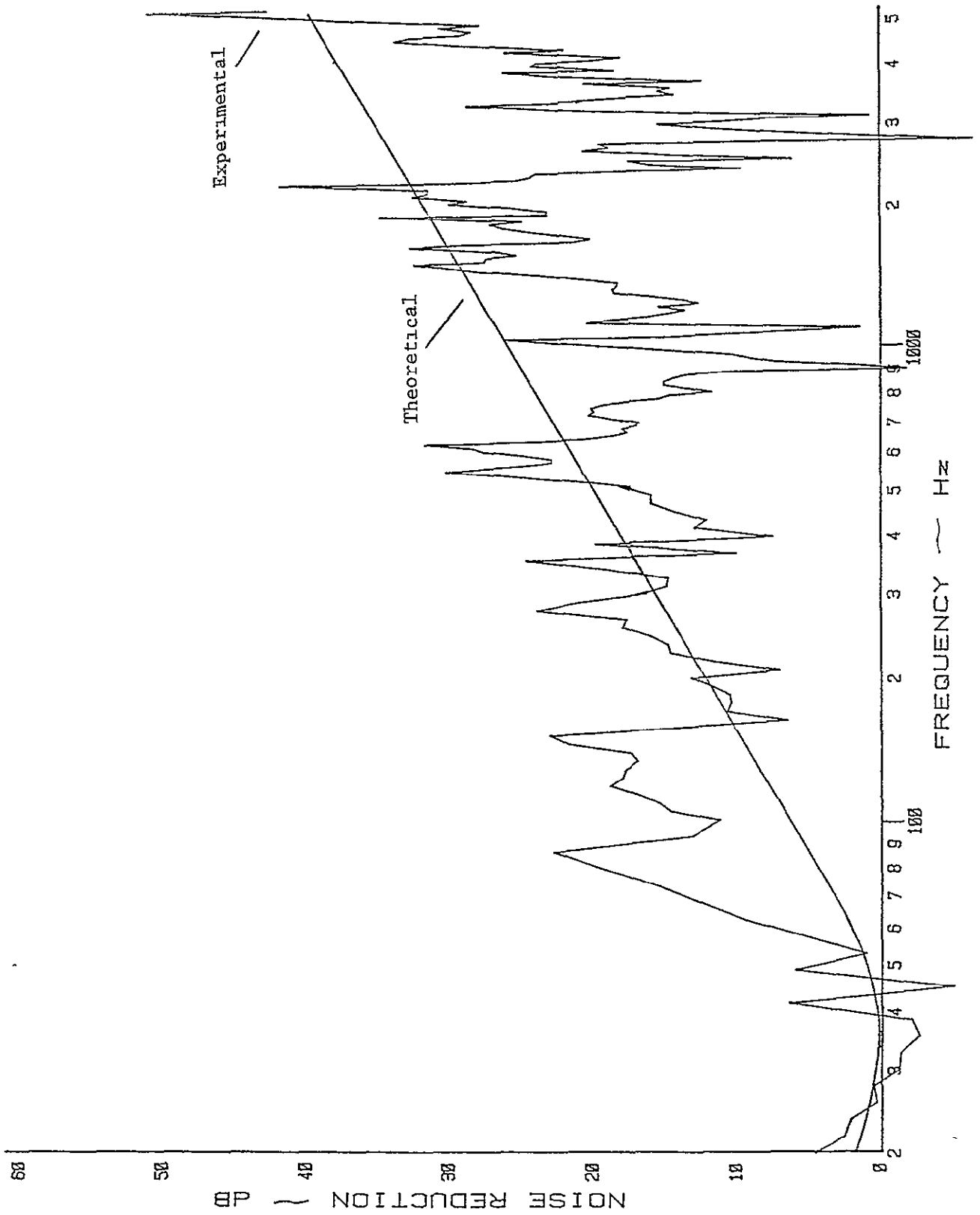

Figure 2.10: Experimental and Theoretical Noise Reduction Characteristics of a .025 Inch Thick Aluminum Panel Under 40° Angle of Sound Incidence.

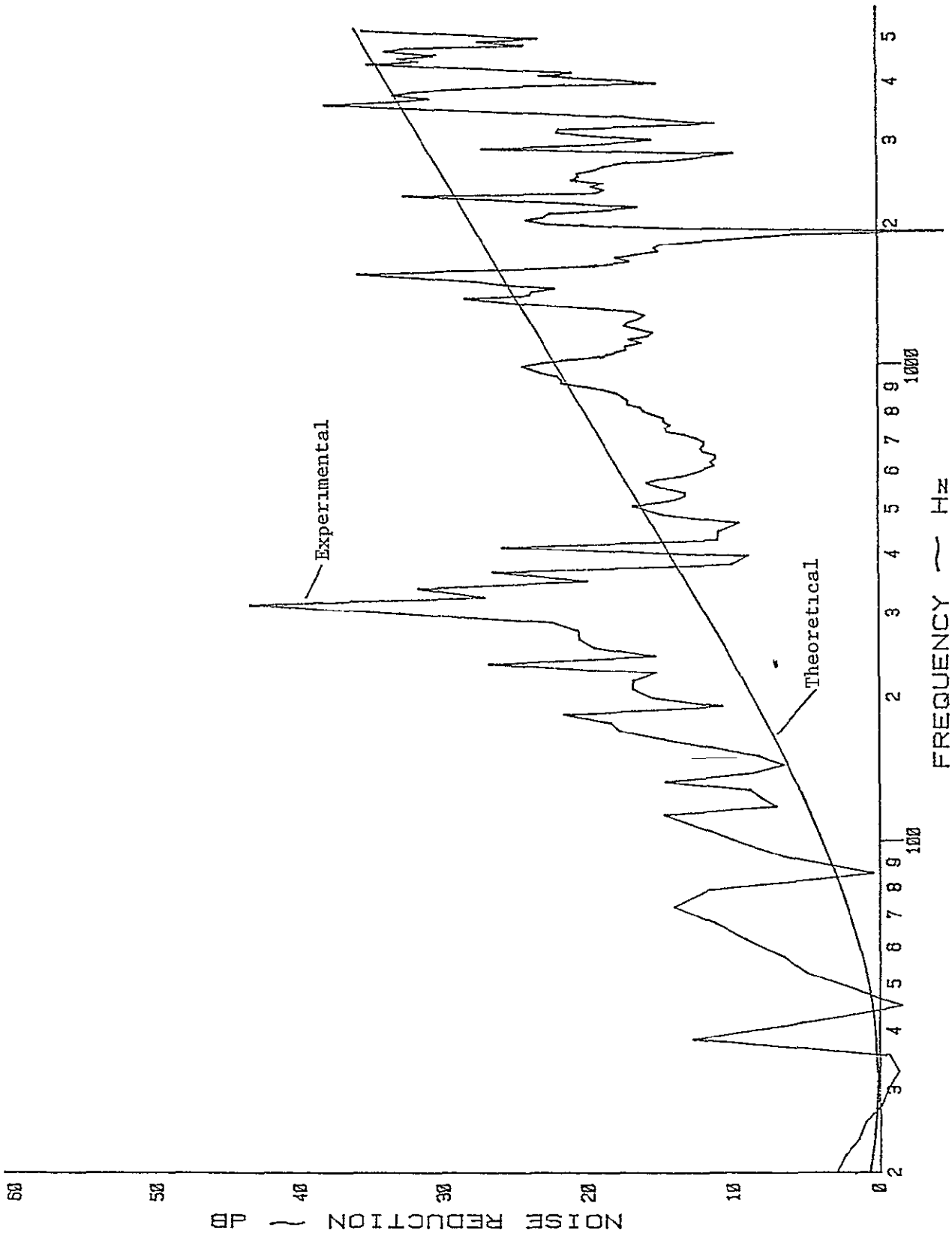

Figure 2.11 Experimental and Theoretical Noise Reduction Characteristics of a .025 Inch Thick Aluminum Panel Under 60° Angle of Sound Incidence.

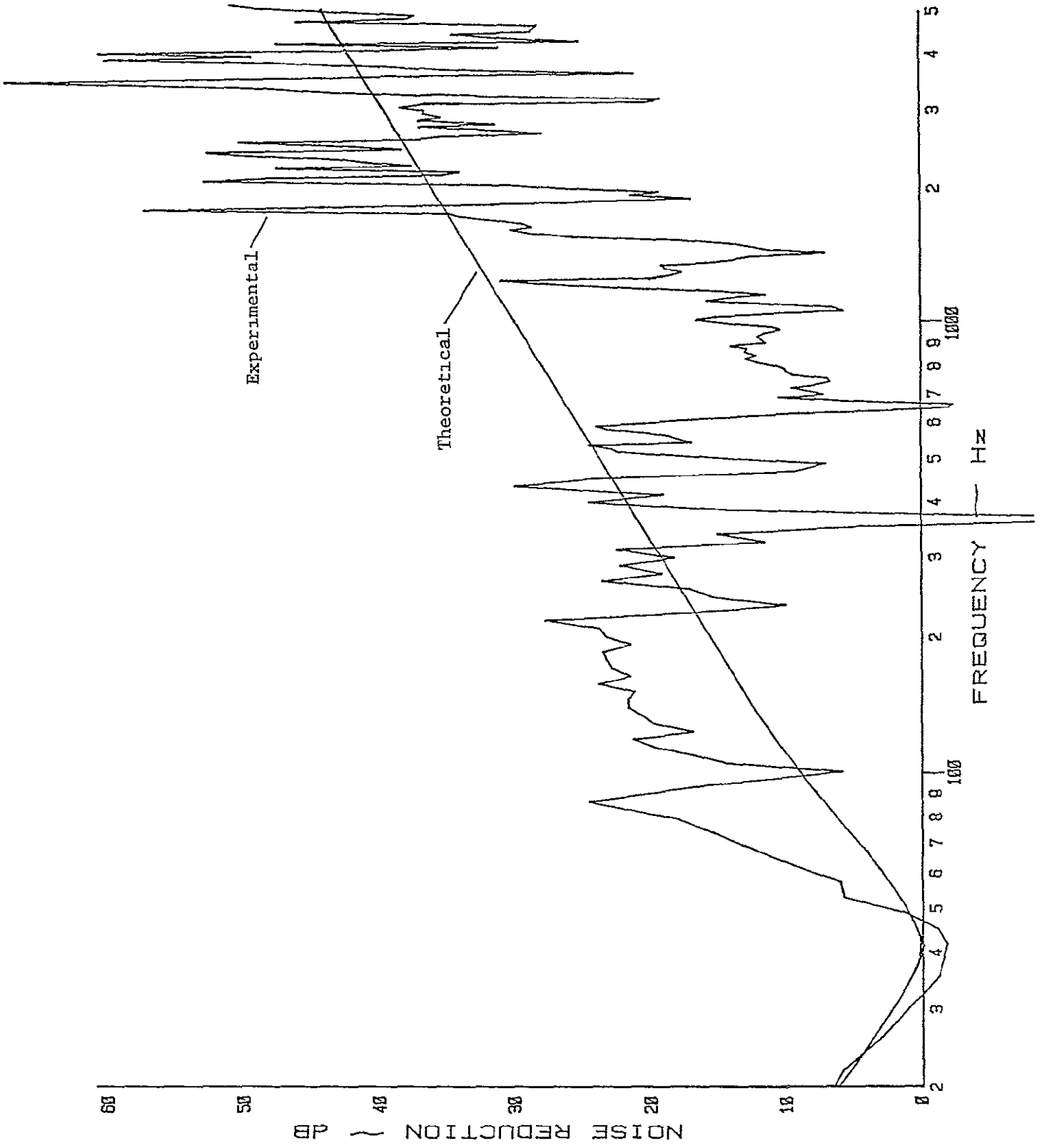

Figure 2.12. Experimental and Theoretical Noise Reduction Characteristics of a .032 Inch Thick Aluminum Panel Under 15° Angle of Sound Incidence.

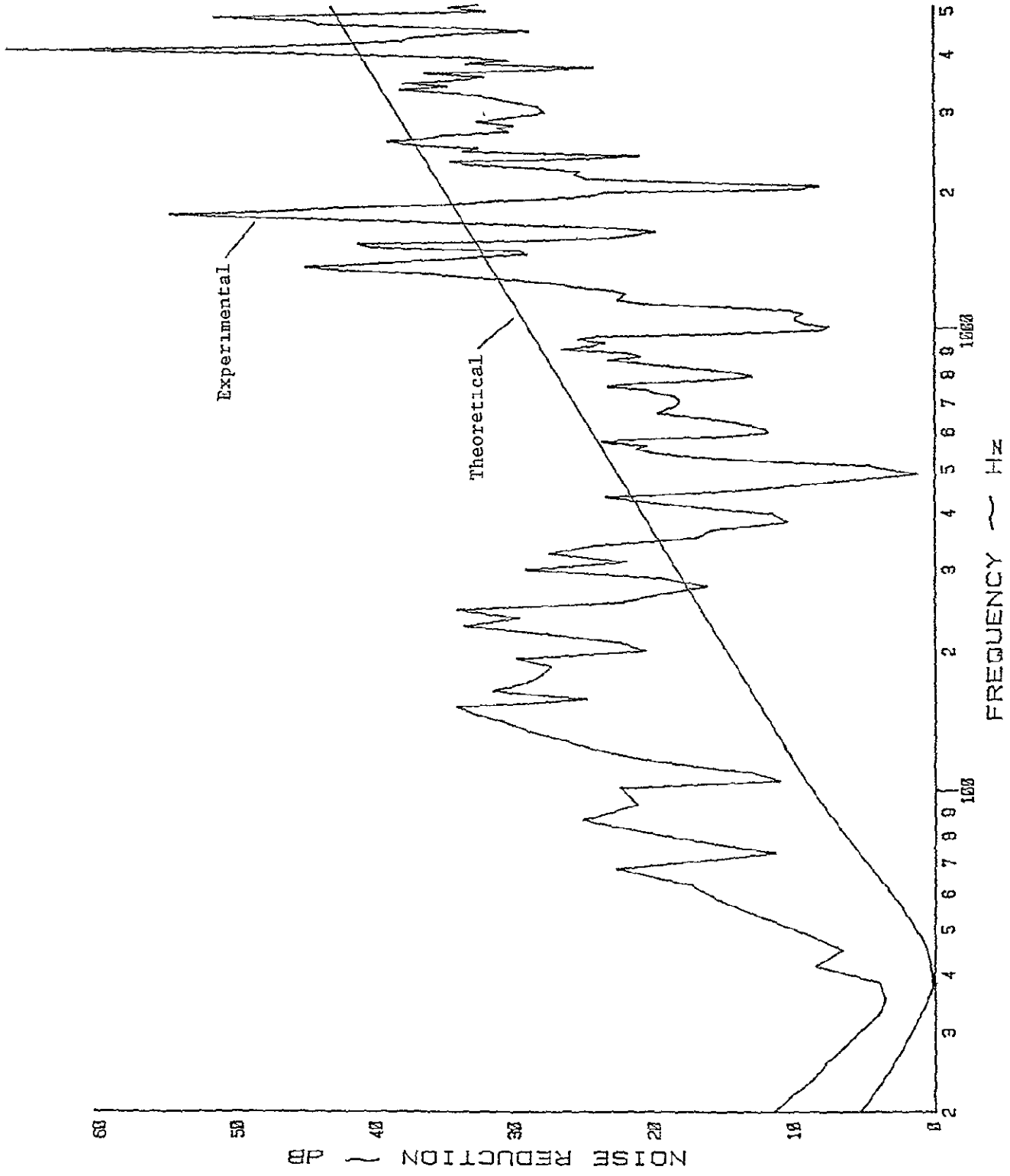

Figure 2.13 Experimental and Theoretical Noise Reduction Characteristics of a .032 Inch Thick Aluminum Panel Under 30° Angle of Sound Incidence.

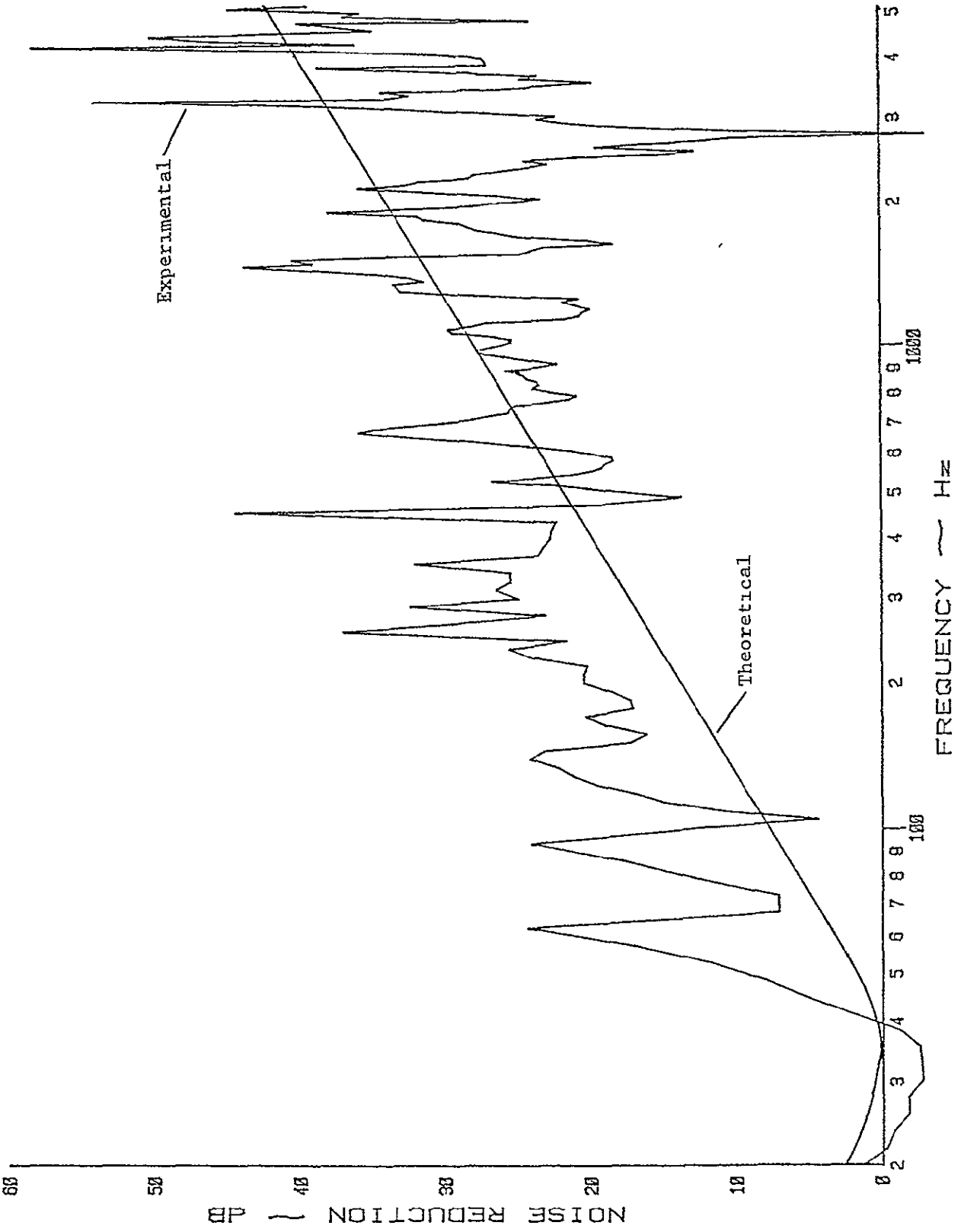

Figure 2.14: Experimental and Theoretical Noise Reduction Characteristics of a .032 Inch Thick Aluminum Panel Under 40° Angle of Sound Incidence.

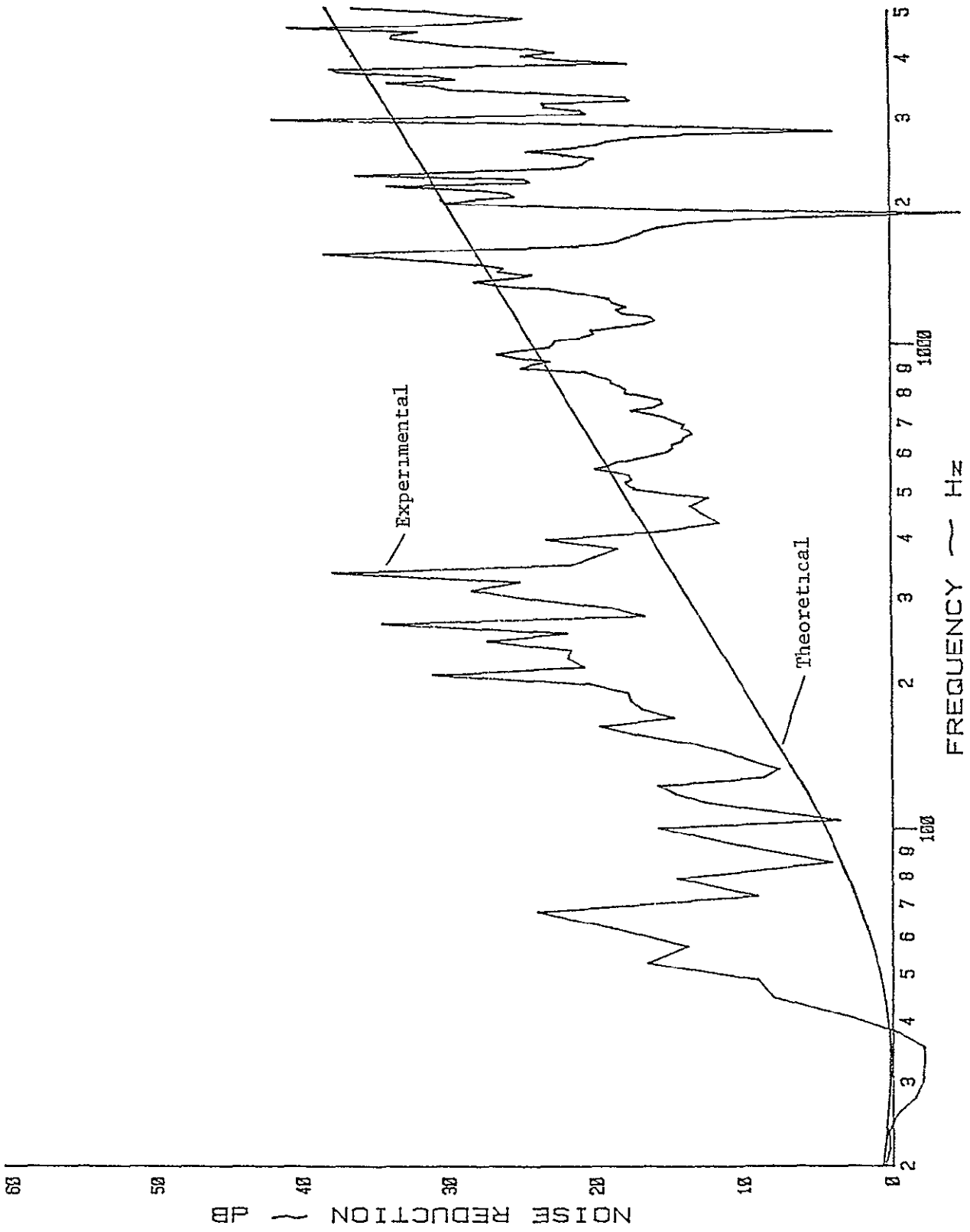

Figure 2.15 Experimental and Theoretical Noise Reduction Characteristics of a .032 Inch Thick Aluminum Panel Under 60° Angle of Sound Incidence.

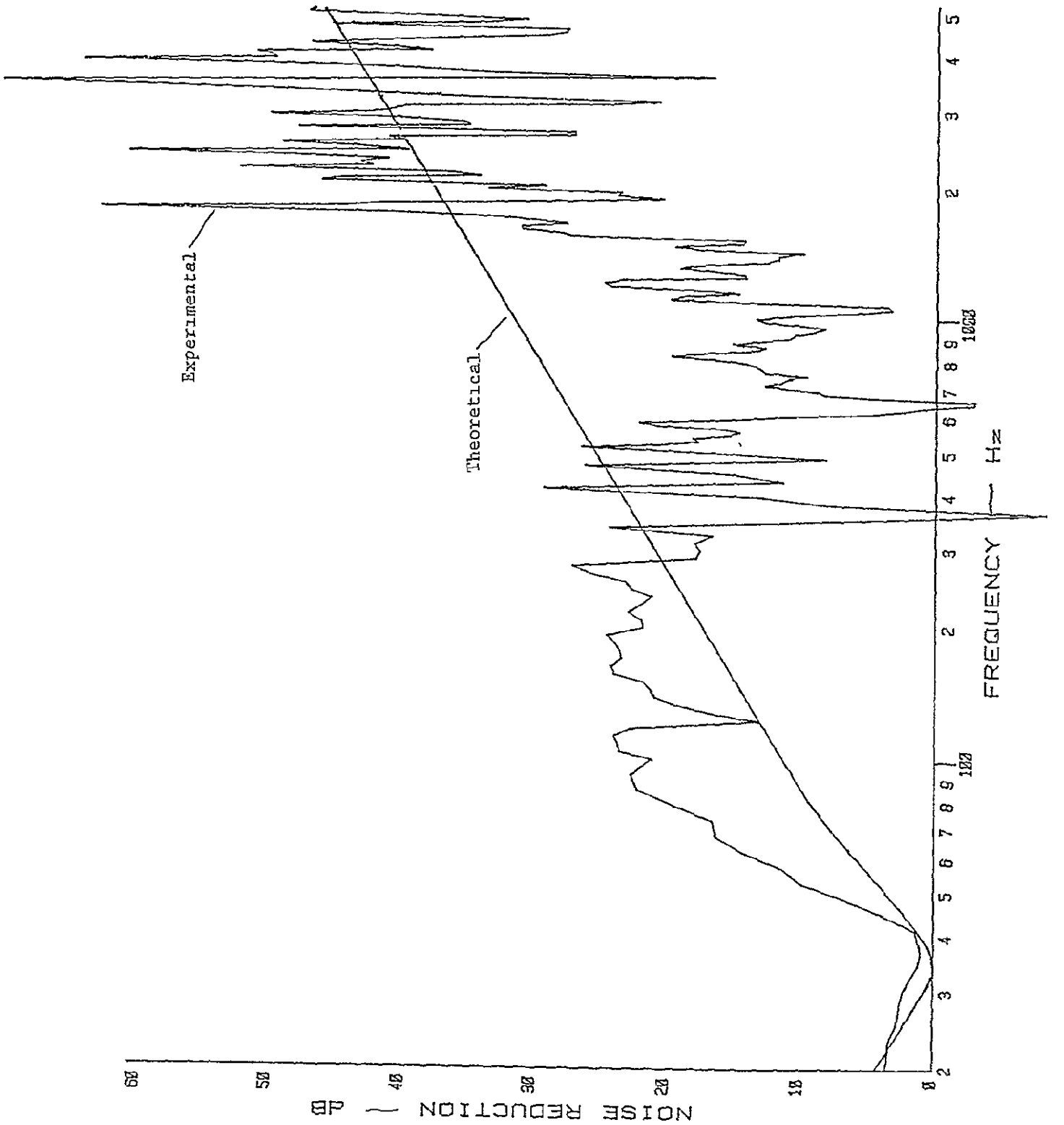

Figure 2.16: Experimental and Theoretical Noise Reduction Characteristics of a .040 Inch Thick Aluminum Panel Under 15° Angle of Sound Incidence.

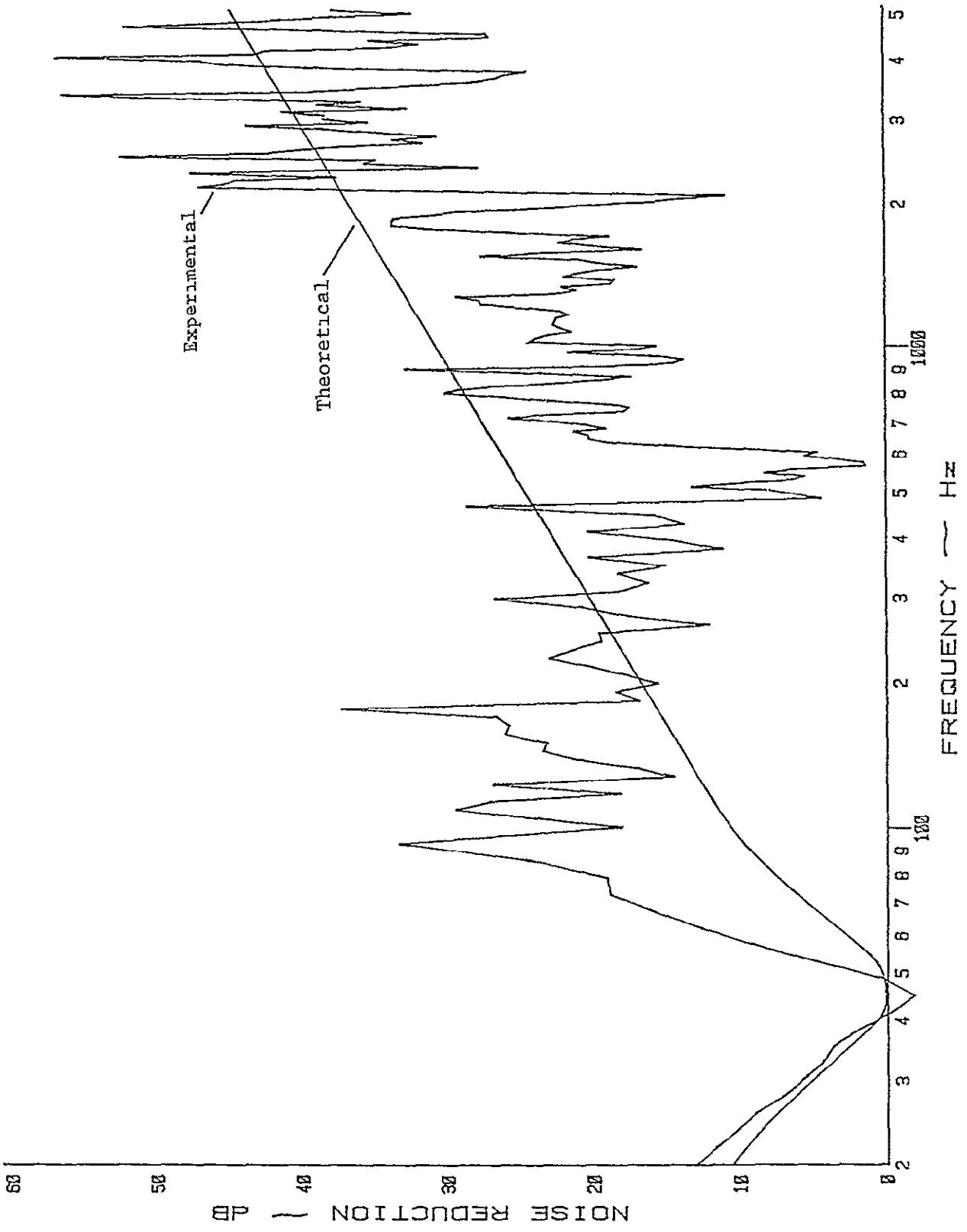

Figure 2.17: Experimental and Theoretical Noise Reduction Characteristics of a .040 Inch Thick Aluminum Panel Under 30° Angle of Sound Incidence.

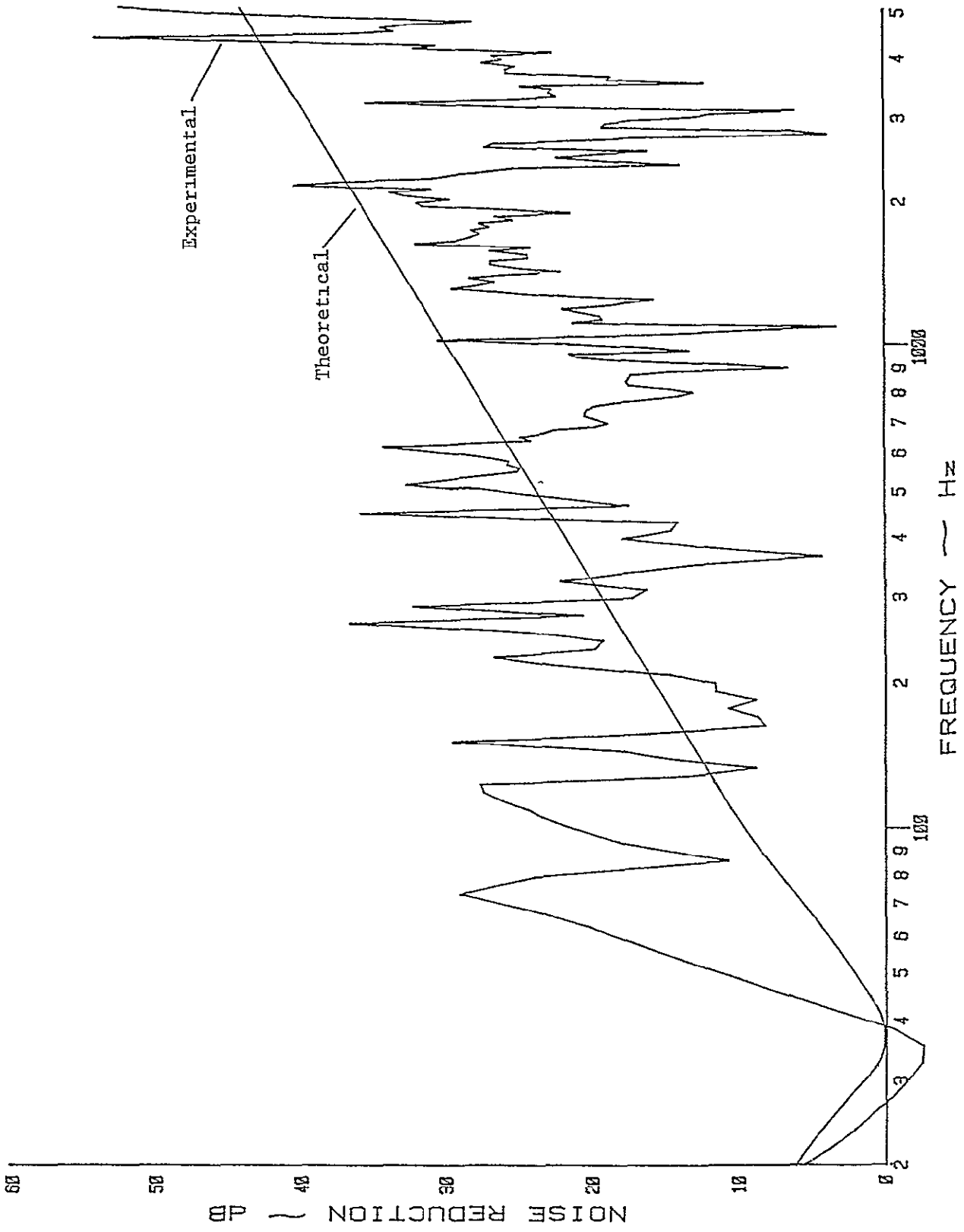

Figure 2.18· Experimental and Theoretical Noise Reduction Characteristics of a .040 Inch Thick Aluminum Panel Under 40° Angle of Sound Incidence.

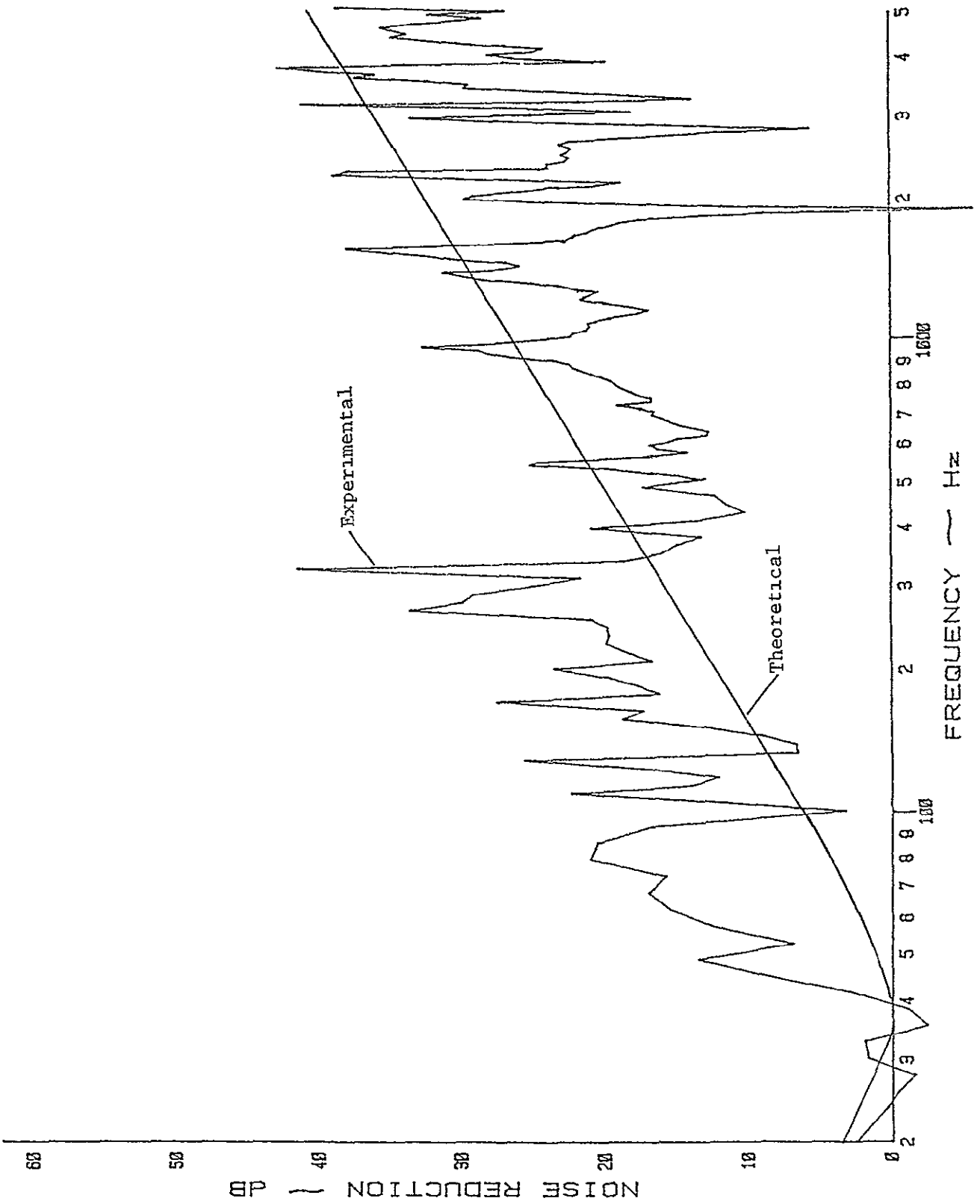

Figure 2.19: Experimental and Theoretical Noise Reduction Characteristics of a .040 Inch Thick Aluminum Panel Under 60° Angle of Sound Incidence.

Table 2.5 Important Hard Wall Cavity Modes in the Frequency Range Below 2000 Hz

$$f_{mnq} = \frac{c}{2}\sqrt{(\frac{m}{\ell_m})^2 + (\frac{n}{\ell_n})^2 + (\frac{q}{\ell_q})^2} \qquad \text{(Ref 3)}$$

where $c = 343.8$ m/s — speed of sound

$\ell_m = 0.635$ m — distance between two cavity walls

$\ell_n = 0.762$ m — distance between two cavity walls perpendicular to the m-direction

$\ell_q = 4.3942$ m — distance between speaker box and cavity back wall (x-direction)

modal number m	n	q	calculated frequency f_{mnq}	modal number m	n	q	calculated frequency f_{mnq}
0	0	1	39.1	2	0	1	542.8
0	0	2	78.2	2	0	2	547.0
0	0	3	117.4	2	1	0	587
0	0	4	156.5	2	1	1	588
0	0	5	195.6	2	1	2	592
0	1	0	225.6	0	3	0	677
0	1	1	228.9	2	2	0	705
0	1	2	238.8	2	2	1	706
0	1	3	254.3	2	2	2	709
1	0	0	270.7	1	3	0	729
1	0	1	273.5	1	3	1	730
1	0	2	281.8	3	0	0	812
1	0	3	295.0	3	1	0	843
1	1	0	352.4	3	1	1	844
1	1	1	354.5	2	3	0	867
1	1	2	360.9	2	3	1	868
1	1	3	371.4	0	4	0	902
0	2	0	451.2	3	2	0	929
0	2	1	452.8	1	4	0	942
0	2	2	457.9	2	4	0	1052
1	2	0	526.2	3	3	0	1057
1	2	1	527.6	4	0	0	1083
1	2	2	531.9	4	1	0	1106
2	0	0	541.4	0	5	0	1128

Table 2.5 Important Hard Wall Cavity Modes in the Frequency Range Below 2000 Hz (continued)

modal number m	n	q	calculated frequency f_{mnq}	modal number m	n	q	calculated frequency f_{mnq}
1	5	0	1160	7	0	0	1894
4	2	0	1173	7	1	0	1908
3	4	0	1214	5	6	0	1914
2	5	0	1251	4	7	0	1914
4	3	0	1277	7	2	0	1947
5	0	0	1353	6	5	0	1977
0	6	0	1354	3	8	0	1979
5	1	0	1372				
1	6	0	1380				
3	5	0	1390				
4	4	0	1410				
5	2	0	1426				
2	6	0	1457				
5	3	0	1513				
4	5	0	1563				
3	6	0	1578				
0	7	0	1579				
1	7	0	1602				
6	0	0	1624				
5	4	0	1626				
6	1	0	1640				
2	7	0	1669				
6	2	0	1685				
4	6	0	1685				
4	6	0	1733				
6	3	0	1759				
5	5	0	1762				
3	7	0	1775				
0	8	0	1805				
1	8	0	1825				
6	4	0	1858				
2	8	0	1884				

flections from the back wall are not measured by the receiver microphone, due to the large amount of absorption material, as indicated by test results in Reference 5. Therefore, standing waves in this direction can be neglected. Cavity modes in the y and z direction, in a plane parallel to the speaker baffle, have a definite effect on the sound measured by the microphones. To explain which modes cause a pressure change at the location of the microphone, first the boundary conditions at the walls have to be considered. Since the walls are assumed rigid, the velocity of the air particles near any wall must be parallel to that wall; i.e., the normal component must be zero. For periodic wave motion, Equation (6) may be rewritten as

$$-\frac{\partial p}{\partial y} = \rho_o \frac{\partial v}{\partial t} = j\omega\rho_o v \tag{39}$$

and therefore

$$v = -\frac{1}{j\omega\rho_o}\frac{\partial p}{\partial y} \tag{40}$$

Application of the boundary conditions at y = 0 and z = 0, where the particle velocities v and w are zero, results in a maximum pressure or pressure antinodes at the wall surfaces. The source and receiver microphones are located in the center of a cross section of the acoustic test facility. All odd modes will have a nodal line across the center of this cross section and will therefore not be measured by one of the microphones. All even modes will have a pressure antinode at the source and receiver microphone location and will therefore cause a peak or a dip in the noise reduction curve. As the pressure is always measured as a positive component, an even mode at the source side of the test panel will cause a peak in the measured noise reduction, while an odd cavity mode will show a dip at that particular frequency.

Important panel modes for flat aluminum simply supported panels of different thicknesses under normal sound incidence are calculated and presented in Table 2.6. The edge conditions of the test panel do not allow a lateral displacement of the edges. No sound pressure will be radiated by the panel edges. The first odd-odd mode (fundamental resonance frequency $f_{1,1}$) will have a maximum displacement of the panel center. The pressure at the receiver side of the panel will be at a maximum, and subsequently the noise reduction will be minimal. A small arrow in Tables 2.6 and 2.7 indicates a dip in the noise reduction curve. An even-even mode produces two nodal lines crossing the center of the panel. Along these nodal lines the panel displacement will be zero and no pressure waves will be radiated. The microphone signal will thus be minimal, and a peak is shown in the noise reduction curve (indicated with an asterisk in Tables 2.6 and 2.7). Table 2.7 presents the most important panel modes for a .025" thick flat aluminum panel with simply supported edge conditions under an oblique angle of sound incidence. The angle of sound incidence will in general not affect the panel modes, as these are characteristics of the panel. The length of the panel, however, will change when another special test section is used ($= \ell_x \cos \theta$). The dimensions of the test panel will affect the modes and the frequency at which the modes occur

Resonance occurs when the frequency of the incident sound wave corresponds to a natural frequency of the panel. At this frequency very little energy is required to force the panel to vibrate, and the high amplitude of this vibration produces a correspondingly high sound pressure level on the opposite side of the panel A condition similar to resonance can occur when sound waves are incident on a panel at an

Table 2.6 Important Panel Modes for Flat Aluminum Simply Supported Panels of Different Thickness Under Normal Sound Incidence

$$f_{m,n} = \frac{\pi}{2}\left(\frac{Et^3}{12(1-\nu^2)M}\right)^{1/2}\left[\left(\frac{m}{\ell_x}\right)^2 + \left(\frac{n}{\ell_y}\right)^2\right] \qquad \text{(Ref 4)}$$

where E = 7 24*10^{10} N/m^2 Young's modulus

t = panel thickness [m]

ν = 33 Poisson's ratio

M = mass per unit area [kg/m^2]

m and n are panel mode numbers (1,2,3)

ℓ_x = 4572 m panel width

ℓ_y = 4572 m panel height

	t [inch] ⟶		016	025	032	040
	modal number		calculated frequency			
	m	n	$f_{m,n}$	$f_{m,n}$	$f_{m,n}$	$f_{m,n}$
→	1	1	9 7	15 1	19 3	24 2
	2	1	24 2	37 8	48.4	60 5
*	2	2	38 7	60 5	77 4	96 7
→	3	1	48 4	75 6	96 7	120 9
	3	2	62 9	98 2	125 7	157 2
	4	1	82 2	128 5	164 4	205 5
→	3	3	87 0	136 0	174 1	217 6
*	4	2	96 7	151 1	193 4	241 8
	4	3	120 9	188 9	241 8	302 3
→	5	1	125 7	196 5	251 5	314 3
	5	2	140 2	219 1	280 5	350 6
*	4	4	154 7	241 8	309 5	386 9
→	5	3	164 4	256 9	328 9	411 1
	6	1	178 9	279 6	357 9	447 3
*	6	2	193 4	302 3	386 9	483 6
	5	4	198 2	309 8	396 6	495 7
	6	3	217 6	340 0	435 2	544 1
→	5	5	241 8	377 8	483 6	604 5
→	7	1	241 8	377 8	483 6	604 5
*	6	4	251 5	392 9	503 0	628 6

Table 2 6 Important Panel Modes for Flat Aluminum Simply Supported Panels of Different Thickness Under Normal Sound Incidence (continued)

	t [inch] ⟶		016	024	032	040
	modal number			calculated frequency		
	m	n	$f_{m,n}$	$f_{m,n}$	$f_{m,n}$	$f_{m,n}$
	7	2	256 3	400 5	512 6	640 8
→	7	3	280 5	438 3	561 0	701 2
	6	5	295 0	460 9	590	737 5
	7	4	314 3	491 2	628.7	785 9
	8	1	314 3	491 2	628 7	785 9
*	8	2	328 8	513 8	657 7	822 1
*	6	6	348 2	544 1	696 4	870 5
	8	3	353 0	551 6	706 1	882 6
→	7	5	357 9	559 2	715 7	894 7
*	8	4	386 9	604 5	773 8	967 2
	7	6	411 1	642 3	822 1	1027 7
	8	5	430 4	672 5	860 8	1076 0
→	7	7	473 9	740 5	947 9	1184 8
*	8	6	483 6	755 6	967 2	1209 0
	8	7	546 5	853 9	1093 0	1366 2
*	8	8	619 0	962 2	1238 0	1547.5

→ denotes odd-odd modes

* denotes even-even modes

Table 2.7 Important Panel Modes for a .025" Thick Flat Aluminum Simply Supported Panel Under Oblique Angle of Sound Incidence

$$f_{m,n} = \frac{\pi}{2} \left(\frac{Et^3}{12(1-\nu^2)M}\right)^{1/2} \left[\left(\frac{m}{\ell_x}\right)^2 + \left(\frac{n}{\ell_y}\right)^2\right] \quad \text{(Ref 4)}$$

where $\ell_x = 4572 \cos\theta$ [m]

where ℓ_x = panel width [m]

θ = angle of sound incidence [degrees]

For the other parameters, refer to Table 2 6

	θ [degrees] ⟶		15	30	40	60
	modal number		calculated frequency $f_{m,n}$			
	m	n				
→	1	1	15 7	17 6	20 4	37 8
*	0	2	30 2	30 2	30 2	30 2
	1	2	38 3	40 3	43 1	60 5
	2	1	40 0	47 9	59 1	128 5
*	2	2	62 6	70 5	91 7	151 1
→	1	3	76 1	78 1	80 9	98 2
→	3	1	80 4	98 2	123 4	279 6
	2	3	100 4	108 3	119 5	188 9
	3	2	103 1	120 9	146 1	302 3
	1	4	129 0	131 0	133 8	151 1
	4	1	137 1	168 8	312 6	491 2
→	3	3	140 9	158 9	183 9	340 0
*	2	4	153 3	161 2	172 4	241 8
*	4	2	159 8	191 4	236 3	513 8
	3	4	193 8	211 6	236 8	392 9
→	1	5	197 0	199 0	201 8	219 1
	4	3	197 6	229 2	274 0	551 6
→	5	1	210 0	259 4	329 5	763 2
	2	5	221 3	229 2	240 4	309 8
	5	2	232 7	282 1	352 1	785 9
*	4	4	250 5	28 1	326 9	604 5
→	3	5	261 8	279 6	304 8	460 9
→	5	3	270 5	319 9	389 9	823 6

Table 2.7 Important Panel Modes for a .025" Thick Flat Aluminum Simply Supported Panel Under Oblique Angle of Sound Incidence (continued)

	θ [degrees] ⟶		15	30	40	60
	modal number		calculated frequency $f_{m,n}$			
	m	n				
	1	6	280 1	282 1	284 9	302 3
	6	1	299 1	370 3	471 1	1095 7
*	2	6	304 4	312 3	323 5	392 9
	4	5	318 5	350 1	394 9	672 5
*	6	4	321 8	392 9	493 8	1118 3
	5	4	323 4	372 8	442 8	876 5
	3	6	344 9	362.7	387 9	544 1
	6	3	359 6	430 7	531 6	1156 1
→	5	5	391 4	440 8	510 8	944 5
*	4	6	401 6	433 2	478 1	755 6
*	6	4	412 5	483 6	584 5	1209 0
	5	6	474 5	523 9	593 9	1027 7
	6	5	480 5	551 6	625 5	1277 0
*	6	6	563 6	634 7	735 6	1360 2

→ denotes odd-odd modes

* denotes even-even modes

oblique angle. At certain frequencies the phases of the incident wave will coincide with the phase of the panel's flexural waves (Figure 2.20).

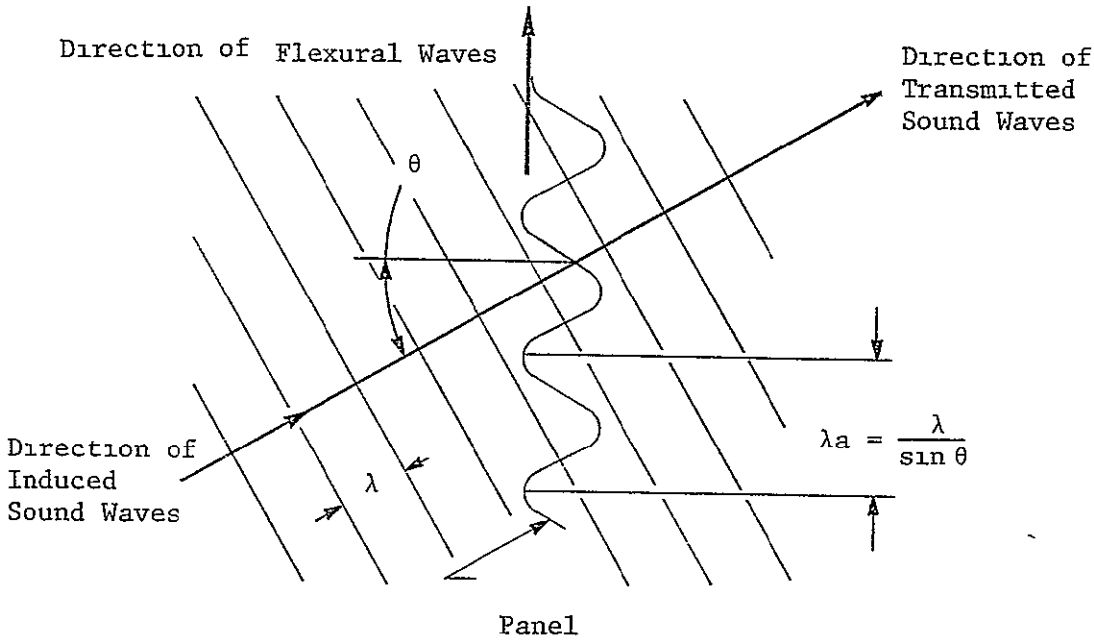

Figure 2.20 Coincidence of Incidence Wave and Flexural Wave in a Panel

If the wavelength of the sound in air is λ and the wave impinges on the panel at an angle θ, then when $\lambda/\sin\theta$ is equal to the wavelength of the flexural wave, the intensity of the transmitted wave approaches that of the incident wave. Wave coincidence can only occur at a frequency which is determined by the material and thickness of the panel. When the coincidence effect occurs, the noise reduction for the panel is greatly reduced. The critical frequency is the lowest frequency at which the coincidence effect can occur. At this frequency the coincidence angle is 90°; that is, the sound wave is traveling parallel to the surface of the panel Below this frequency, the wavelength in air is greater than the bending wavelength in the panel. Table 2.8 presents the critical frequencies of infinite aluminum panels of 5 different thicknesses.

Table 2.8 Critical Frequencies of Different Infinite Aluminum Panels

$$f_c = \frac{c}{2\pi}\sqrt{\frac{M*12(1-\nu^3)}{Et^3}}$$

where f_c = critical frequency [Hz]

c = 343.8 m/s (speed of sound)

E = $7.24*10^{10}$ N/m^2 (Young's modulus)

t = panel thickness [m]

ν = .33 Poisson's ratio

M = mass per unit area [kg/m^2]

Thickness t:	Critical frequency f_c:
.016	30340
.020	24272
.025	19417
.032	15170
.040	12136

The identification of the coupled panel cavity resonance frequencies and the separate panel and cavity modes in the experimental results will be done in a separate study under the same NASA contract. Table 2.9 gives some of the major cavity modes for each of the special test sections, as found in the test results:

Table 2.9 Some Important Experimental Cavity Modes for Each of the Special Test Sections

	frequency at which major dips occur* (Hz)			
15°-test section	352	660	1020	
30°-test section	340	490	1020	2000
40°-test section	900	1050	2600	3100
60°-test section	1800	2600	3100	

* All values are approximations.

Comparing the results from Figure 2 4 through Figure 2.19, it appears that increasing the angle of sound incidence results in a lower noise reduction. As opposed to tests under normal angle of sound incidence, hardly any stiffness region is perceptible because of a major shift of the resonance frequency to lower frequencies. As an example, the resonance frequency of 63 Hz for a panel under normal sound incidence dropped to 33 Hz for a panel under an oblique angle of incidence. This is mainly due to the edge conditions of the test panel and the change in source and receiver cavities. (To determine the fundamental panel/cavity resonance frequency under normal sound incidence, neither the extension tube nor one of the special test sections was used.)

Conclusions·

· The theoretical predictions for the noise reduction of panels under an oblique angle of sound incidence follow the experimental results reasonably well.

· Increasing the angle of sound incidence results in a lower noise reduction over the whole frequency region.

· Only even cavity modes will have a pressure antinode of the location of one of the microphones. An even mode at the source side of the panel will cause a peak in the measured noise reduction, while an even cavity mode at the panel's receiver side will cause a noise reduction dip at that frequency.

· An even-even panel mode causes a peak in the noise reduction curve, while the odd-odd panel modes are responsible for the major dips in the noise reduction curve.

• At the critical frequency the coincidence effect will occur and decrease the noise reduction notably. This frequency is located in the higher frequencies, out of the range of interest.

CHAPTER 3

DESIGN AND CONSTRUCTION OF SPECIAL TEST DEVICES

Special test devices are designed and constructed to study the effect of curvature, angle of sound incidence and bonded or riveted edge conditions.

3.1 Introduction

To obtain a plane wave approximation at the panel's surface, the distance from the speakers to the test panel has to be large compared to the width of the panel. To achieve this, a 30.5"-long extension tube was used for the tests. The fiberglass that had been attached to the walls of the extension tube was covered by 3/4" inner walls, made out of particle board. This provided an 18 x 18 inch path for the sound to travel without being absorbed by the fiberglass material. This ensures that the sound level at the receiver side of the test panel will be high enough to be measured by the microphone and analyzed by the real time analyzer. To investigate the effect of curvature, angle of sound incidence and edge conditions for different panel thicknesses, only one parameter was changed at a time, so that only its effect would be indicated by the test results. Table 3.1 gives a summary of all the tests done to study the parameters mentioned above.

3.2 Design Considerations for Special Test Devices

Four special devices were designed and constructed·

1. one to test flat panels

Table 3.1 Summary of Curved and Inclined Panels Used on Special Test Mountings in Noise Reduction Tests

Thickness	Material	Bonded (B) Riveted (R)	Radius of Curvature	Angle of Inclination	Panel Number
.016"	Al	B	R= 10"	-	#206
.016"	Al	R	R= 10"	-	#207
.016"	Al	B	R= 20"	-	#208
.016"	Al	R	R= 20"	-	#209
.016"	Al	B	-	0^{o}	#210
.016"	Al	R	-	0^{o}	#211
.016"	Al	B	-	60^{o}	#212
.016"	Al	R	-	60^{o}	#213
.020"	Al	B	R= 10"	-	#214
.020"	Al	R	R= 10"	-	#215
.020"	Al	B	R= 20"	-	#216
.020"	Al	R	R= 20"	-	#217
.020"	Al	B	-	0^{o}	#218
.020"	Al	R	-	0^{o}	#219
.020"	Al	B	-	60^{o}	#220
.020"	Al	R	-	60^{o}	#221
.032"	Al	B	R= 10"	-	#222
.032"	Al	R	R= 10"	-	#223
.032"	Al	B	R= 20"	-	#224
.032"	Al	R	R= 20"	-	#225
.032"	Al	B	-	0^{o}	#226
.032"	Al	R	-	0^{o}	#227
.032"	Al	B	-	60^{o}	#228
.032"	Al	R	-	60^{o}	#229

2. one to test flat panels with a 60° sound incidence*

3. one to test curved panels with a radius of 10 inches

4. one to test curved panels with a radius of 20 inches

In all configurations, panels with bonded as well as riveted edge conditions were tested. To obtain these edge conditions, the panels were attached to aluminum strips by bonding or riveting. These aluminum strips were clamped to the special test device by a one-inch-wide steel strap and screws, evenly spaced along each side To maximize sound insulation and prevent structural vibration, strips of ducting tape were placed between the aluminum strips and the edges of the special test devices. The same ducting tape was also applied between the aluminum strips and the steel straps for the same reasons. Design drawings of the four special test devices 1 to 4 are depicted in Figures 3 1 to 3.4 respectively. To install these special test devices between the extension tube and the Beranek tube, an adapter was designed and constructed; it is shown in Figure 3.5. The four holes shown on the plan view match up with the four studs shown in each of the special test device illustrations (Figures 3.1 to 3 4). Figure 3.6 shows the special test device for curved panels installed in the acoustic test facility. Figure 3.7 illustrates the way the 10-inch-radius curved panel is attached to the aluminum strips. To compare the test results for the various configurations, major parameters were kept constant.

---

* The angle of sound incidence is here defined as the angle between the direction of the sound and the plane of the panel.

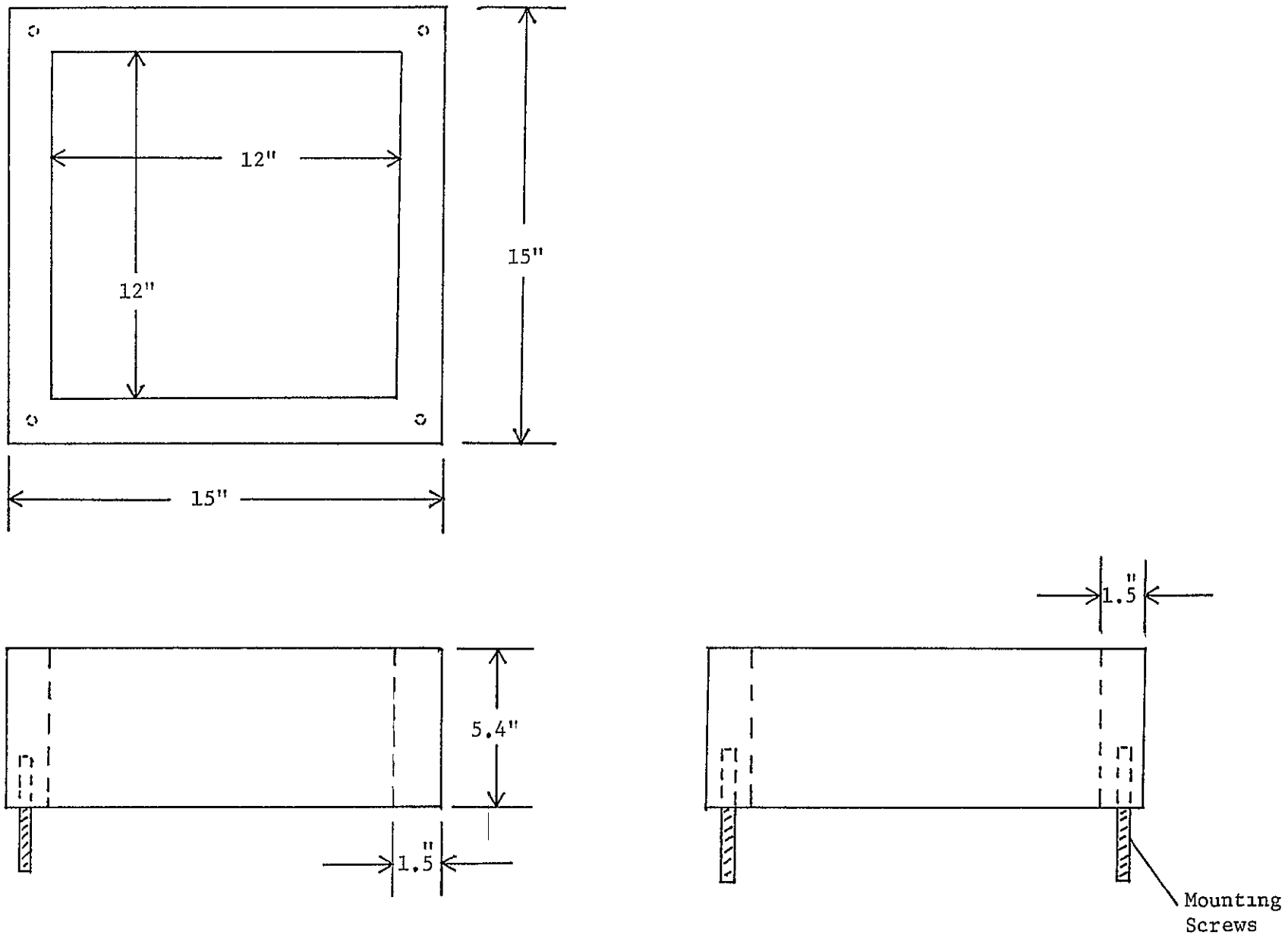

Figure 3 1 3-View of Special Test Mounting Used for a Panel Under Normal Sound Incidence

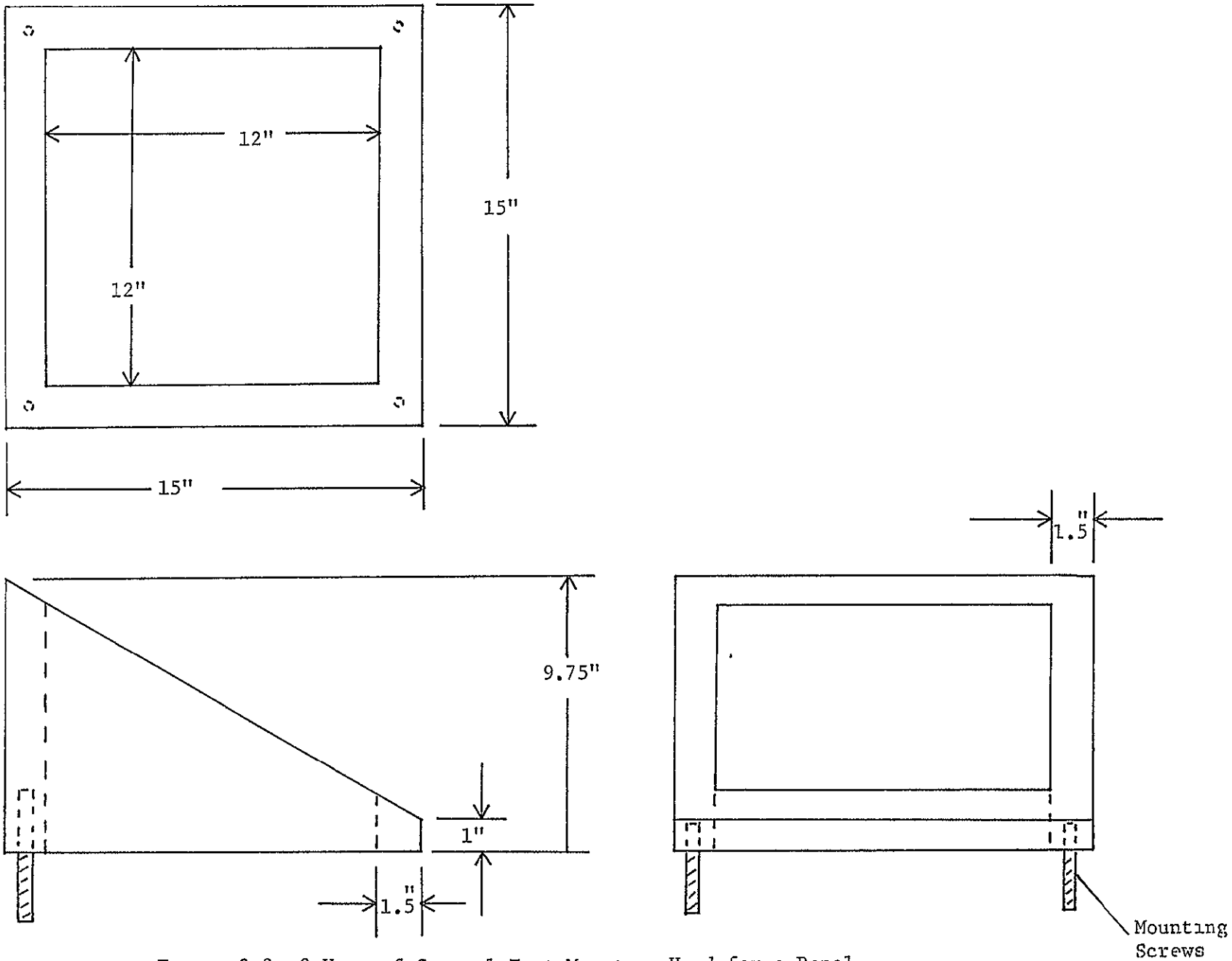

Figure 3.2 3-View of Special Test Mounting Used for a Panel Under 60° Angle of Sound Incidence

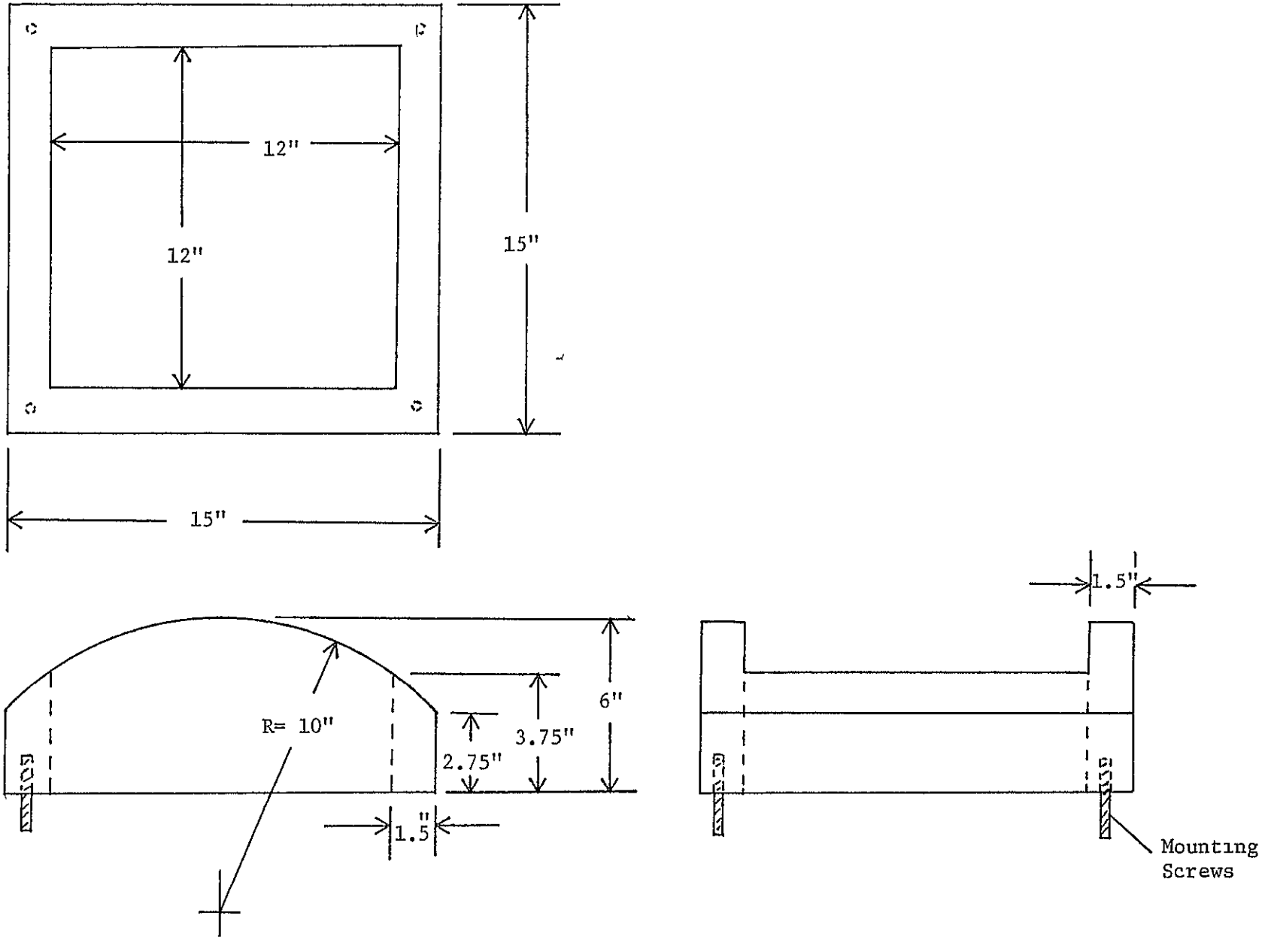

Figure 3.3 3-View of Special Test Mounting Used for a Curved Panel with a 10" Radius

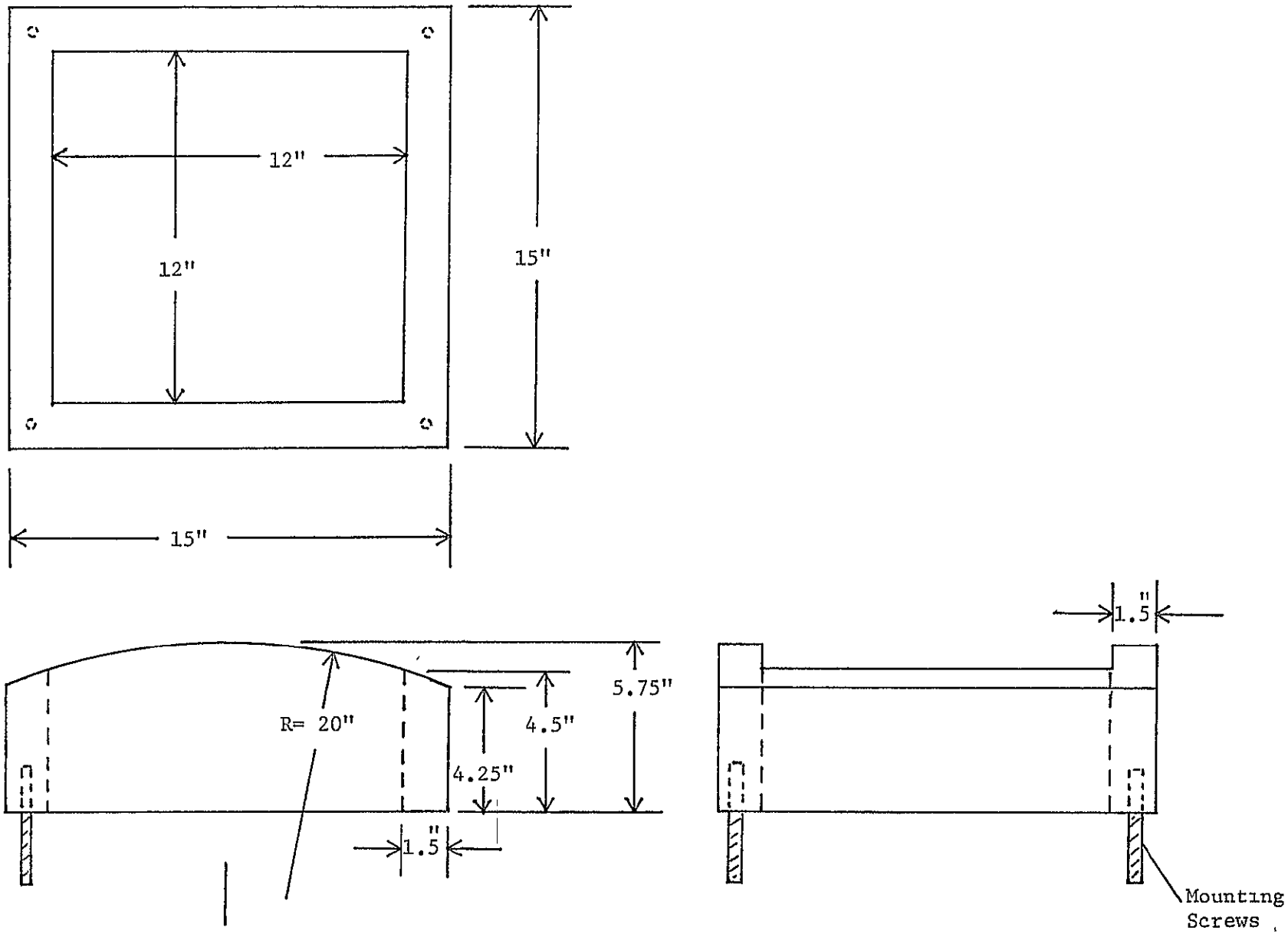

Figure 3 4 3-View of Special Test Mounting Used for a Curved Panel with a 20" Radius

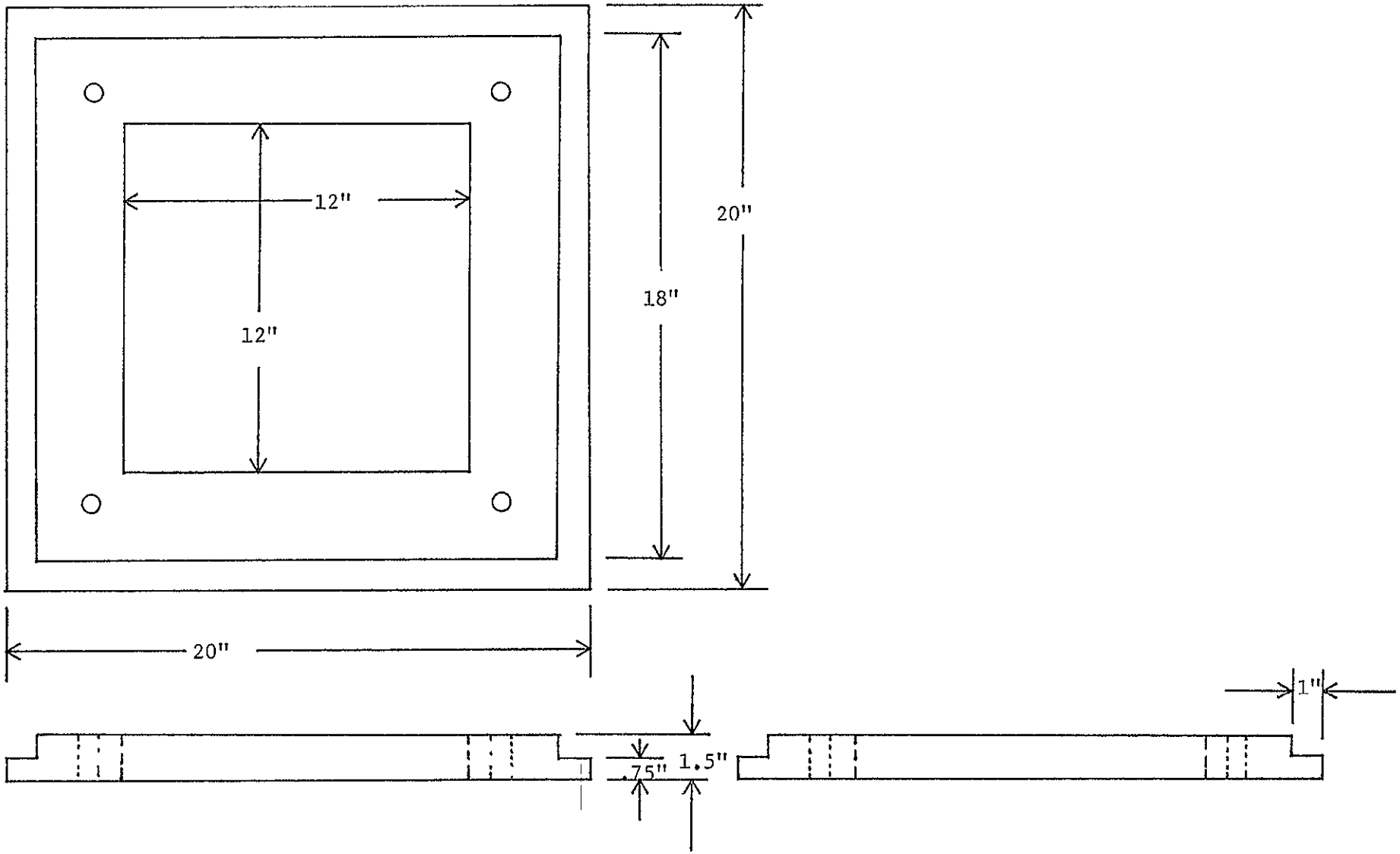

Figure 3 5 3-View of Adapter Used for Installing Special Test Mountings

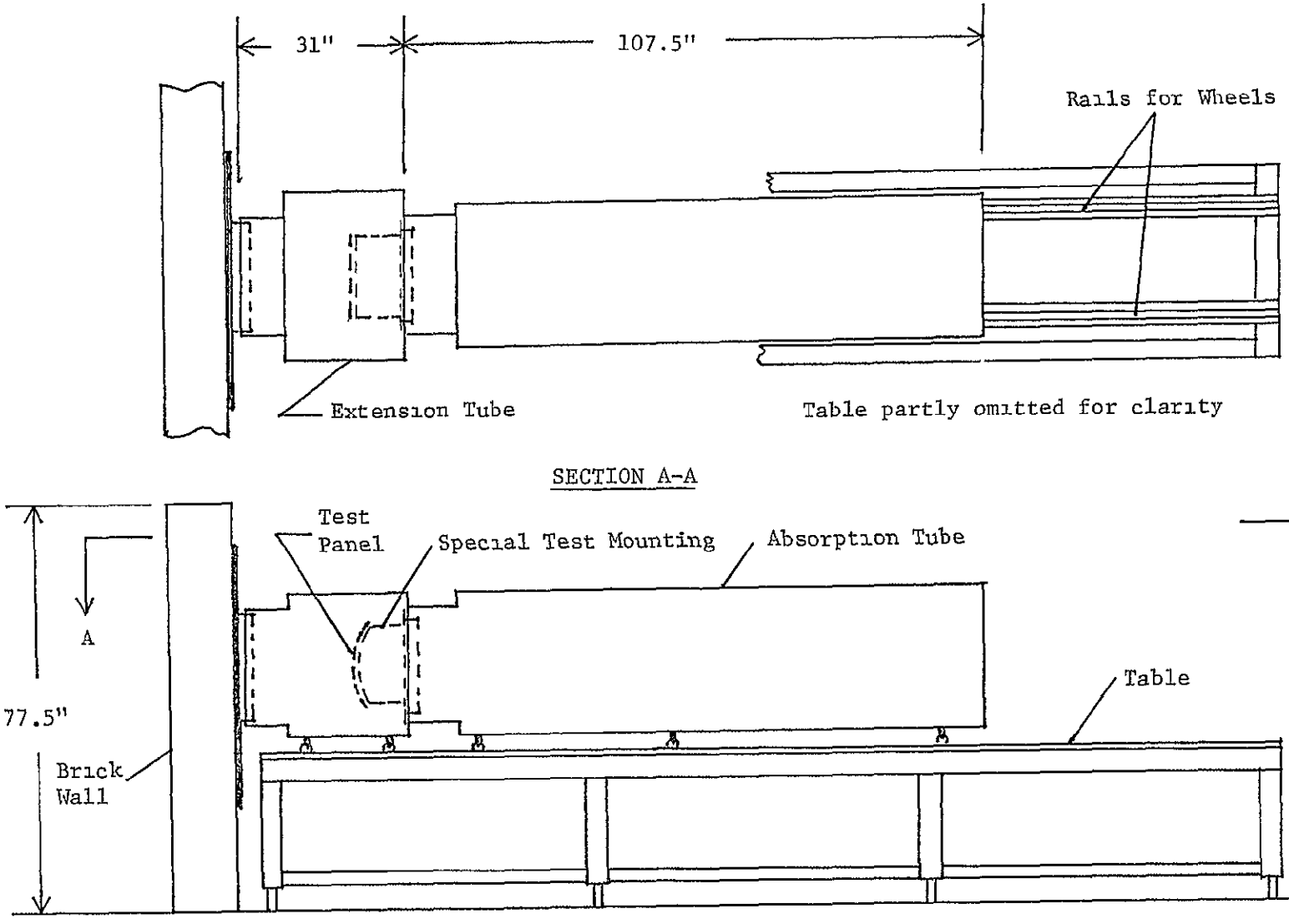

Figure 3.6 KU-FRL Acoustic Test Facility Showing Placement of Special Test Mountings

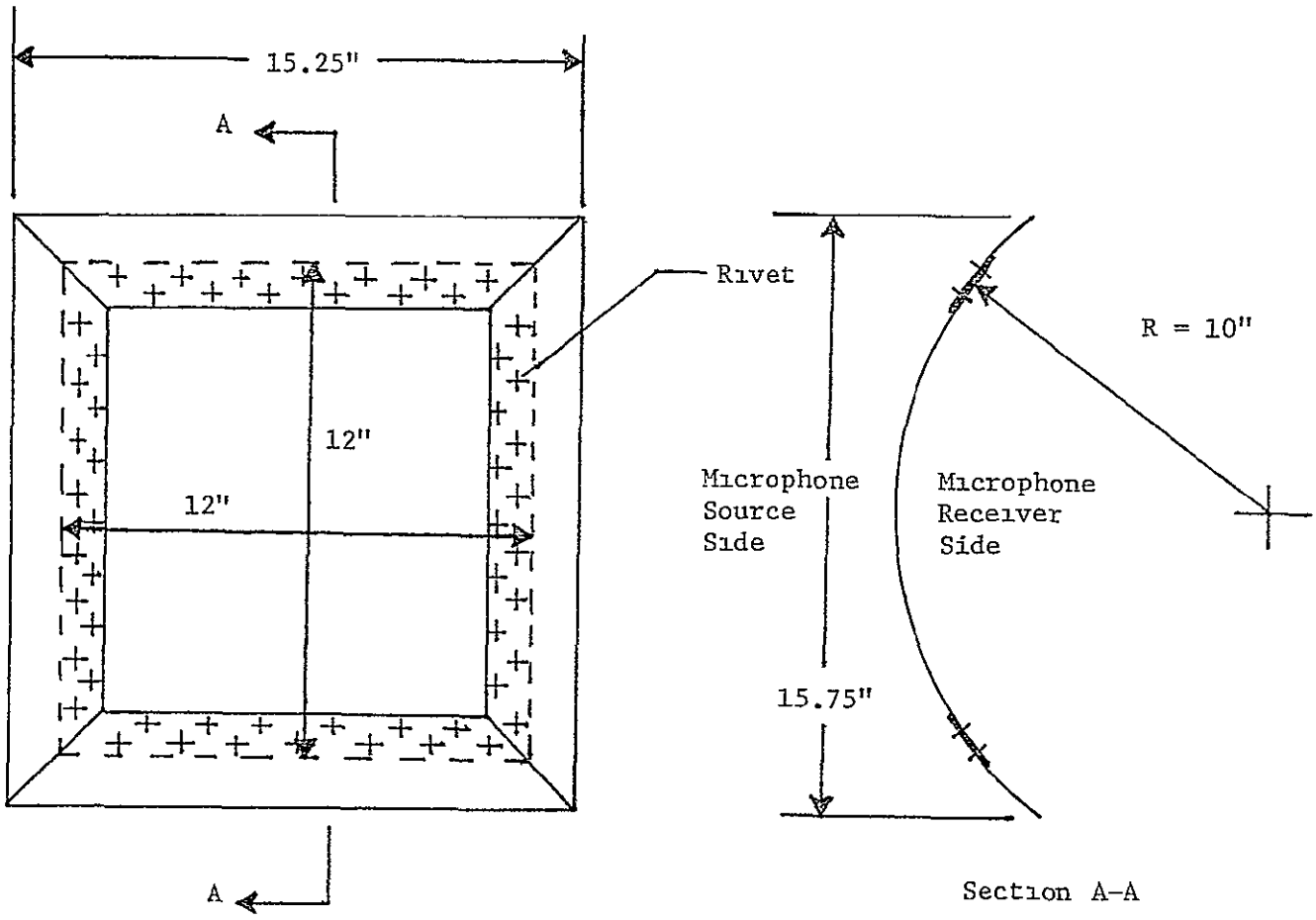

Figure 3 7: The 10" Radius Curved Panel Attached to Four Aluminum Strips

1. distances to the microphones

A source and a receiver microphone on both sides of the test panel are used for each noise reduction test. The distances from the centroid of the test panel to these microphones were kept constant, whether the test panel was curved, flat or under an oblique angle of sound incidence. The distance from centroid to source microphone is 2.25 inches, while the corresponding distance to the receiver microphone is 14.50 inches. The receiver microphone is located at a fixed position in the Beranek Tube. The source microphone is mounted on a stand in the extension tube. It is located closer to the panel's surface to avoid the possibility of its measuring reflections that are not incident on the test panel or reflected by the panel.

2. cavity volumes

The special test devices are designed such that the cavity volume behind each panel is the same. It is realized that the same cavity volume does not necessarily mean the same cavity effect on the behavior of the panel But because these cavities have no back panel (they are backed by the Beranek Tube), the assumption of the same cavity effect can be justified. The cavity volume for each special test device is 717 $inch^3$.

3. sound passage cross-sectional area

The interior dimensions of all four special test devices

were 12 inches by 12 inches, making a cross sectional area of 144 $inch^2$.

CHAPTER 4

EFFECT OF CURVATURE AND RIVETED OR BONDED EDGE CONDITIONS ON THE NOISE REDUCTION OF AN ALUMINUM PANEL

A comparison of the test results for riveted and bonded edge conditions of flat and curved panels is given in the first section of this chapter. In the second section a theoretical analysis is presented to predict the effect of curvature for an aluminum panel. This prediction then is compared to the experimental results. The results are discussed for the stiffness-controlled region and mass-controlled region that are defined in the introduction.

4.1 Effect of Riveted or Bonded Edge Conditions

The effect of realistic edge conditions will be discussed for flat and curved panels respectively. All considerations are based on experimental results obtained in the KU-FRL acoustic test facility, using special test devices (Chapter 3). The exposed part of the panel has a projected area of 12 x 12 inches in all cases.

4.1.1 Flat Panels

Stiffness-controlled region

Test results have been obtained for bonded and riveted edge conditions by testing flat aluminum panels of three thicknesses. These experimental results are depicted in Figures 4.1 through 4.6. Riveting thin aluminum panels applies stresses to the panels, which give the panel more resistance to deflections. Therefore, in the stiffness-controlled frequency region, a slightly better noise reduction occurs for the riveted aluminum panels than for the bonded

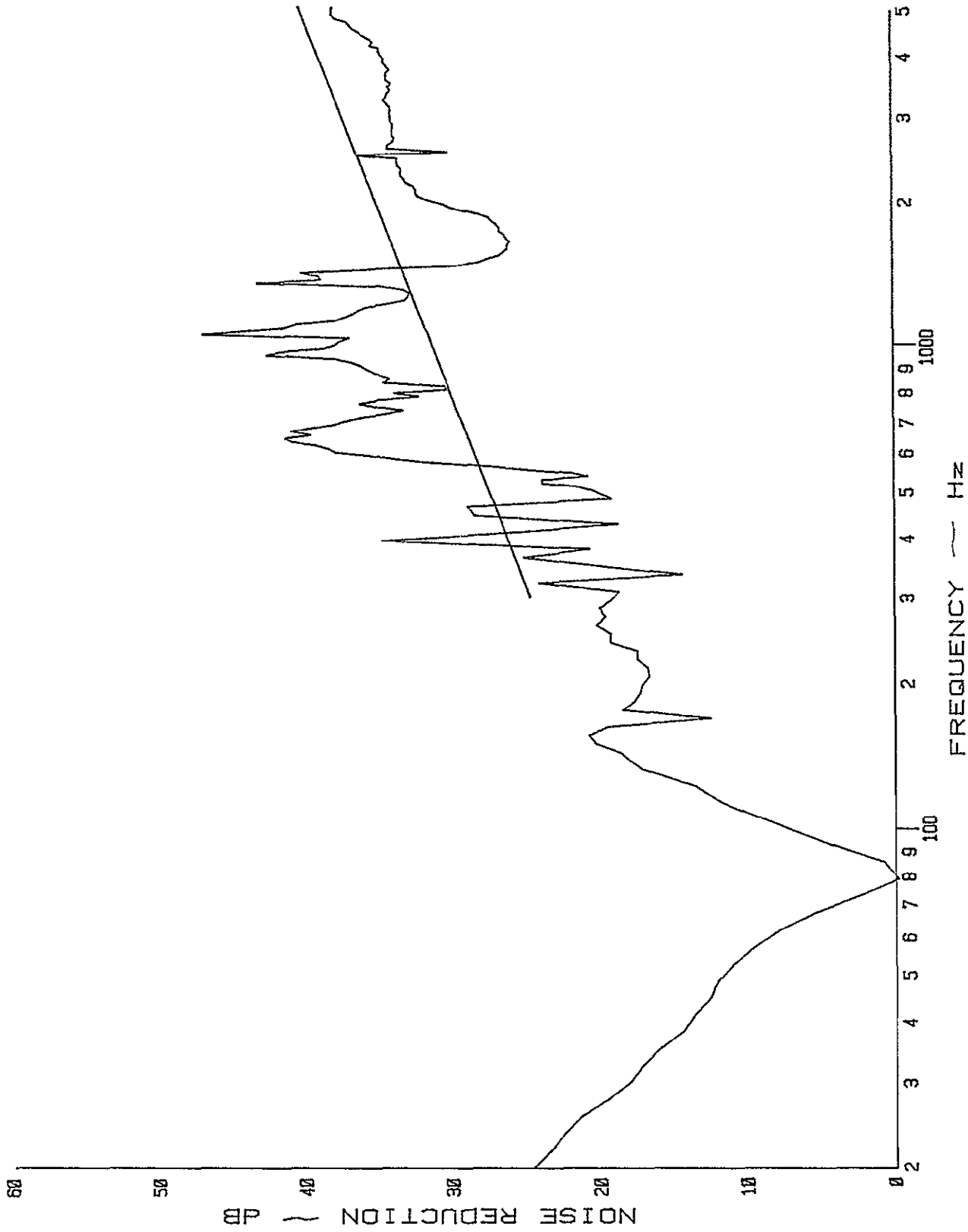

Figure 4.1. Noise Reduction Characteristics of a .016 Inch Thick Flat Aluminum Panel with Riveted Edge Conditions.

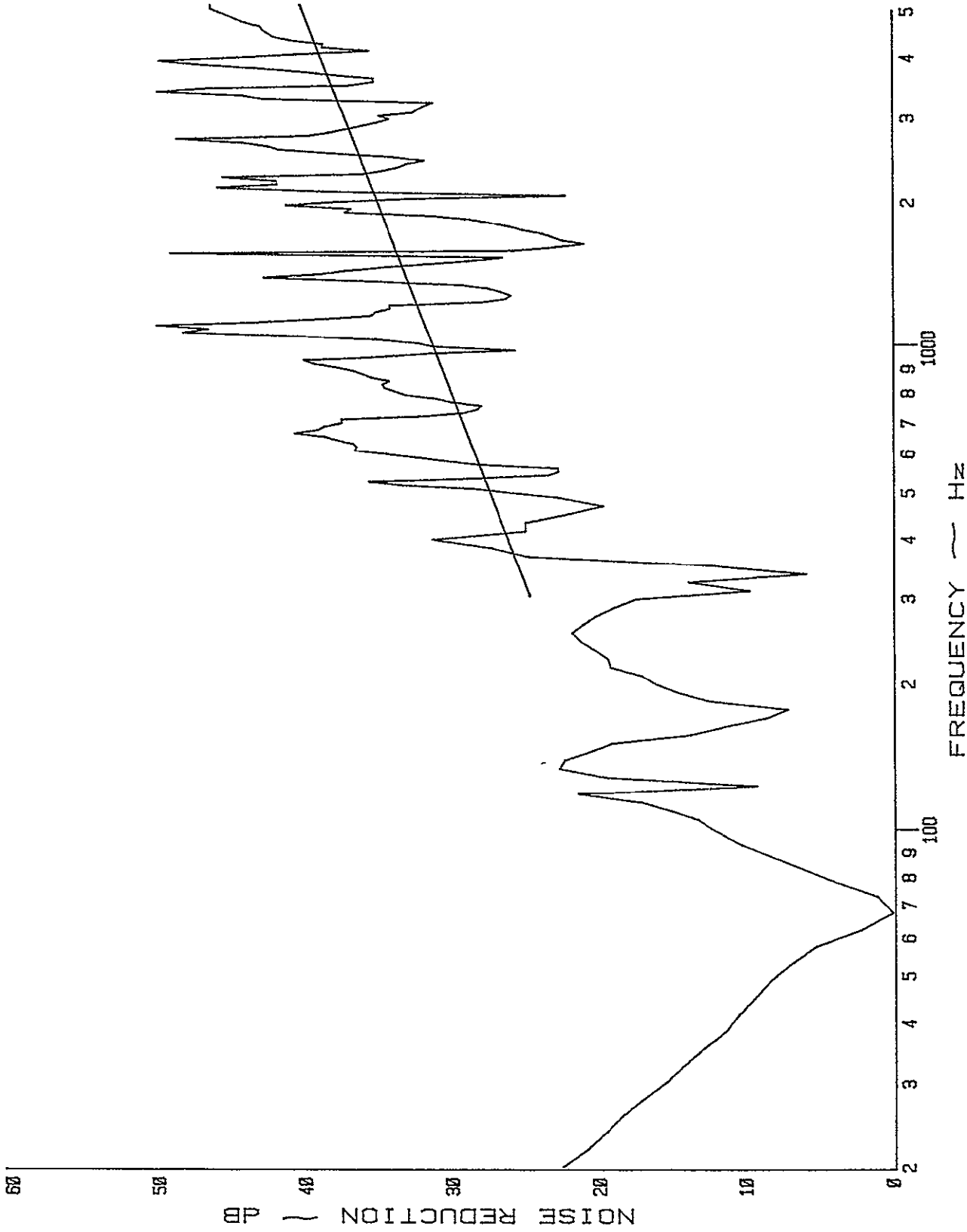

Figure 4.2 Noise Reduction Characteristics of a .016 Inch Thick Flat Aluminum Panel with Bonded Edge Conditions.

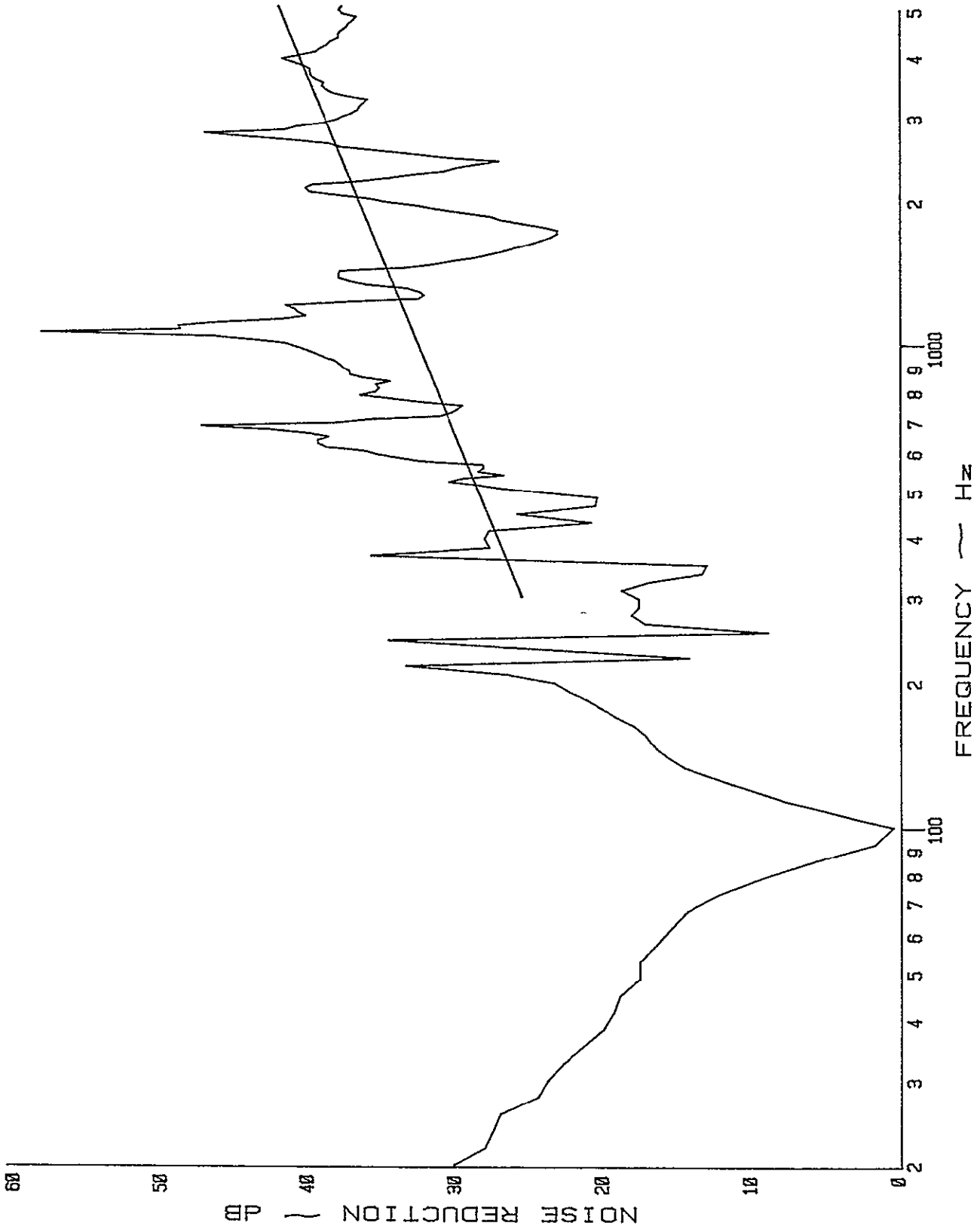

Figure 4.3. Noise Reduction Characteristics of a .020 Inch Thick Flat Aluminum Panel with Riveted Edge Conditions.

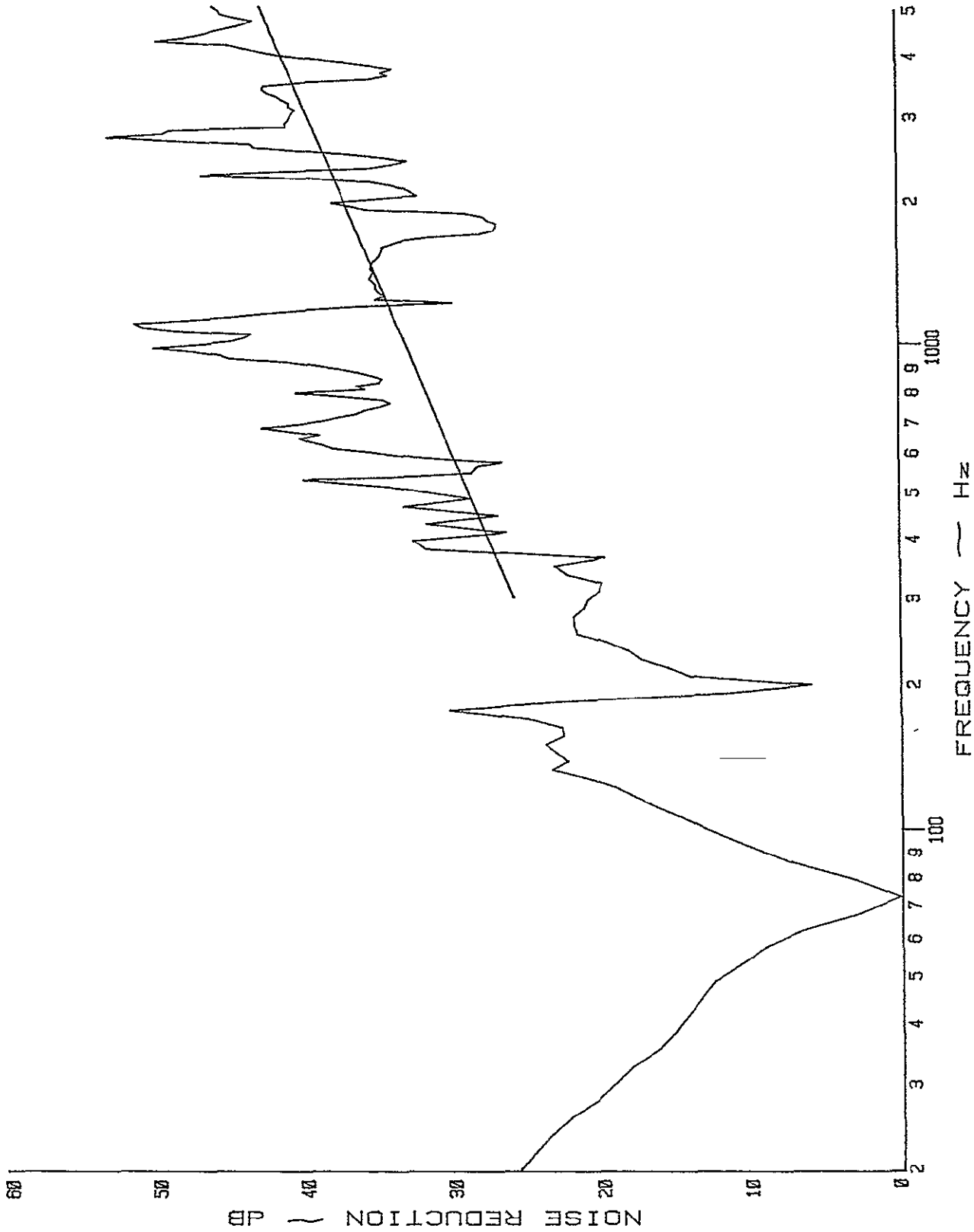

Figure 4.4 Noise Reduction Characteristics of a .020 Inch Thick Flat Aluminum Panel with Bonded Edge Conditions.

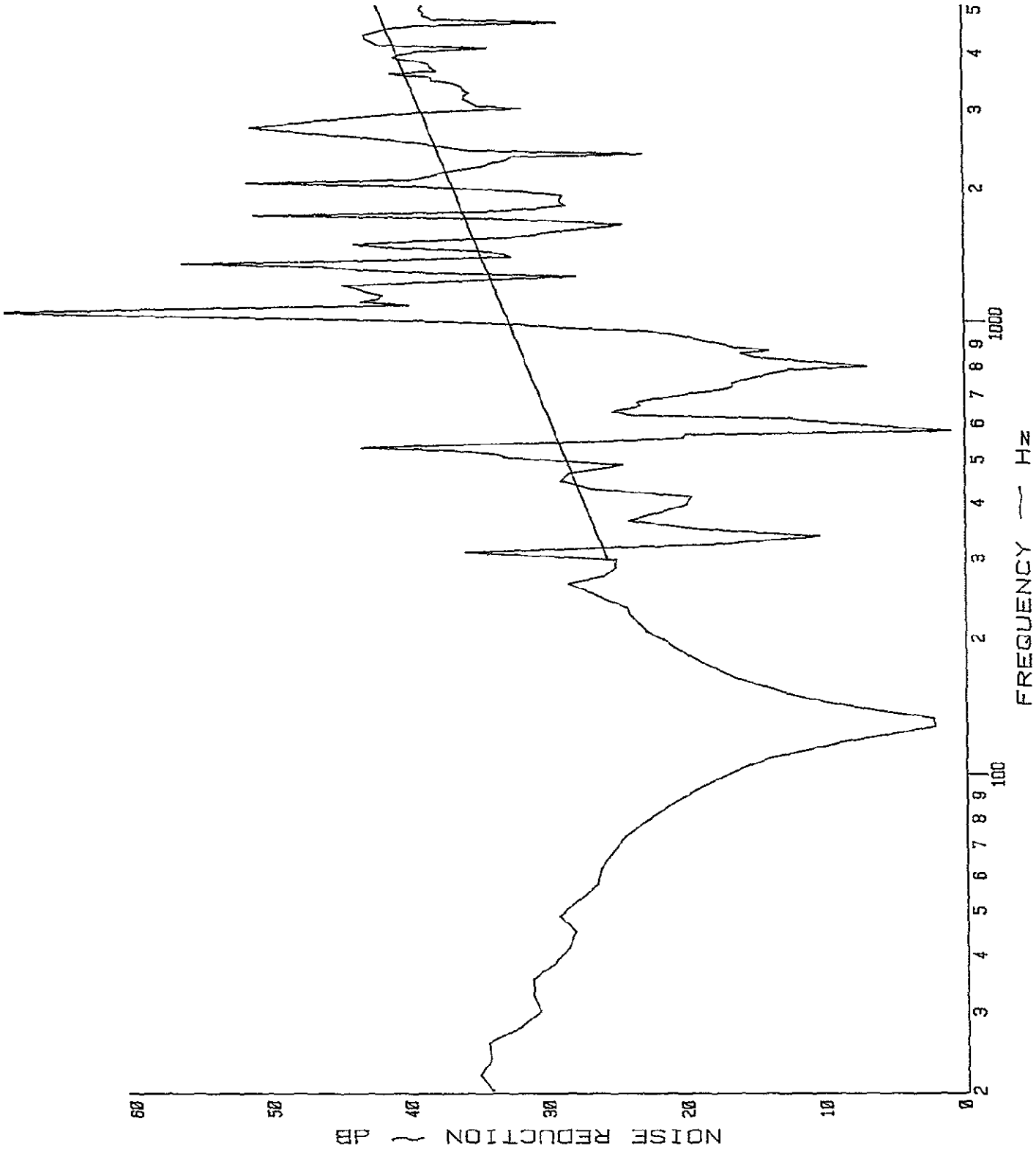

Figure 4.5. Noise Reduction Characteristics of a .032 Inch Thick Flat Aluminum Panel with Riveted Edge Conditions.

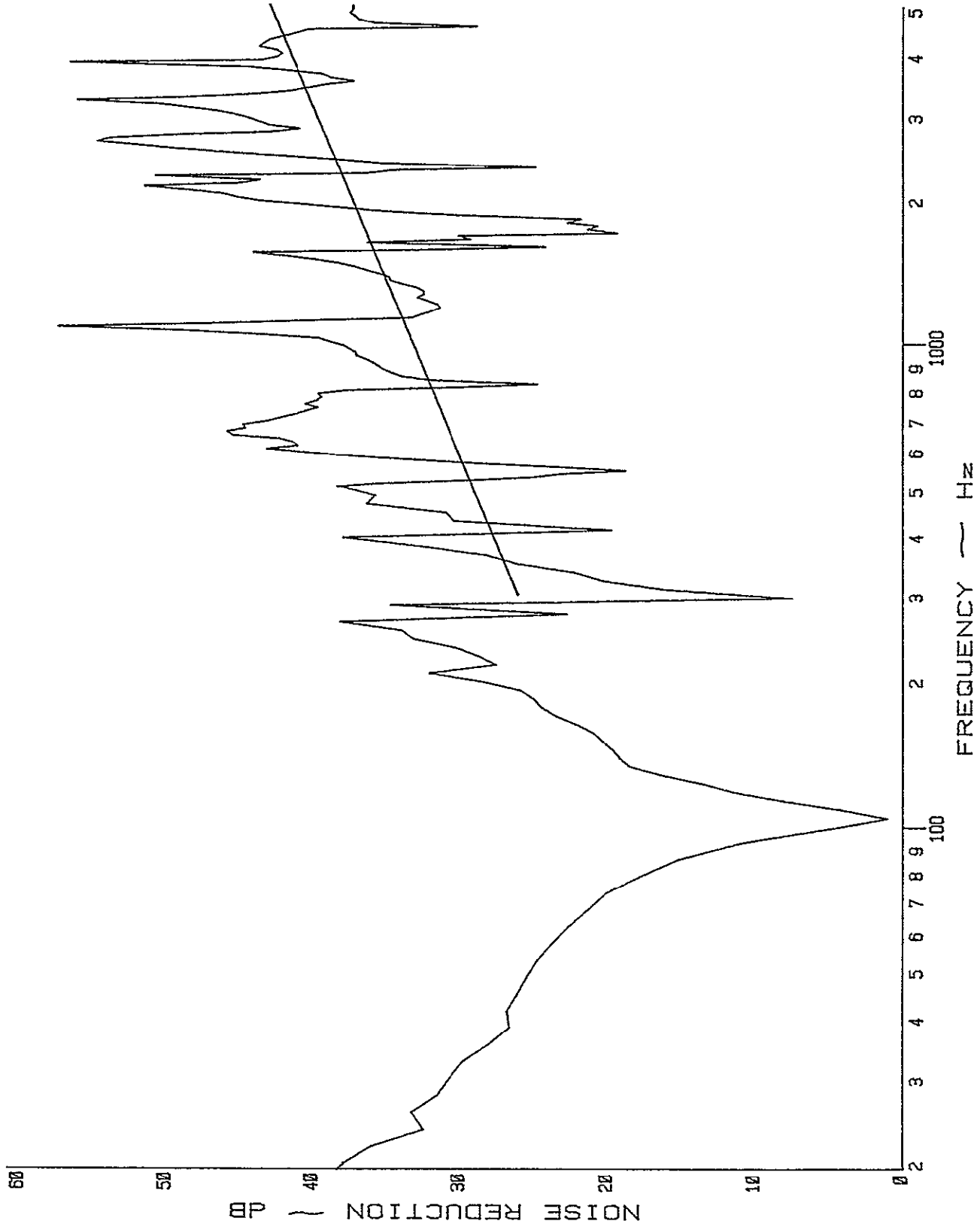

Figure 4 6. Noise Reduction Characteristics of a .032 Inch Thick Flat Aluminum Panel with Bonded Edge Conditions.

aluminum panels. The increase in noise reduction, due to riveting, ranges from 2 dB to 4 dB.

Mass-Controlled Region

To be able to compare the experimental results in the mass-controlled region, the least squares line of the noise reduction in this region has been computed and drawn in the graphs. The total mass of a riveted panel and that of a bonded panel of the same nominal thickness are approximately the same. For this reason there is no difference in noise reduction between the bonded and the riveted panels. Because the noise reduction for the riveted panels does not change in the mass-controlled region, but increases in the stiffness-controlled region, the fundamental panel/cavity resonance frequency shifts to a higher value for these panels (Figure 1.1).

Conclusions

· The noise reduction in the stiffness-controlled region is higher for riveted panels than for bonded panels, due to the panel stresses caused by the riveting process.

· The noise reduction of riveted panels matches the noise reduction of the bonded panels in the mass-controlled region, because the total mass of both panel types is the same.

· The fundamental panel/cavity resonance frequency will be experienced at a higher frequency for the riveted panels than for the bonded panels.

4.1.2 Curved Panels

The effect of realistic edge conditions of curved panels can be determined by analyzing Figure 4.7 through Figure 4.18. Bonded and riveted panels with a thickness of .016", .020" and .032" and a curvature radius of respectively 20" and 10" have been tested. The frequency region 20-5000 Hz will be divided into two regions of interest:

- low-frequency region $f < 500$ Hz
- high-frequency region $f > 500$ Hz

The first major dip in noise reduction (located around 150 Hz) is not represented by the first panel mode as in the case of a flat panel. The first panel/cavity mode, at which the largest deflections occur, originates at the so-called ring frequency (Refer to definition in Section 4.2). It seems that the low-frequency region is stiffness controlled, while the high-frequency region is related to the mass of the panel.

Low-Frequency Region

Curvature adds stiffness to the panel, as will be discussed in the second section of this chapter. Flat panels are affected by the riveting procedure, which also adds stiffness to the panel. As the additional stiffness caused by curving the panel is dominant, the edge conditions become important, being boundary conditons for a vibrating panel. The adhesive, used to bond the panels, is applied along the four edges of the panel and creates continuously fixed edge conditions. The riveted panels, however, will have crevices in the space between the rivets, where the panel will have free boundary

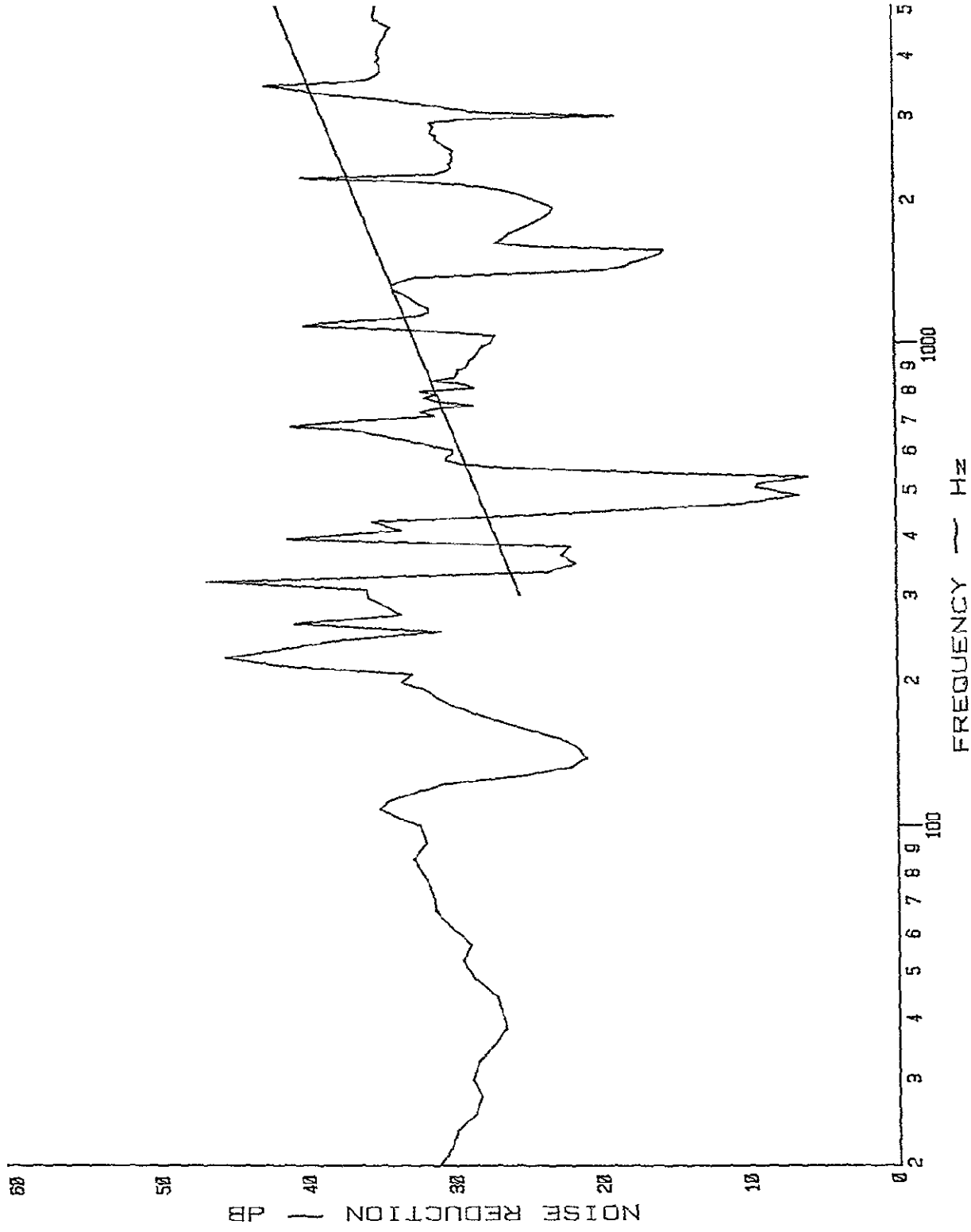

Figure 4.7 Noise Reduction Characteristics of a .016 Inch Thick Curved Aluminum Panel with a Curvature Radius of 20 Inches and Riveted Edge Conditions.

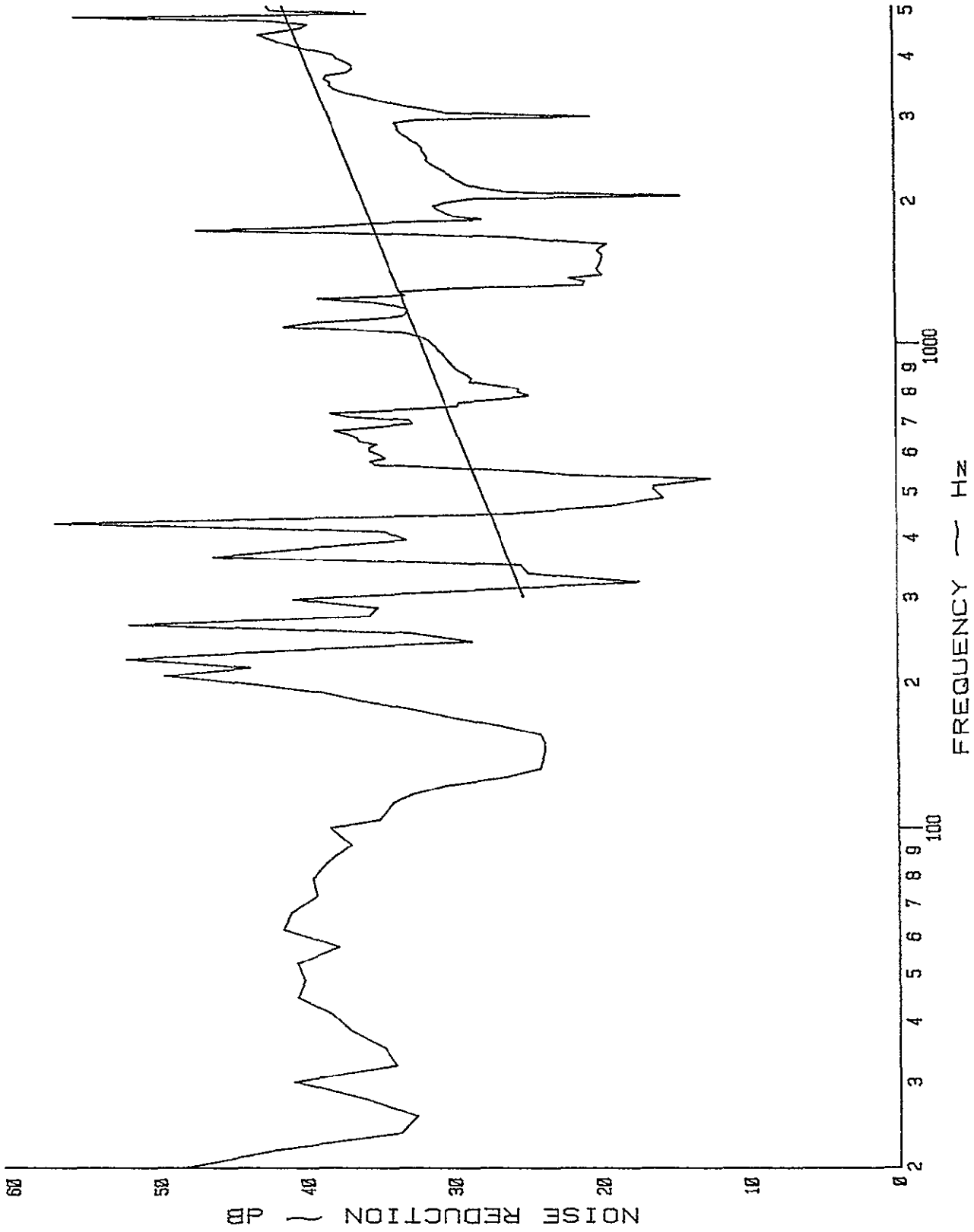

Figure 4.8 Noise Reduction Characteristics of a .016 Inch Thick Curved Aluminum Panel with a Curvature Radius of 20 Inches and Bonded Edge Conditions.

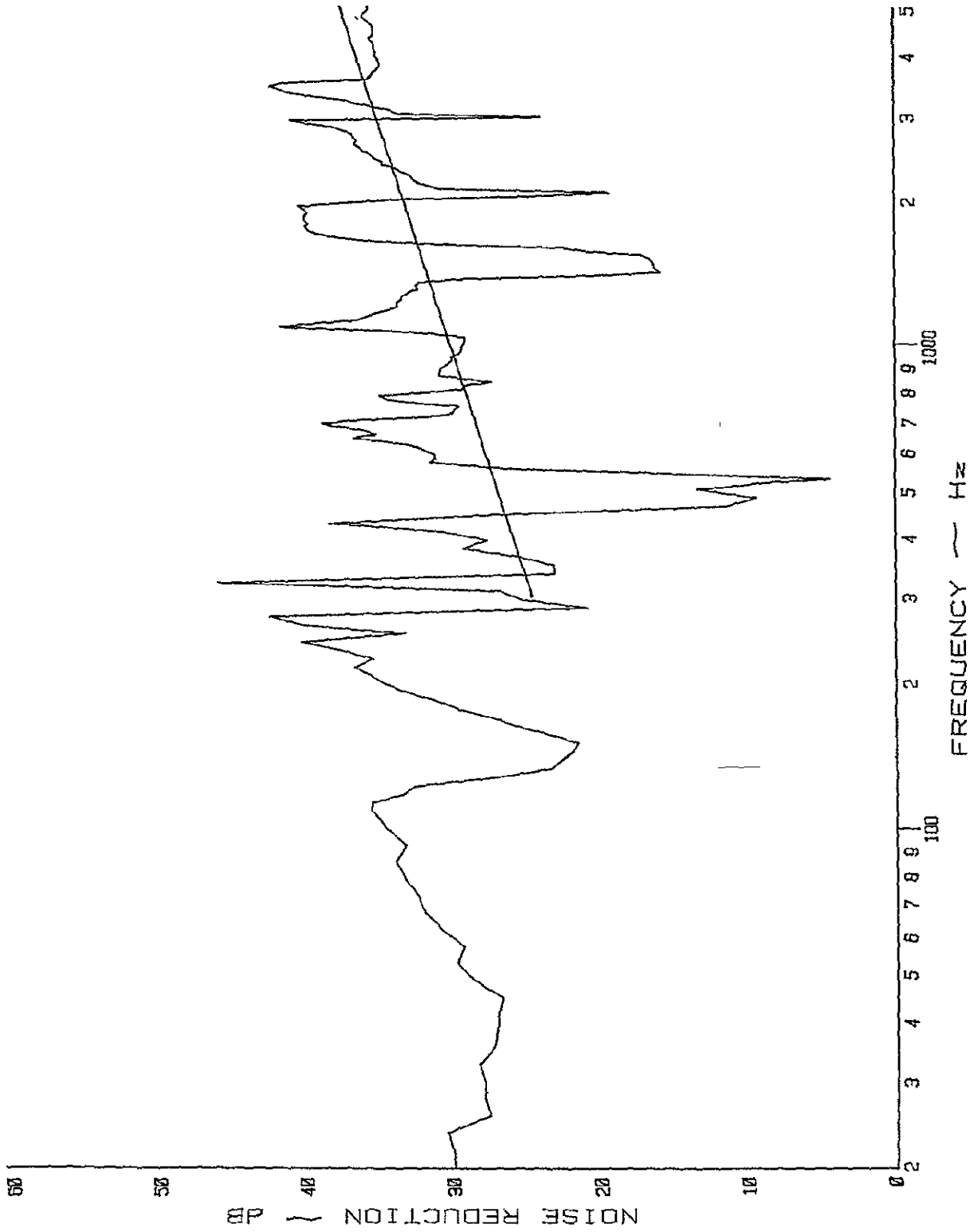

Figure 4.9. Noise Reduction Characteristics of a .020 Inch Thick Curved Aluminum Panel with a Curvature Radius of 20 Inches and Riveted Edge Conditions.

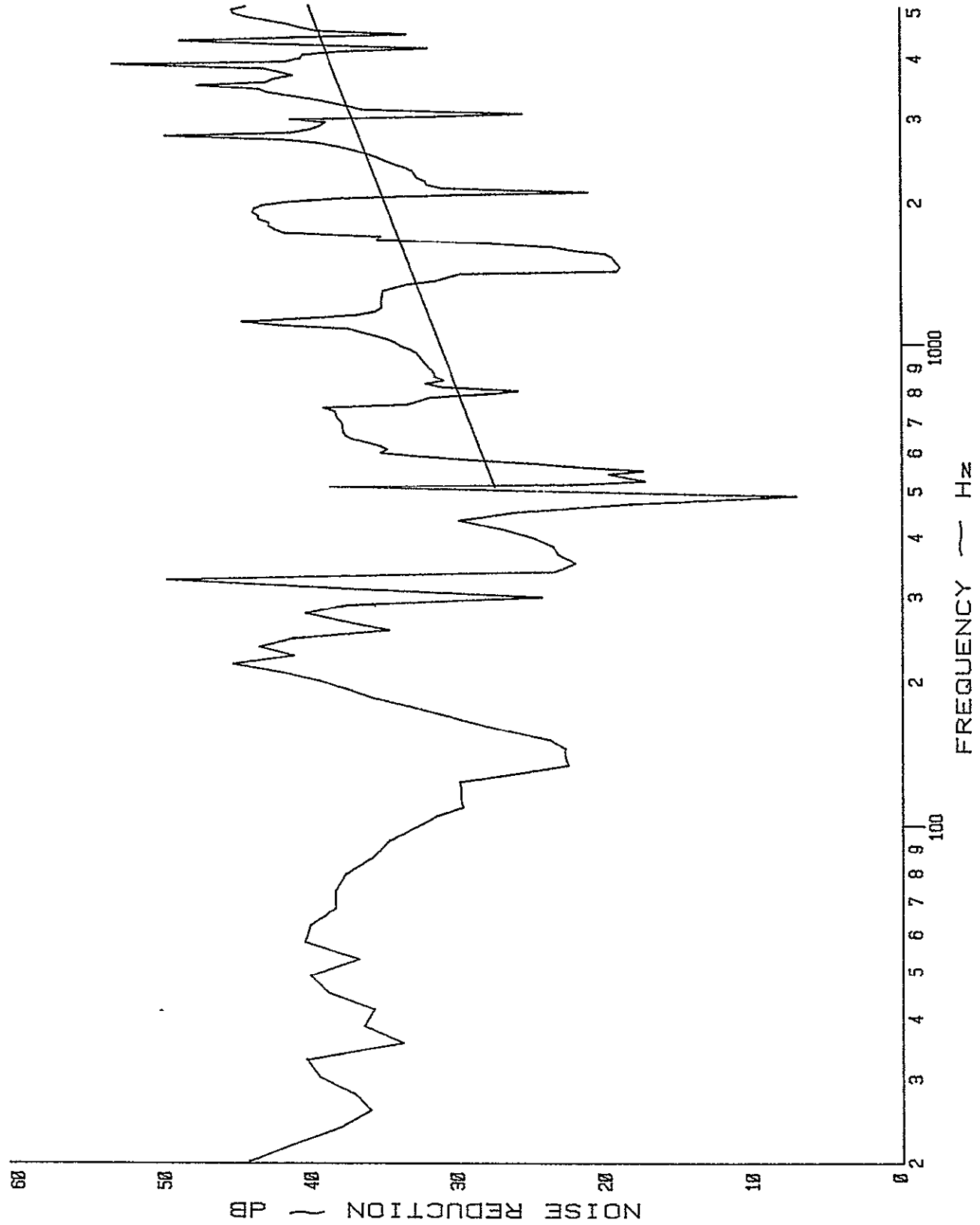

Figure 4.10 Noise Reduction Characteristics of a .020 Inch Thick Curved Aluminum Panel with a Curvature Radius of 20 Inches and Bonded Edge Conditions.

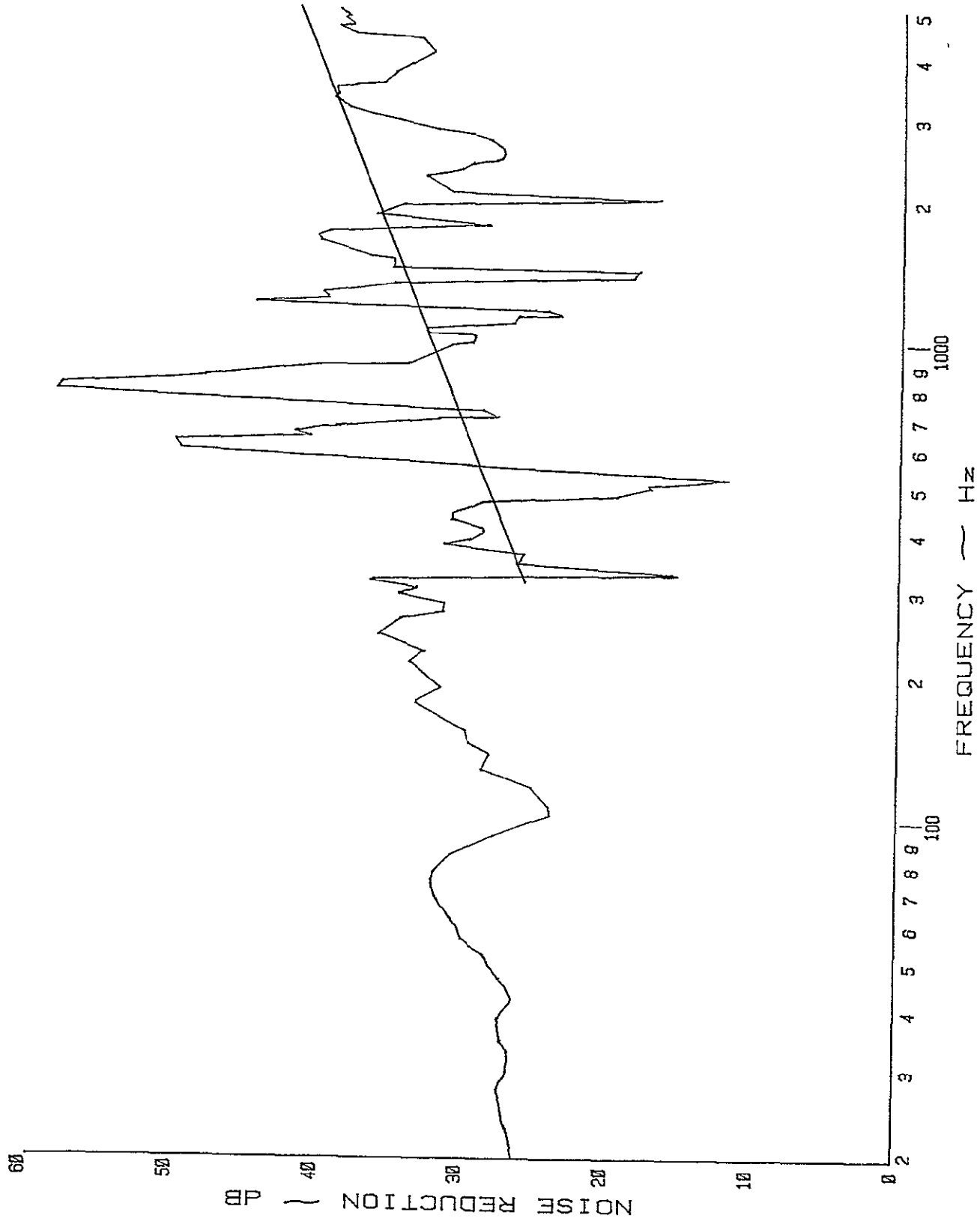

Figure 4.11: Noise Reduction Characteristics of a .032 Inch Thick Curved Aluminum Panel with a Curvature Radius of 20 Inches and Riveted Edge Conditions.

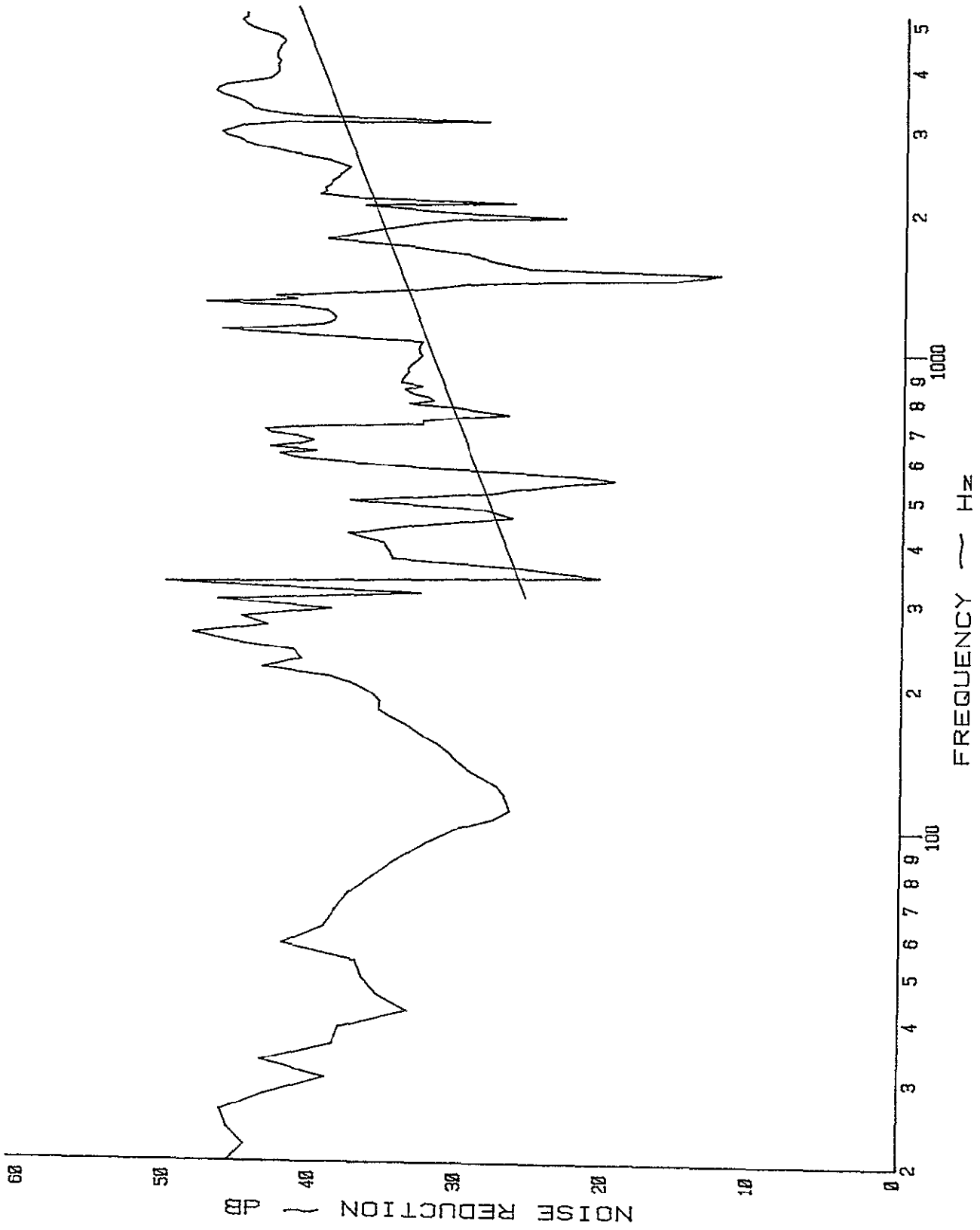

Figure 4.12. Noise Reduction Characteristics of a .032 Inch Thick Curved Aluminum Panel with a Curvature Radius of 20 Inches and Bonded Edge Conditions.

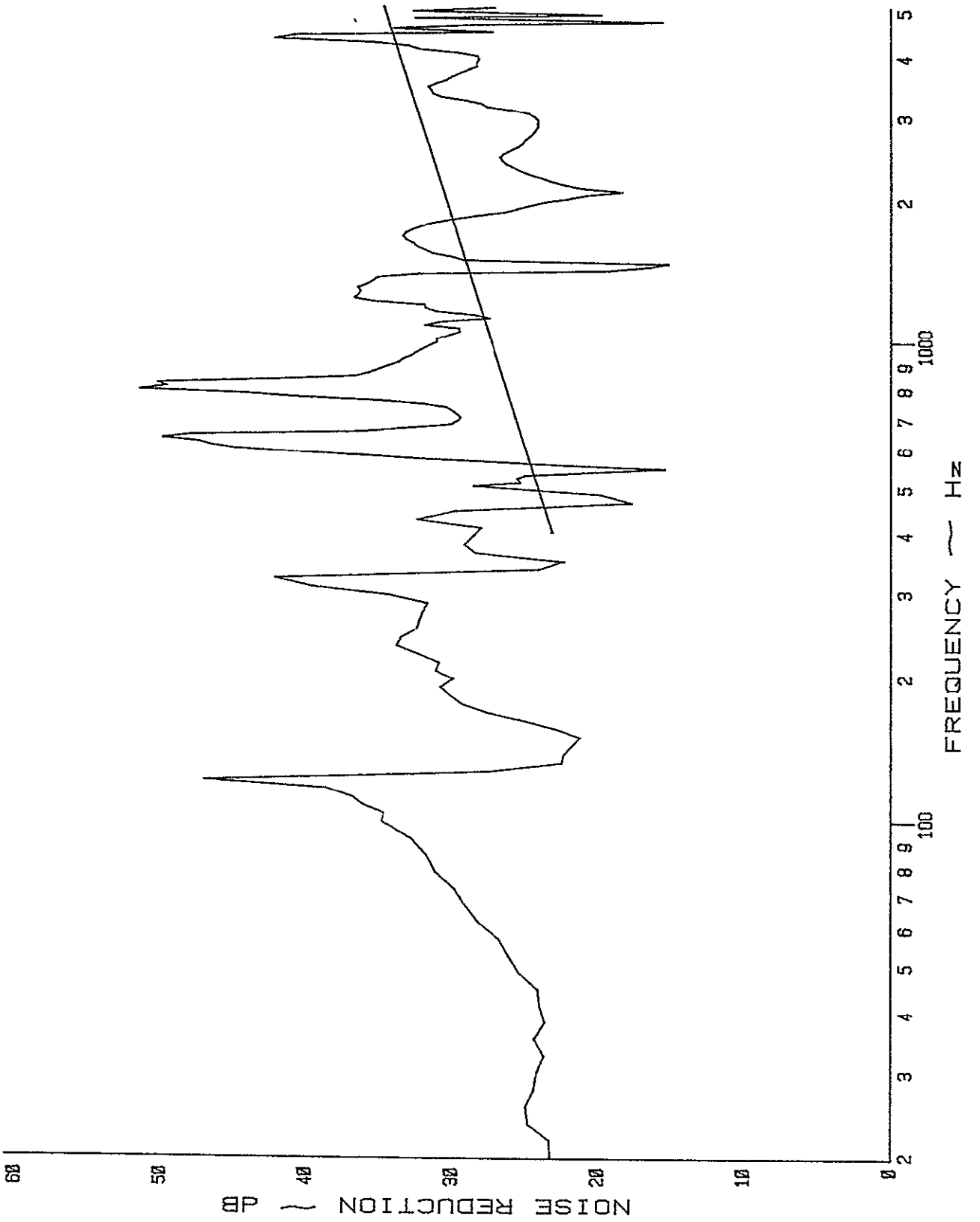

Figure 4.13. Noise Reduction Characteristics of a .016 Inch Thick Curved Aluminum Panel with a Curvature Radius of 10 Inches and Riveted Edge Conditions

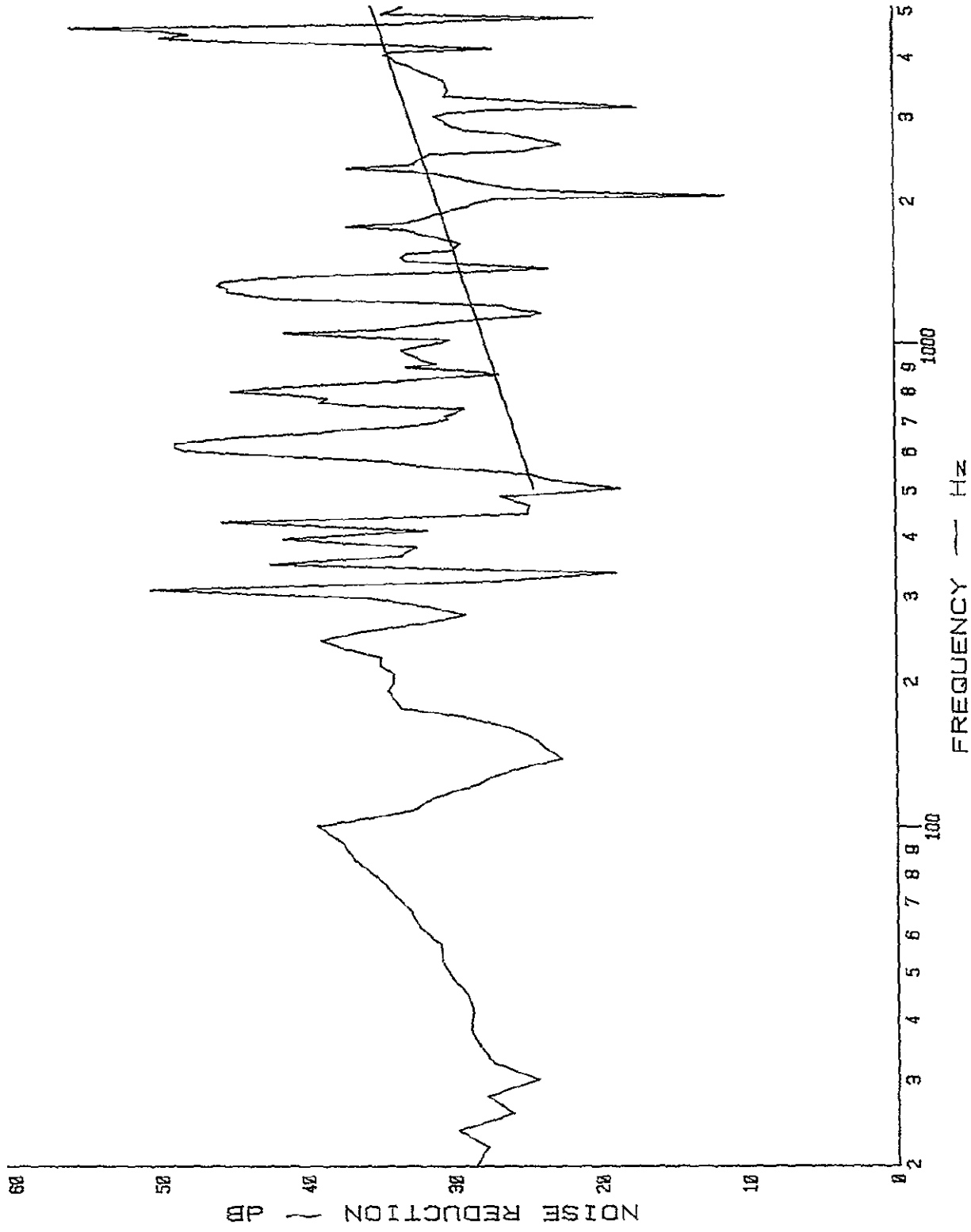

Figure 4.14: Noise Reduction Characteristics of a .016 Inch Thick Curved Aluminum Panel with a Curvature Radius of 10 Inches and Bonded Edge Conditions.

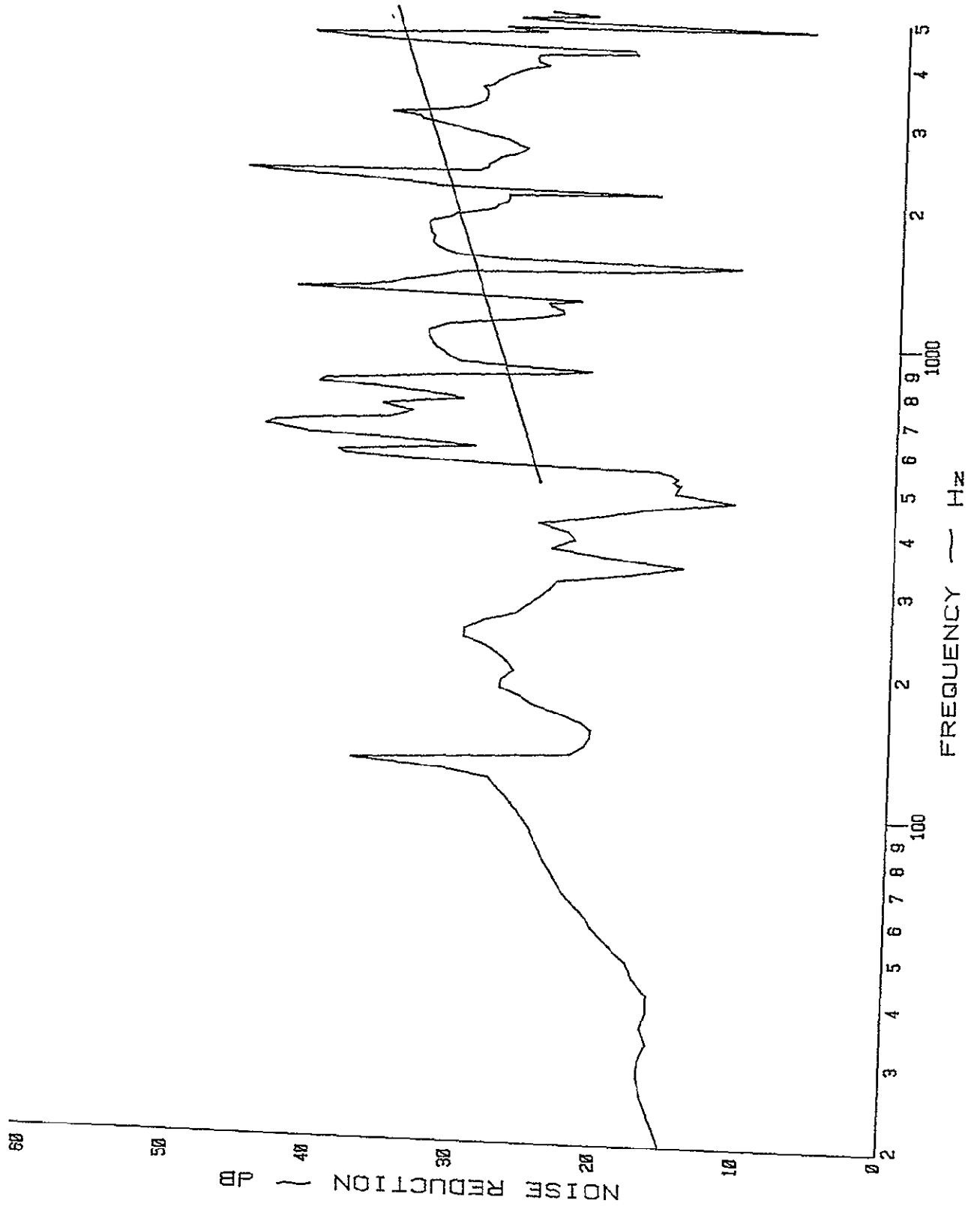

Figure 4.15 Noise Reduction Characteristics of a .020 Inch Thick Curved Aluminum Panel with a Curvature Radius of 10 Inches and Riveted Edge Conditions.

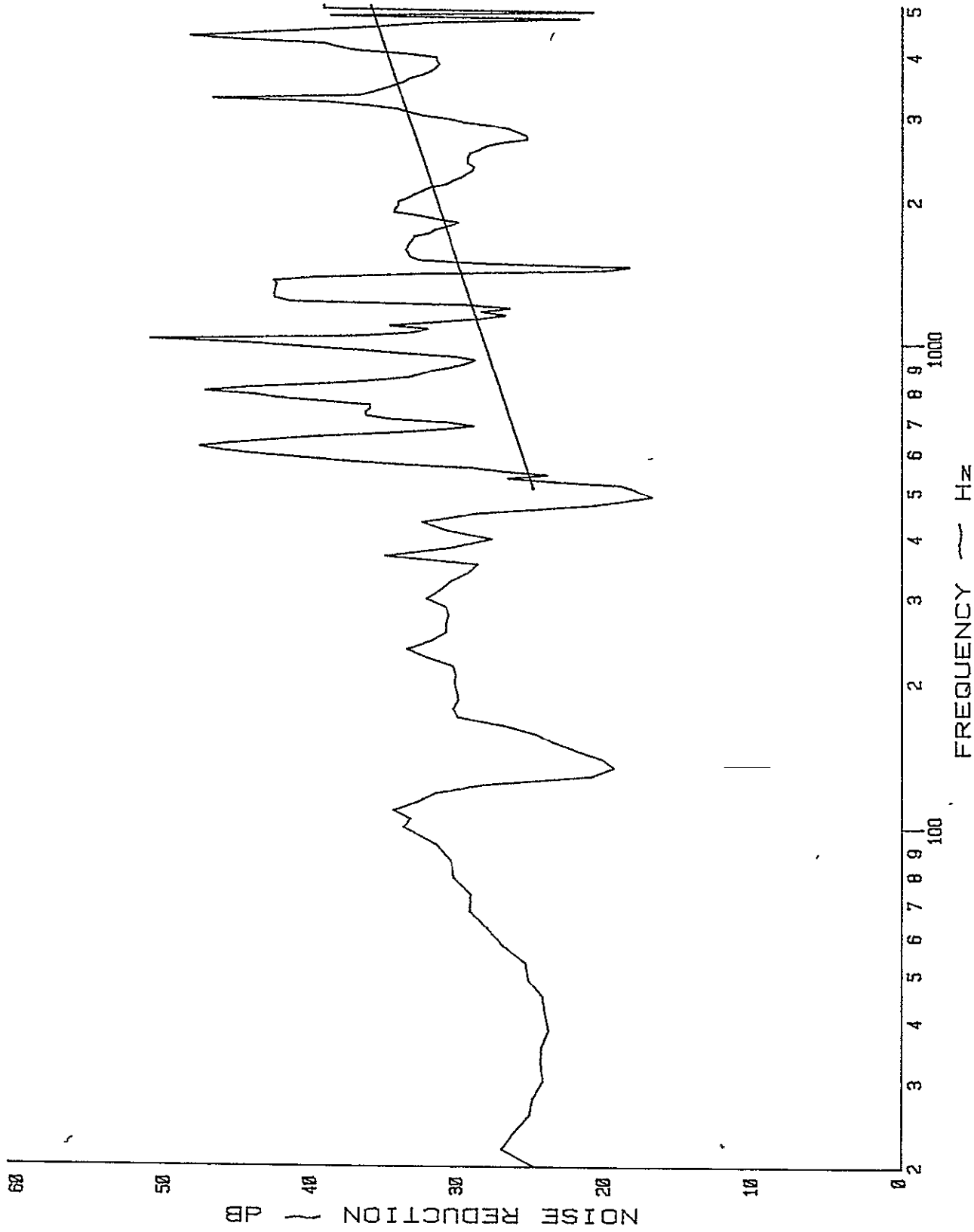

Figure 4 16: Noise Reduction Characteristics of a .020 Inch Thick Curved Aluminum Panel with a Curvature Radius of 10 Inches and Bonded Edge Conditions.

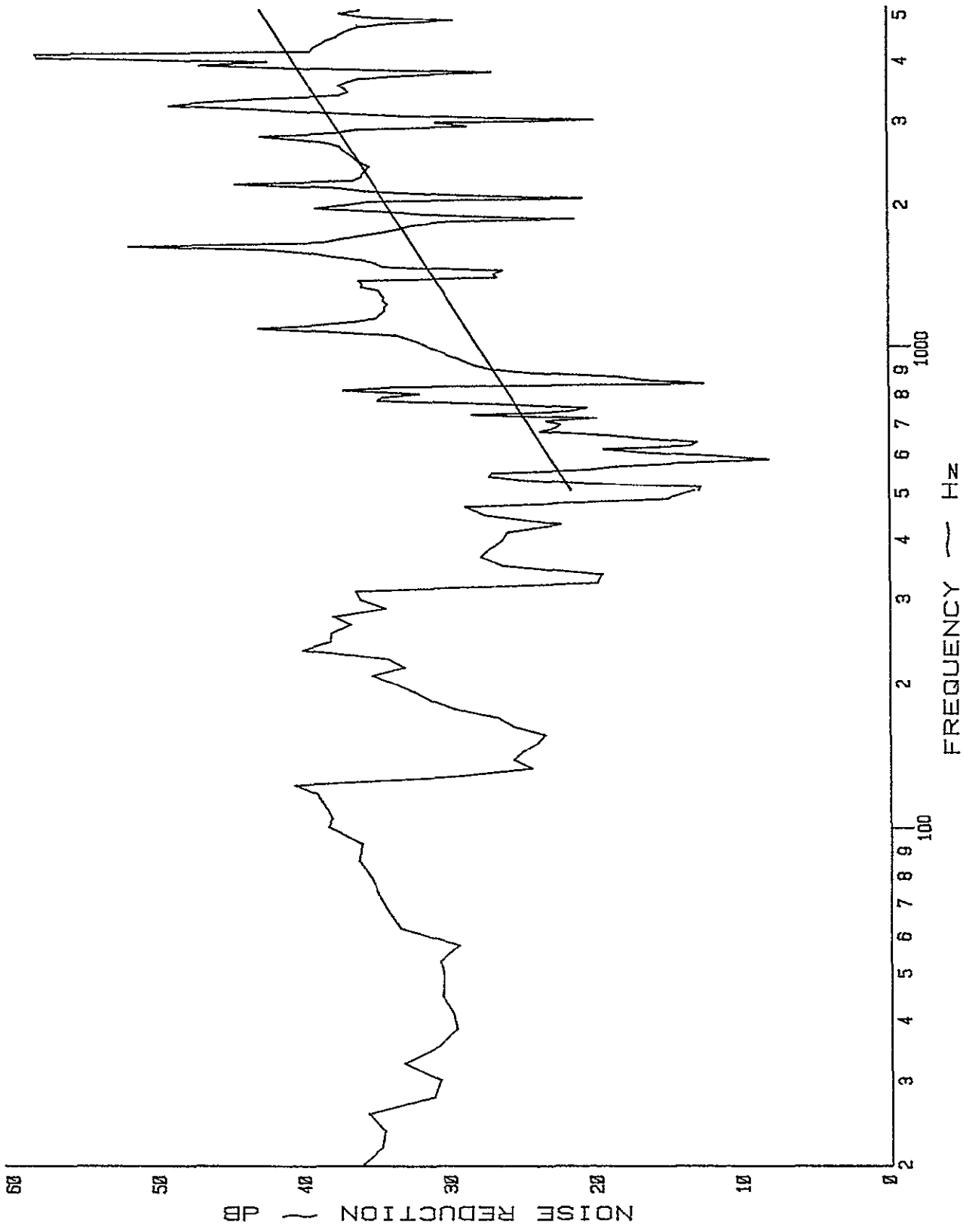

Figure 4.17· Noise Reduction Characteristics of a .032 Inch Thick Curved Aluminum Panel with a Curvature Radius of 10 Inches and Riveted Edge Condtions.

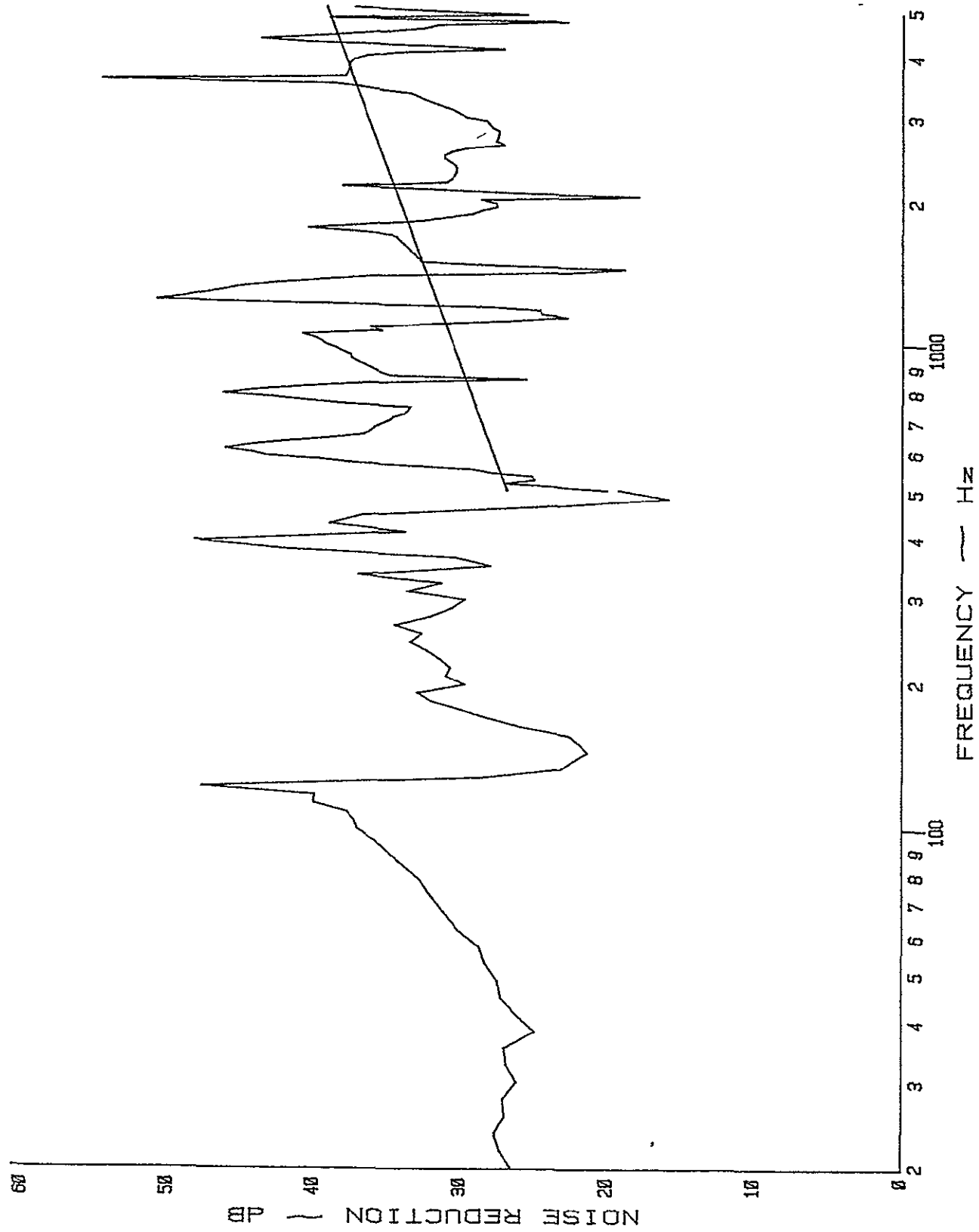

Figure 4.18 Noise Reduction Characteristics of a .032 Inch Thick Curved Aluminum Panel with a Curvature Radius of 10 Inches and Bonded Edge Conditions.

conditions. For these reasons, higher noise reduction is measured for a bonded panel than for a riveted panel in the low-frequency region.

High-Frequency Region

The noise reduction of a panel is mass dependent in the high-frequency region. The total mass of the bonded test panel equals the total mass of the riveted panel. To compare the results in this high-frequency region, the least squares line is computed for each test panel and drawn in the graphs. Figures 4.7 through 4.18 show that the noise reduction does not change between bonded panels or riveted panels, in the same configuration and under matching conditions.

Conclusions

- In the low-frequency region the bonded panels give better noise reduction characteristics than do the riveted panels.
- In the high-frequency region different edge conditions do not change the noise reduction of a panel, if the total mass does not alter.

4.2 Effect of Curvature

First a theoretical analysis is given which includes the effect of panel curvature. An analysis then is given of the experimental results, and theory and experiment are compared. Each section contains its own conclusions.

4.2.1 Theoretical Analysis

To include the effect of curvature, Reference 1 gives, for the impedance of a cylindrical panel with internal damping:

$$Zp = \eta M\omega \left\{\left(\frac{f}{f_c}\right)^2 + \left(\frac{f_R}{f}\right)^2\right\} + iM\omega \left\{1-\left(\frac{f}{f_c}\right)^2 - \left(\frac{f_R}{f}\right)^2\right\} \qquad (41)$$

For this panel impedance it is assumed that only pressure waves are incident in the direction of the plate's x-axis (Figure 2.1) and no membrane stresses are present. The critical frequency f_c is given by:

$$f_c = \frac{c^2}{2\pi} \left(\frac{M}{D}\right)^{1/2} \tag{42}$$

where: M = mass per unit area = 2700 xt (t in meters)

The flexural rigidity D is expressed by.

$$D = Et^3/12(1-\nu^2) \tag{43}$$

where: E = Young's modulus = $7.24*10^{10}$ N/m^2

t = panel thickness [m]

ν = Poisson's ratio = .33

The ring frequency f_R is defined by

$$f_R = \frac{(Et/M)^{1/2}}{2\pi R} \quad \text{(mode: m=1, n=0)} \tag{44}$$

where R is the radius of the curvature.

The ring frequency from Equation (44) is for a cylindrical shell extending to infinity in the length-direction. The first prossible mode will be the m=1, n=0 mode. This mode is impossible for a curved panel, simply supported or clamped along four edges. The first curved panel mode will be the m=1, n=1 mode. For a panel either simply supported or clamped on four edges the ring frequency will be given by

$$f_R = \frac{(Et/M)^{1/2}}{4\pi R} \quad \text{(mode m=1; n=1)} \tag{45}$$

Internal damping is included in Equation 41 by assuming a loss factor $n=10^{-2}$.

The critical frequency is the lowest frequency at which the coincidence effect can occur. At this frequency the coincidence

angle is 90°, that is, the sound pressure wave is traveling parallel to the surface of the panel. Below this frequency, the wavelength in air is greater than the bending wavelength in the panel. The critical frequency is calculated for panels with various thickness. The results are given in Table 4.1.

Table 4.1 Calculated Critical Frequencies for Aluminum Panels for Various Thicknesses

Thickness t [inch]	Critical frequency f_c [Hz]
.016	32439
.020	25710
.025	20568
.032	16069
.040	12855

The ring frequency is the frequency at which a traveling stress wave in a pipe, due to an oscillating point force, will arrive at the opposite side of the pipe in phase with the driving force, due to a delay of exactly one period. Table 4.2 gives the ring frequency for two test panels of different curvature.

Substituting the panel impedance Equation (41) into Equation (29), the noise reduction equation for part of an "infinite" curved panel, backed by a closed fiberglass-filled cavity, becomes:

$$NR = 10 \log \left[\left\{ \eta \frac{M\omega}{\rho c} \left\{ \left(\frac{f}{f_c}\right)^2 + \left(\frac{f_R}{f}\right)^2 \right\} + \frac{A\rho c \ (1-\tan^2 k\ell)}{(\rho c + B \tan k\ell)^2 + (A \tan k\ell)^2} + 1 \right\}^2 + \right.$$

$$\left. + \left\{ \frac{M\omega}{\rho c} \left\{ \left(\frac{f}{f_c}\right)^2 + \left(\frac{f_R}{f}\right)^2 - 1 \right\} + \frac{\{(A^2 + B^2 - (\rho c)^2\} \tan k\ell + B\rho c \ (\tan^2 k\ell - 1)}{(\rho c + B \tan k\ell)^2 + (A \tan k\ell)^2} \right\}^2 \right] \quad (46)$$

The theoretical noise reduction of two curved aluminum panels has been calculated for thicknesses of .016" and .032" and curvature radii of R = 10" and R = 20" using Equation (46). The results are given in Table 4.2 and depicted in Figure 4.19. To compare these results with the noise reduction characteristics of flat aluminum panels .016" and .032' thick, the noise reduction of such panels is calculated for the same frequencies and illustrated in Figure 4.19.

Conclusions

- Curving a panel will make that panel stiffer, which increases the noise reduction considerably below the frequency of largest panel displacement.
- The fundamental panel/cavity resonance frequency shifts to the ring frequency of that panel when curvature is applied.
- The ring frequency is much higher than the fundamental panel/cavity resonance frequency.
- A thicker panel with the same radius of curvature will have better noise reduction characteristics than a thinner panel.
- Increasing the panel curvature results in an increase of the noise reduction characteristics of that panel.
- The ring frequency is independent of the thickness of the panel

4.2.2 Experimental Results

The experimental noise reduction graphs are shown in Figures 4.1 through 4.18. In analyzing these test results, the following four phenomena have to be considered.

-C-2

Table 4.2 Calculated Noise Reduction for Curved Aluminum Panels of Two Different Thicknesses

thickness t [inch] →			.016			.032	
ring frequency f_R [Hz] →			811	1622		811	1622
critical frequency f_c [Hz] →			32439			16069	
frequency f [Hz] ↓	radius of curvature R [inch] →	∞	20	10	∞	20	10
16		17.2	56.6	68.6	30.0	62.6	74.6
32		10.5	50.5	62.6	23.5	56.6	68.8
63		2.3	44.6	56.7	15.7	50.6	62.8
125		4.2	38.5	50.7	1.5	44.5	56.8
250		12.0	31.7	44.5	16.2	37.8	50.6
500		17.2	23.8	38.0	23.0	29.2	44.9
811			3.7	32.1		4.48	38.1
1000		23.7	13.3	28.9	29.9	20.1	34.7
1622			25.5	.92		31.7	4.2
2000		30.3	28.7	20.9	36.3	34.6	26.6
4000		36.4	35.9	34.7	42.4	41.4	40.2
5000		38.15	37.7	36.9	44.2	43.1	42.3

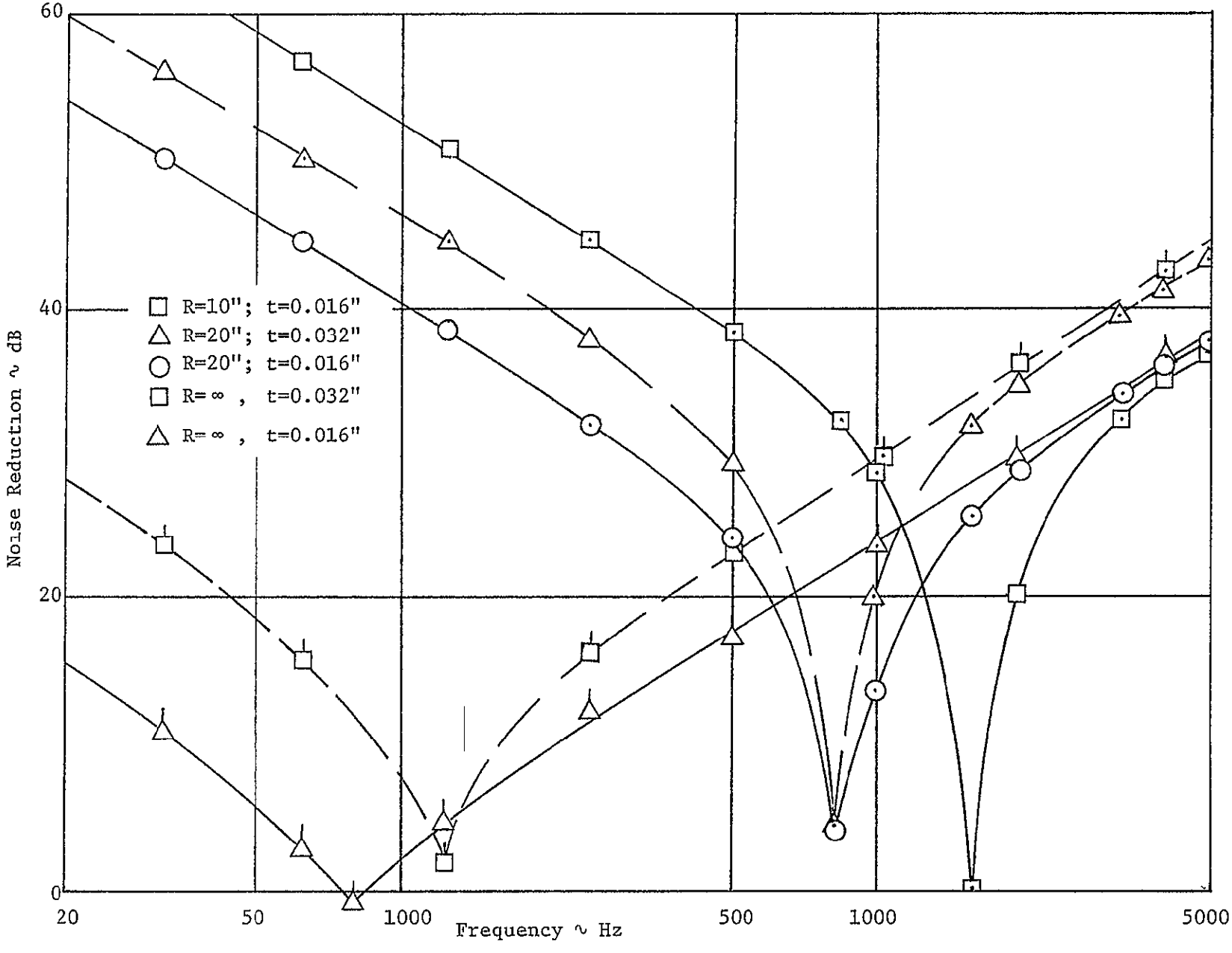

Figure 4.19 Theoretical Noise Reduction of a 12"x12" Aluminum Panel for Three Curvature Radii and Two Thicknesses

1. The curvature of a panel increases its stiffness at low frequencies, which results in a noise reduction increase.
2. In the vicinity of the ring frequency, the noise reduction is proportional to the radius of panel curvature.
3. Increasing the panel curvature will shift the ring frequency into a higher frequency region.
4. The curved panel is hit by a plane wave. Due to the curvature, the angle of incidence of the sound wave will be oblique all over the panel surface, except along the line thorugh the center of the panel parallel to the speaker baffle.

A combination of these four factors will determine whether the noise reduction for a particular panel will increase or decrease when (more) curvature is applied.

Analysis of the test results of the .016", .020" and .032" thick flat and curved panels (Figures 4.1 through 4 18) led to the following observations.

Low-Frequency Region

Curving a flat test panel results in a big noise reduction increase, due to the stiffening effect. At the fundamental resonance frequency of the flat panels, the noise reduction of the curved panels is up to 40 dB higher. Bonded or riveted edge conditions as well as thickness appear to affect this increase in noise reduction in the following way (Figures 4.1 through 4.12)

	.016"	.020"	.032"
bonded panels	40 dB	39 dB	28 dB
riveted panels	34 dB	35 dB	23 dB

Applying more curvature to an already curved panel by decreasing the curvature radius R from 20" to 10" did not result in a higher noise reduction. A higher noise reduction was expected because the sharper curvature of the panel would result in a stiffer panel. The reason is that, having a plane pressure wave, the local angle of incidence between this acoustic wave and the panel surface is oblique, except at the panel's centerline parallel to the speaker baffle. As concluded in Chapter 2, an oblique angle of sound incidence indicates a lower noise reduction As this effect prevails when changing from a 20" to a 10" curvature radius, the noise reduction decreases. Bonded or riveted edge conditions and thickness affect this decrease in noise reduction in the following way (Figure 4.7 through 4.18)

Frequency = 40 Hz	.016"	.020"	.032"
bonded panels	8 dB	10 dB	10 dB
riveted panels	4 dB	10 dB	4 dB

High-Frequency Region

The following sequence of test configurations will be discussed for three panel thicknesses (.016", .020" and .032")

flat panel - curved panel (R = 20") - curved panel (R = 10")

The bonded and riveted edge conditions do not affect the noise reduction characteristics of the panels in the high frequency region. The total mass of test panels of the same thickness in different configuration changes because the projected exposed area is kept constant The panel with a curvature radius of 10" is consequently the heaviest. This, combined with the effect of a local oblique angle of sound incidence, led to the following results· (least squares line, f = 2000 Hz)

Table 4.3 Important Panel Modes for Curved Simply Supported Aluminum Panels (Dimensions: 12" x 12" x .016")

$$f^2_{m,n} = \frac{Em^4}{4\pi^2\rho R^2[m^2+n^2(a/b)^2]^2} + f^2_{m,n_{flat}} \qquad \text{(Ref 6)}$$

where E = 7 24 x 10^{10} N/m^2 elasticity modulus

R = radius of curvature [m]

a = b = 3048m panel dimensions

$$f_{m,n} = \frac{\pi}{2}\left(\frac{Et^3}{12(1-\nu^2)M}\right)^{1/2} \cdot \left(\frac{m^2}{a^2}+\frac{n^2}{b^2}\right) \qquad \text{(Ref 4)}$$

where M = mass per unit area [kg/m^2]

ν = Poisson's ratio

m and n are panel modes (1,2,3,)

Curvature R [inch] →		∞	20	10
modal number		calculated frequency $f_{m,n}$		
m	n			
1	1	21 76	811 5	1622
2	1	54 4	1299 0	2596 3
2	2	87 0	815 8	1624 7
3	1	108 3	1464 2	2922 3
3	2	141 5	1132 0	2250 8
3	3	195 9	834 5	1634 1
4	1	185 0	1538 1	3059 4
4	2	217 6	1316 0	2604 9
4	3	272 0	1073 3	2094 3
4	4	348 2	882 7	1659 3
5	1	282 9	1585 4	3132 7
5	2	315 6	1433 7	2814 9
5	3	370 0	1249 0	2414 3
5	4	446 1	1085 2	2028 1
5	5	544 1	976 7	1711 1
6	1	402 6	1629 0	3182 6
6	2	435 2	1523 6	2952 5
6	3	489 7	1387 2	2641 5
6	4	565 8	1257 6	2316 5
6	5	663 8	1165 0	2026 7
6	6	783 4	1127 7	1801 6

- .016"-thick panels.

Following the configuration sequence, first an increase of 1 dB is observed, followed by a decrease of 5 dB.

- .020" and .032"-thick panels:

Following the configuration sequence, a decrease of 2 dB is followed by another 3 dB decrease in noise reduction.

Important calculated panel modes of simply supported, 12" x 12" x .016", aluminum panels are given in Table 4.3. The calculation is based on the work of Getline (Reference 6), which states that the frequency of a curved panel is the frequency of a flat panel plus the curvature effect:

$$f^2_{m,n} = \frac{Em^4}{4\pi^2\rho R^2[m^2+n^2(a/b)^2]^2} + f^2_{m,n_{flat}} \qquad (47)$$

where $f_{m,n_{flat}}$ is given by the equation in Table 2.6. The identification of these panel modes will occur in a future report under the same NASA Grant 1301. Some definite cavity modes can be identified from the experimental results (Figure 4.1 through Figure 4.18). They are presented in Table 4.4 They appeared to be identical for the test section with a 20" curvature radius as for the test section with the 10" curvature radius.

Table 4.4 Some Important Cavity Modes for the Curved Test Sections (Curvature Radii 20" and 10") as Found in the Experimental Noise Reduction Curves (Figures 4.1 through 4.18)

Curvature Radius [Inch]	Experimental Frequency f [Hz]*				
R = 20	145	340	520	1450	2050
R = 10	145	340	520	1450	2050

*approximate values

Conclusions

• Curving a flat aluminum test panel greatly increases the noise reduction in the low frequency region, due to its stiffening effect.

• Applying more curvature to an already curved panel reduces the noise reduction in the low-frequency region, due to a local oblique angle of sound incidence.

• A trade-off between curvature radius and panel thickness is necessary to determine the highest noise reduction in the high-frequency region.

CHAPTER 5

DESIGN AND CONSTRUCTION OF A TENSION DEVICE

In this chapter the design and construction of a tension device is discussed. This tension device is used for acoustical testing of panels under either uniaxial or biaxial stresses with the KU-FRL acoustic test facility.

5.1 Introduction

Aircraft fuselage panels are part of the airplane's bearing structure and are exposed to shear and tension loads in the plane of the panel. In the case of curved panels or a pressure difference over the panel, additional radial tensile stresses occur (the hoop stresses). These loads will affect the stiffness of these panels and therefore their acoustic properties.

To investigate the effect of in-plane stresses on the noise reduction characteristics of a flat panel, a tension device has been designed and constructed to apply uniaxial and biaxial stresses to a flat panel. Panels can be exposed to a plane sound wave under normal or oblique angles of sound incidence.

5.2 Design Considerations

The following design criteria were considered:

1. The tension device should allow application of in-plane stresses to a flat panel in two perpendicular directions, independent of each other.

2. A design maximum panel stress of 10,000 psi, which is the equivalent of 20% of the yield stress of an aluminum panel, is required.
3. The tension device must have the capability to test panels under an oblique angle of sound incidence, by using the special test sections of 75, 60 and 50 degrees*, as well as under normal sound incidence.
4. The entire tension device must be movable and operational, independent of the original acoustic test facility.
5. Test panels used in former tests must be usable in the tests with the tension device.
6. Clamped edge conditions of the test panels are required
7. No sound should reach the receiver microphone other than through the test panel.

5.3 Design and Construction

5.3 1 Maximum Force

A maximum panel stress of 10,000 psi in a 0.040 x 20 x 26.11 inch aluminum panel (50° sound incidence) and a safety factor of 3 results in a maximum design load of 31,330 lb., to be exercised by the actuator.

5.3.2 The Frame

The tension device is basically built up out of four heavy steel I-beams, supported by two horizontal tubes. Four clamping plates clamp

* The angle of sound incidence is here defined as the angle between the direction of the sound and the plane of the test panel.

the test panel along the four edges. Two adjacent clamping plates are attached to the frame by angles. Two hydraulic actuators are attached to the steel frame and the two other clamping plates and take care of the stresses applied to the test panel in two mutually perpendicular directions. The actuators are of the push-cylinder type and can exercise a maximum hydraulic pressure of 3000 psi. The frame can be moved in any direction on four steel swivel casters, which are mounted at the ends of the horizontal tubes. During the tests, the frame is aligned to the Beranek Tube and is fixed to the floor by four screw jacks. The design of the tension device and its position in the acoustic test facility is shown in Figures 5.1 to 5.6.

5.3.3 Other Components of the Tension Device

The frame, support angles, and clamping plates are made out of ASTM 36 Steel and are constructed by a local steel company. Parts that needed machining were contracted out to a local machine shop or to the University machine shop. Assembling of the tension device and the design and construction of the hydraulic system were done by the members of the FRL Noise Group. Almost all connections consist of joints of high-strength bolts and nuts. The lower horizontal I-beam is connected to the vertical I-beams by joints in such a way that it can be easily removed to clear the tension device from the test facility. To adjust the tension device in vertical direction, to level it off and to make it stable, the device is resting on four screw jacks. These screw jacks have a special ball-and-socket construction between the spindle and the base plate. The width of the frame is determined by the length of the test panel. The length of the test panel varies

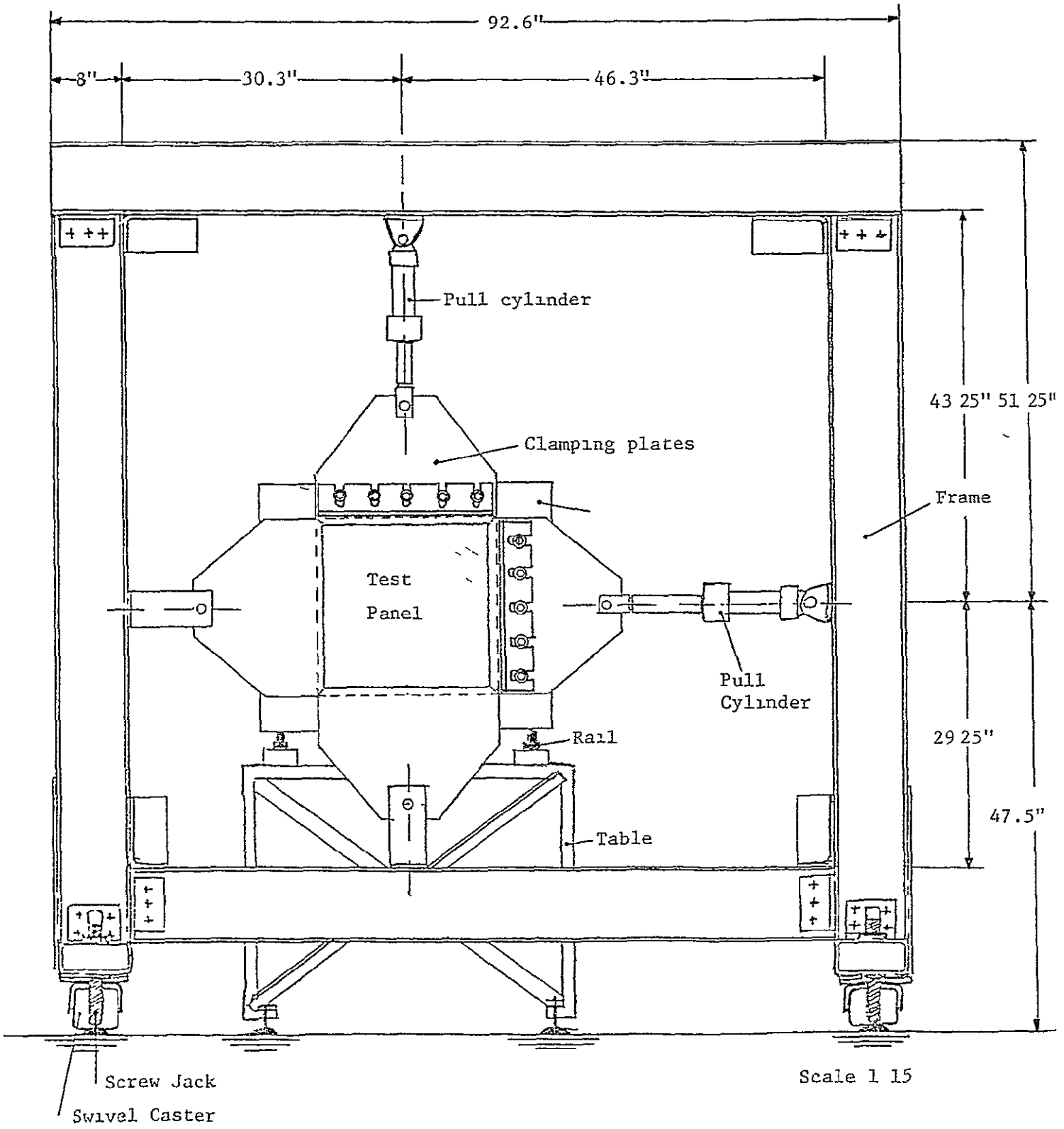

Figure 5.1 View of Tension Device

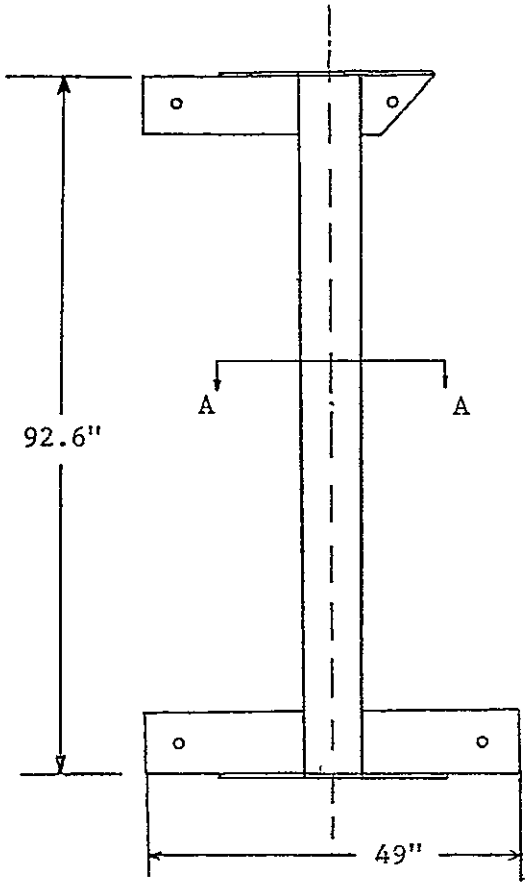

a) Topview

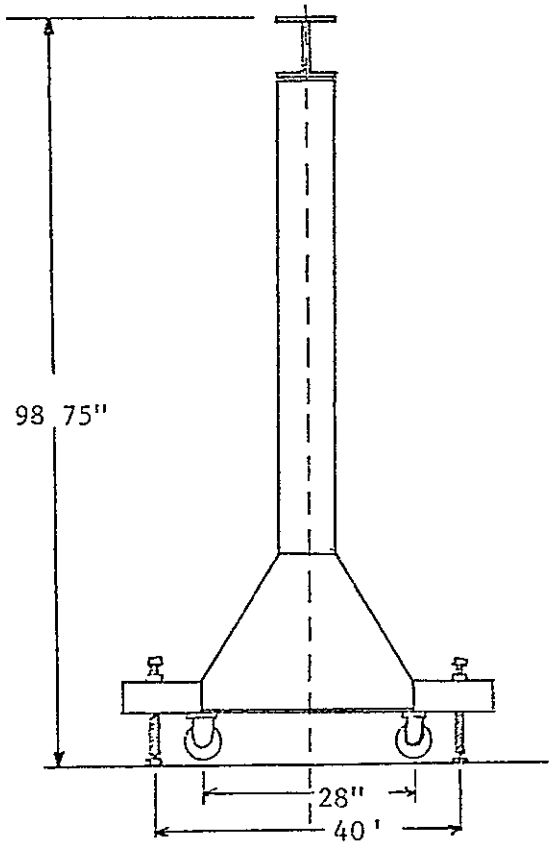

b) Sideview

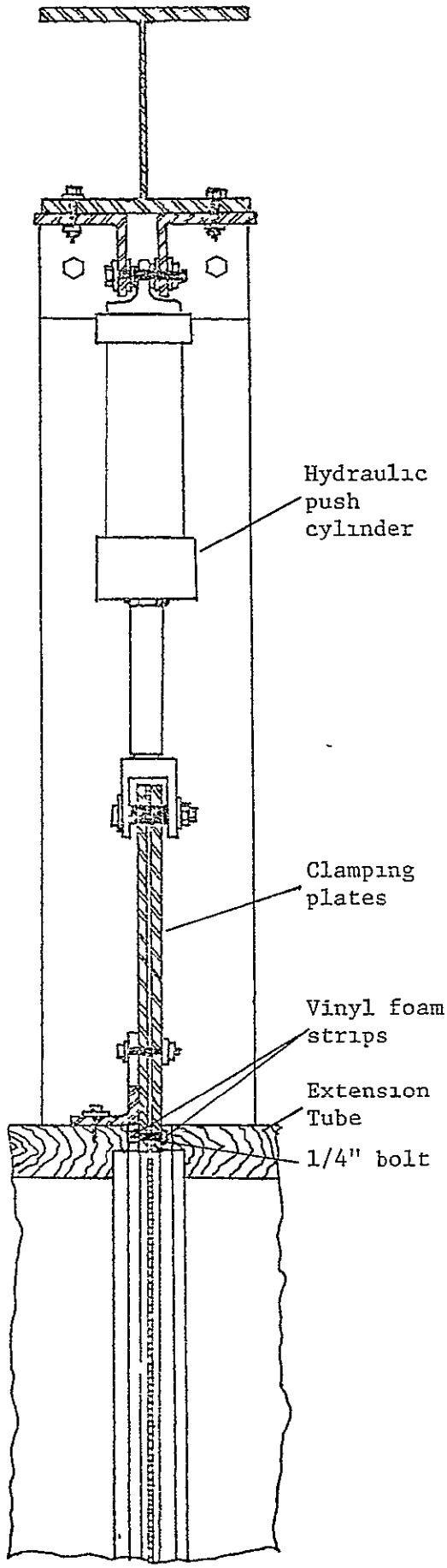

c) Cross-Section A-A

Figure 5.2 A Three-View of the Tension Device

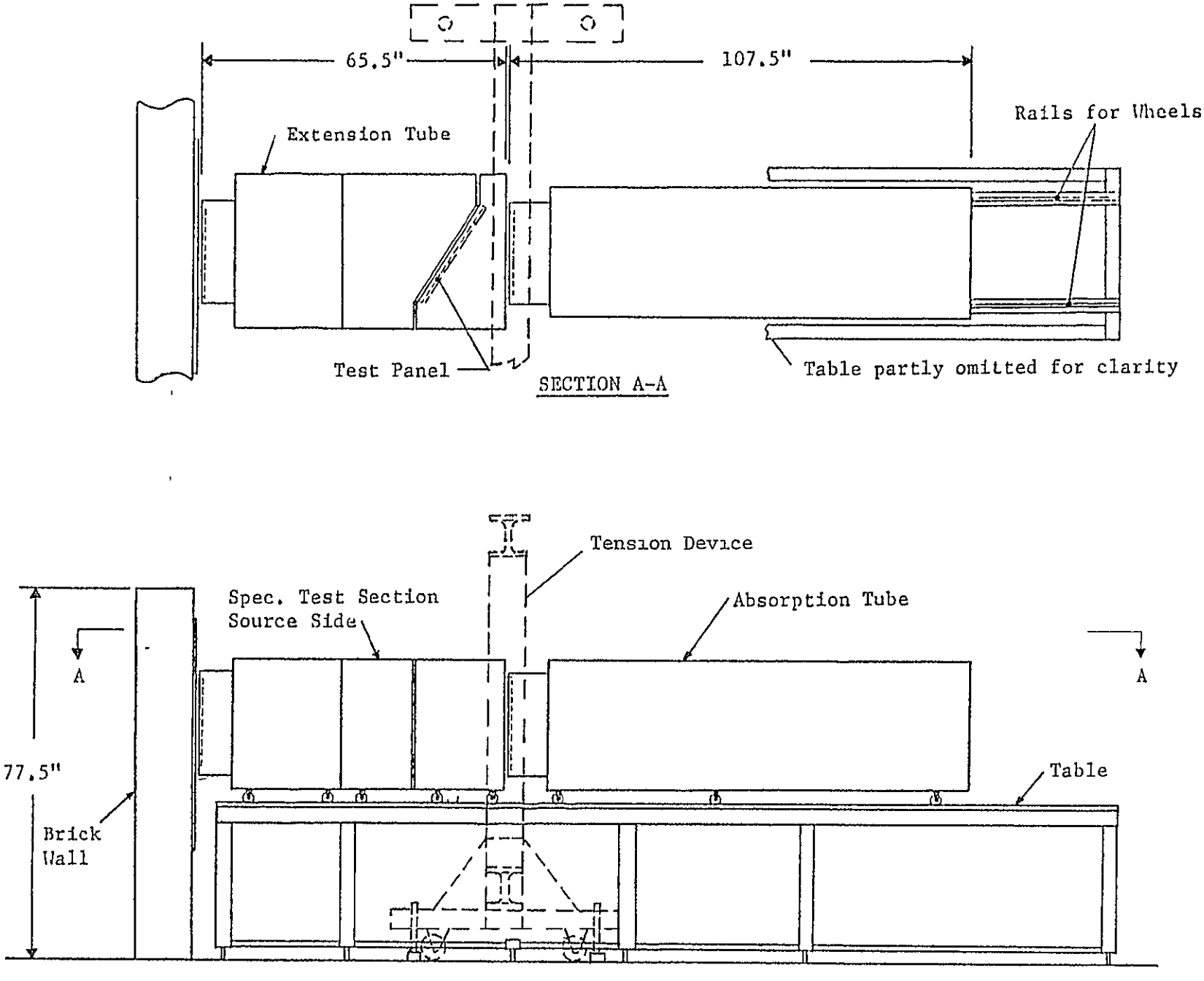

Figure 5.3 Position of the Tension Device in the KU-FRL Acoustic Test Facility

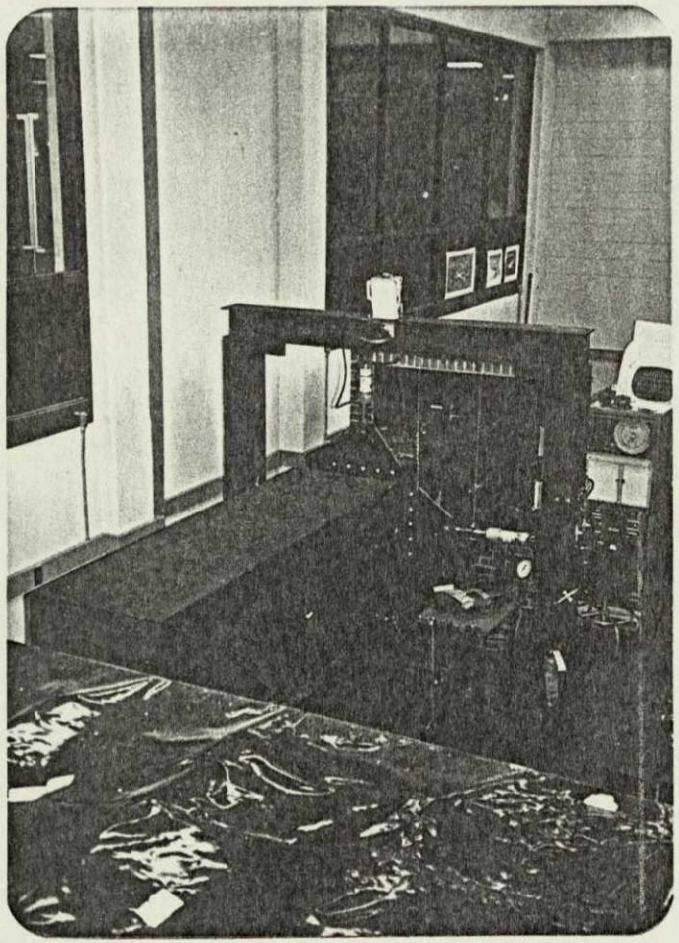

Figure 5.4: General View of the KU-FRL Acoustic Test Facility with the Tension Device

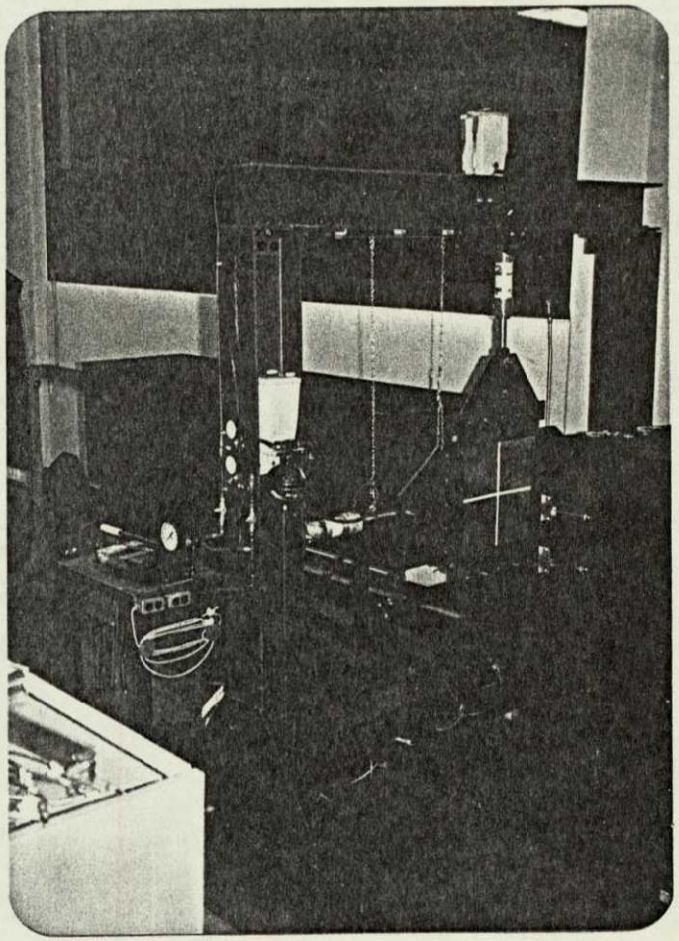

Figure 5.5: Front View of the KU-FRL Tension Device

Table 5.1· Various Distances (Defined in Figure 5.6) for Different Angles of Sound Incidence and Mounting Angles.

Mounting Angle	Angle of Sound Incidence		Distance ~ Inch		
	P	Q	a	b	c
I	60°	90°	6.5	1.55	24.25
II	50°	75°	5.0	2.7	22.6

5.3.4 Clamping Plates

Each side of the test panel is clamped between two uniform .5-inch-thick clamping plates with an overlap of 1 inch. Nine .25-inch bolts, at the same mutual distance along each side of the panel, are tightened with a torque of 100 in-lb to ensure a uniform distribution of the clamping forces and high shear loads. This torque of 100 in-lb is the maximum torque that can be applied to the bolts without damage to the thread. Special attention will be paid to tightening the bolts in a sequence such that a uniform clamping distribution will be obtained. In this way it can be assumed that the test panel's edges are clamped.

5.3.5 Structural Vibration and Safety Considerations

To minimize vibrations of the whole system inside the frame (connections, clamping plates, actuators and test panel), two support angles are attached to the Beranek Tube and fix the clamping plates at the actuator sides of the Beranek Tube. To prevent damage to the Beranek Tube, these angles are designed with slots to provide an

unrestricted movement of the clamping plates in case of a panel failure. When a panel failure occurs, all movements will take place in the plane of the frame and will be damped and stopped by the actuators. The clamping plates are secured to allow movement in only one direction to ensure safety in case of a failure in the hydraulic system and/or a tear-out of the test panel.

5.3.6 Sealing of the Gap Between the Tubes and Test Panel

A special closed cell vinyl foam has been applied along the edges of the tubes on both sides of the test panel/clamping plates to seal the source and receiver rooms. The whole system is kept together under light pressure without hindering movements perpendicular to the Beranek Tube axis. The sealing strip has good resilient and damping properties. At the corners of the panel caulking cord is applied to seal the crevices between the clamping plates. A special damping material (GAF) is attached to the inside edges of both tubes to further minimize any vibration other than that of the test panel. Initial tests proved the reliability of the whole system: Sound can only reach the receiver microphone through the test panel, and no vibrations of the clamping plates could be measured.

5.3.7 Hydraulic System

The hydraulic system consists of two separate systems actuated by one hydraulic hand pump. The two systems are separated by valves, and the pressure in each line can be determined by a pressure gauge. Each system contains an actuator, an accumulator and an oil reservoir.

The hand pump with oil reservoir is connected to both systems by a quick-connect, self-closing coupling. The accumulator, actuators and hand pump are borrowed from Gates Learjet Aircraft Corporation. Figure 5.7 gives a schematic view of the hydraulic system. The distinctive parts are interconnected by hoses and .25-inch-diameter steel tubes.

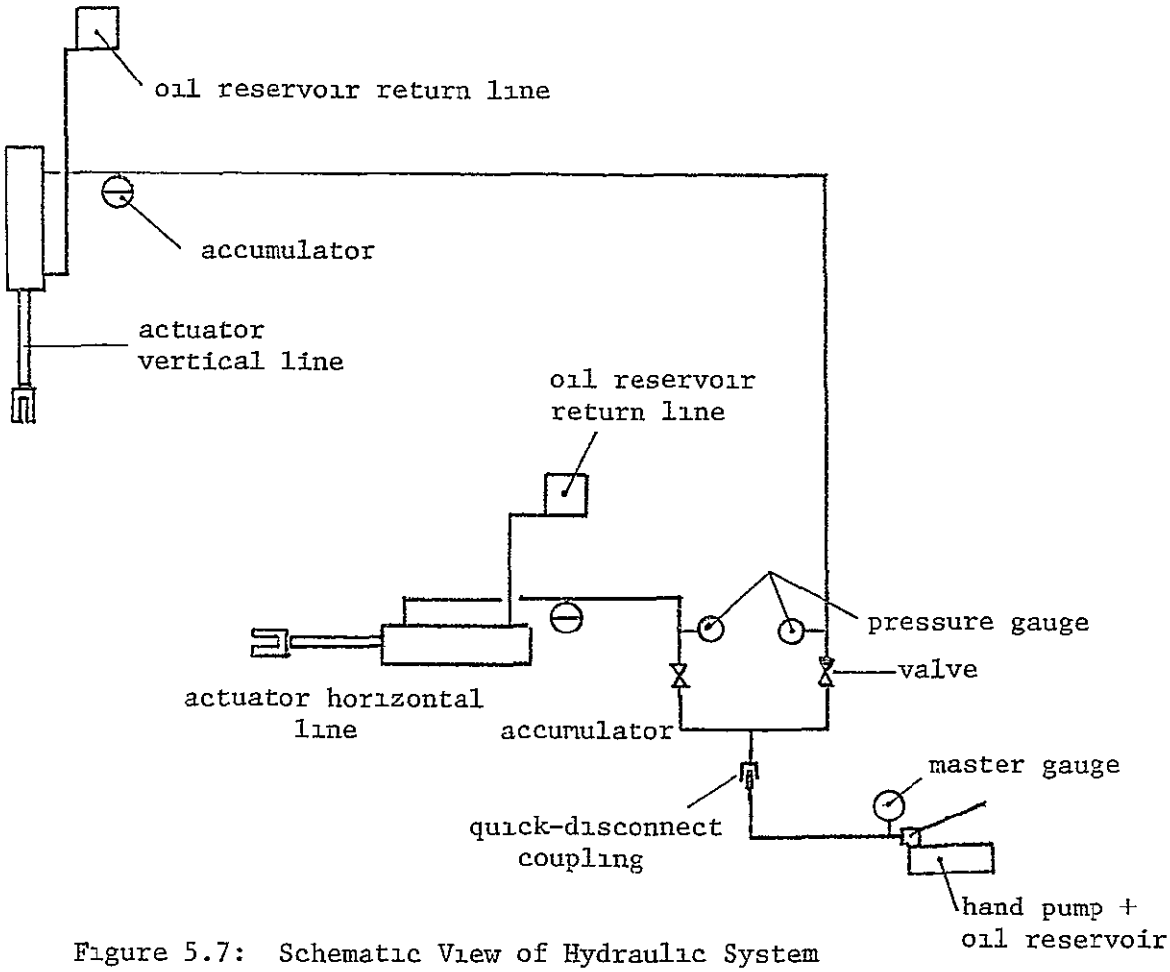

Figure 5.7: Schematic View of Hydraulic System

The hand pump with oil reservoir is mounted on a movable table and can be disconnected from the system to prevent unauthorized use. A maximum pressure of 3000 psi can be obtained by using the hand pump, sufficient to provide the required stresses in the panel. The effective piston area is about 3.8 square inches. The accumulators are filled with nitrogen under a 750 psi pressure to stabilize the pressure lines and to prevent pressure losses during the tests (Figure 5.8).

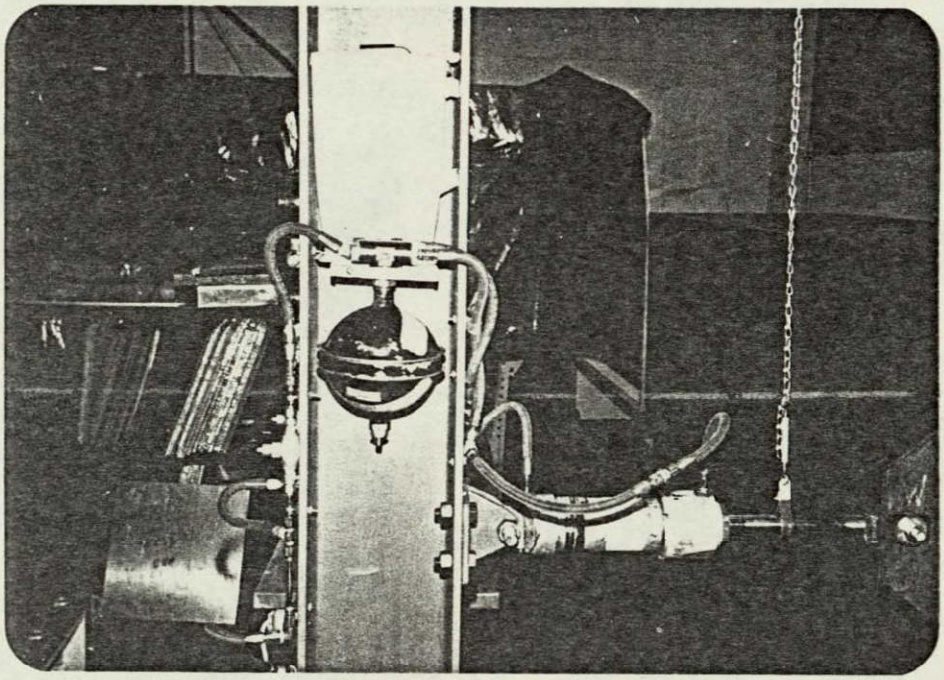

Figure 5.8: The Accumulator in the Horizontal Line of the Hydraulic System.

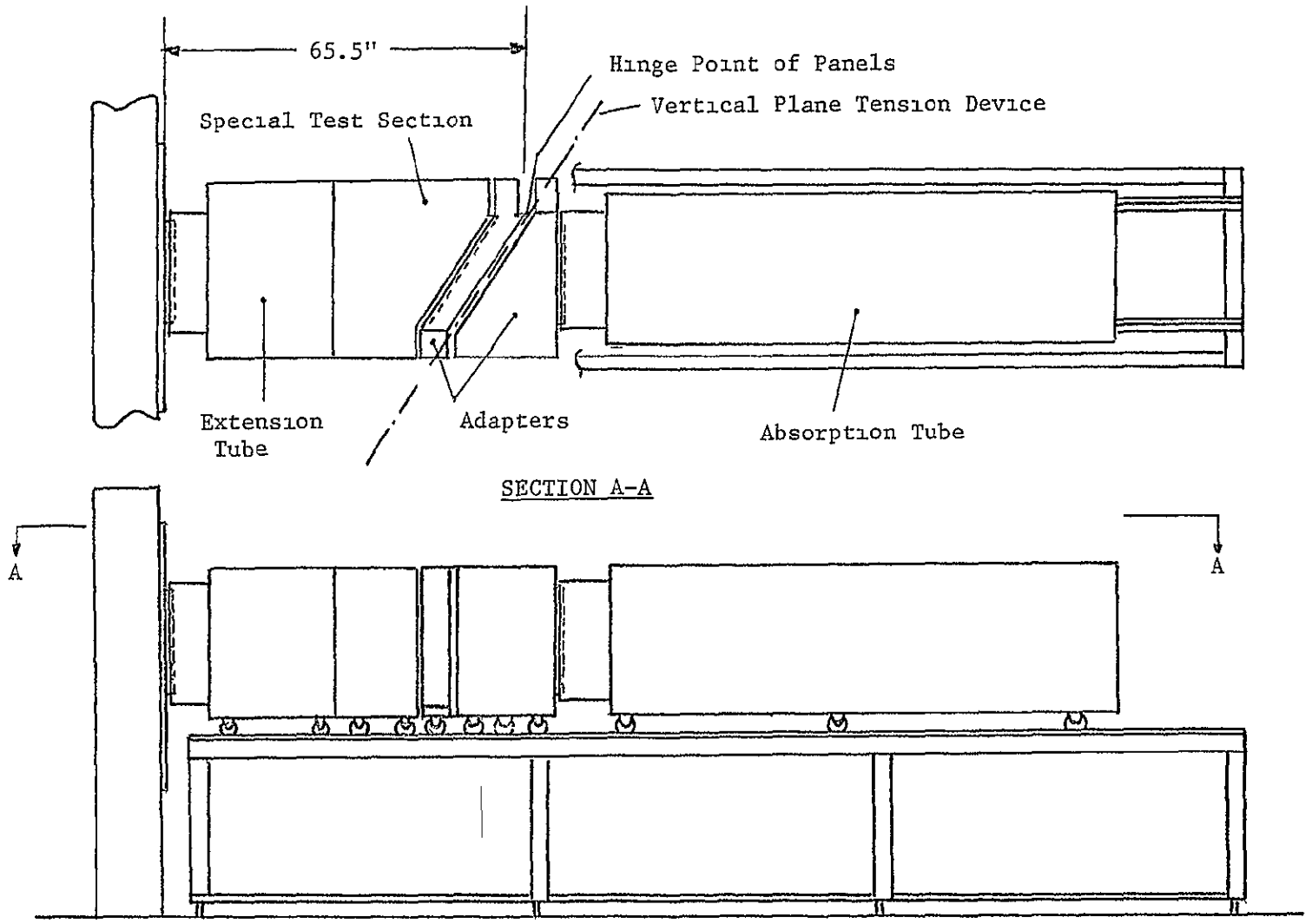

Figure 5 9 Proposed Form of Adapter for Simultaneous Testing Under Oblique Angle of Sound Incidence and Stress.

input of the loudspeakers. Inquiry made of the manufacturer of the loudspeakers revealed that there is presently no more powerful loudspeaker of the same diameter on the market. Because some doubts had also been raised in using the special test sections (Chapter 2), only the extension will be used for tests with panels under stress. The extension tube has been rotated 180°. The new test configuration is depicted in Figure 5.10. The distance from the test panel to the loudspeakers has been decreased by about 30 inches by deleting the special test section. Because the tension device was moved to another location, the table needed a second modification (Figure 5.10) Test results show a sound level at the receiver side of the panel that is high enough to be measured by the receiver microphone for all required tests. A new adapter design is needed to facilitate the testing of panels under stress and under an oblique angle of sound incidence. This will be done in the near future.

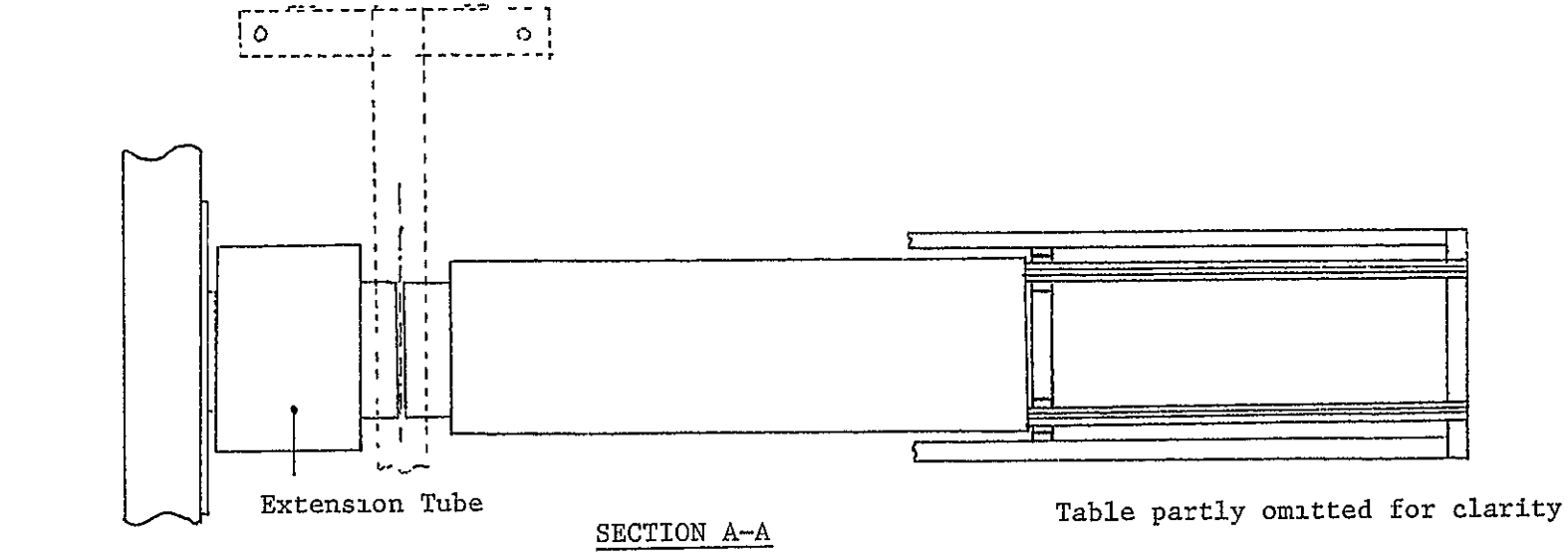

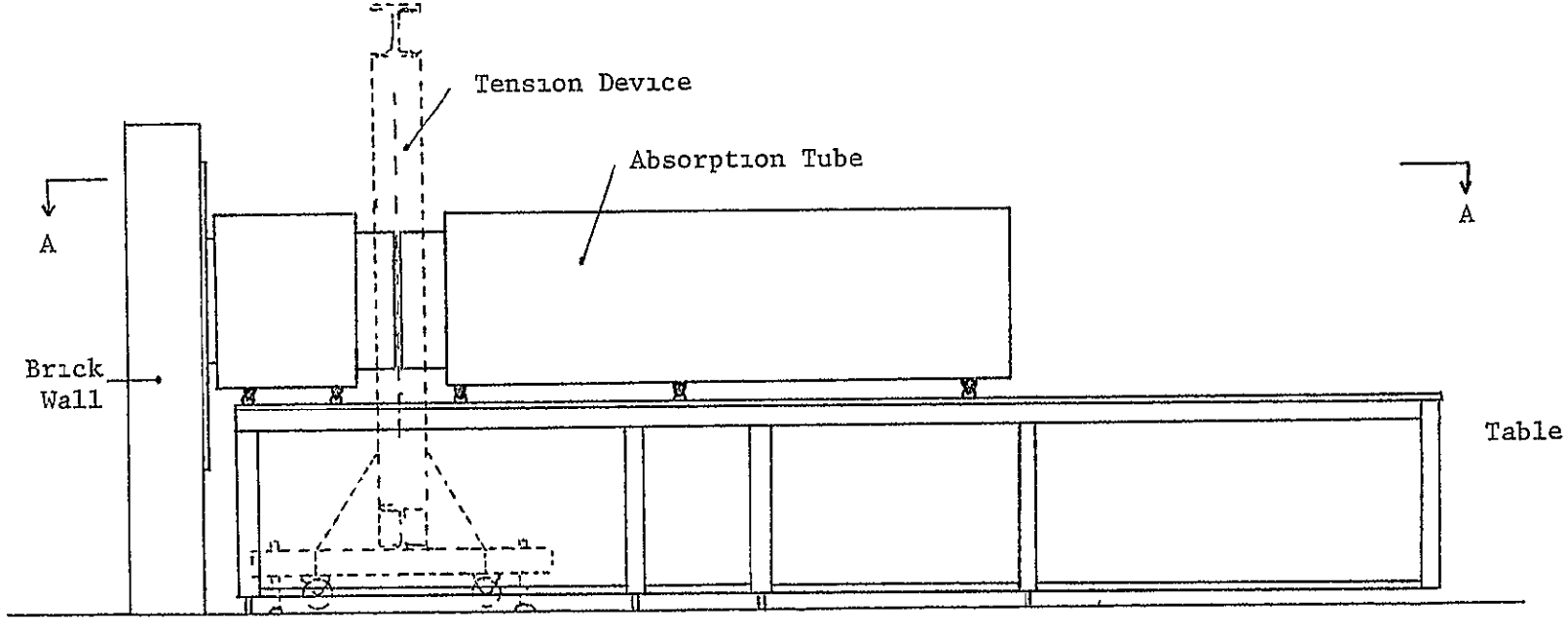

Figure 5.10· New Position of the Tension Device

CHAPTER 6

INITIAL NOISE REDUCTION RESULTS FOR A PANEL UNDER UNIAXIAL STRESS

First the calibration of the measuring devices and the monitoring of the applied stresses will be discussed in this chapter. The initial test results for a panel under uniaxial stress will be analyzed hereafter.

6.1 Calibration and Monitoring of the Applied Stresses

Originally, strain gauges were used to calibrate the forces exercised by the actuators. Strain gauges were also used to monitor the load-time history during testing Opposite each actuator, strain gauges were attached on both sides of the clamping plate mounting angles. Using a Wheatstone bridge and a digital signal conditioner, the strain in the angles can be determined. This strain is a measure of the applied stress in the panel. The mounting angles with four strain gauges installed were calibrated under compression. A special adapter was made to introduce the load at the mounting holes of the angles (Figure 6.1). However, during the calibration tests, the required sensitivity could not be obtained with the available equipment Furthermore, bending in the angles caused a severe distortion of the strain output. A satisfactory solution to these problems has been found in the use of a load cell instead of strain gauges. The load cell is a measuring device that gives a force-proportional signal to a force meter (Figure 6 2). In this way the force exercised by each actuator can be determined The load cell itself is calibrated by the force meter. The

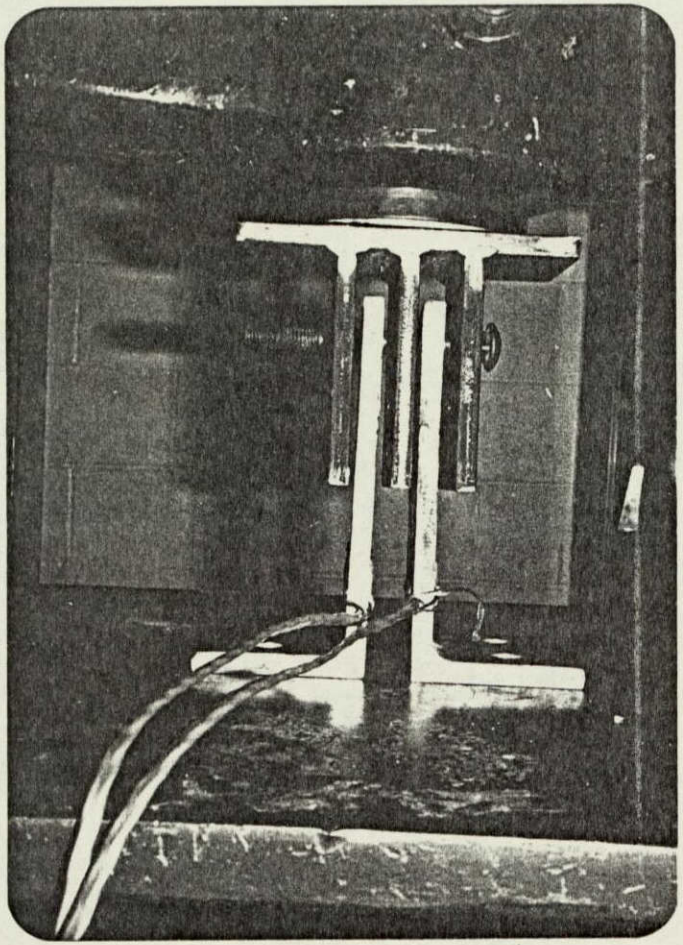

Figure 6.1: Mounting Angle and Adapter Under Compression Load at Calibration

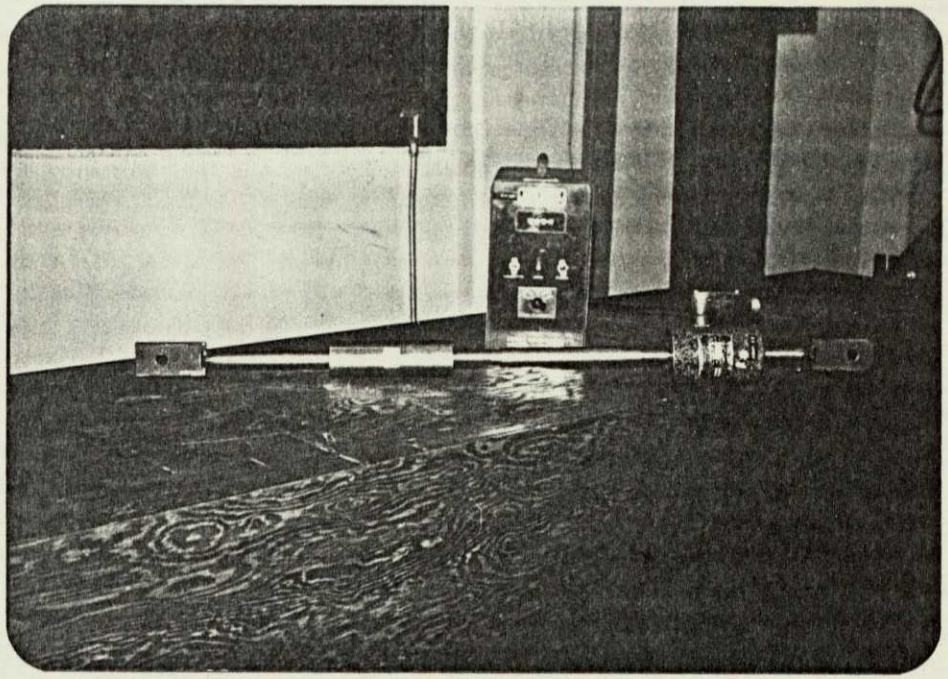

Figure 6.2: Load Cell with Adapter and Force Calibrator

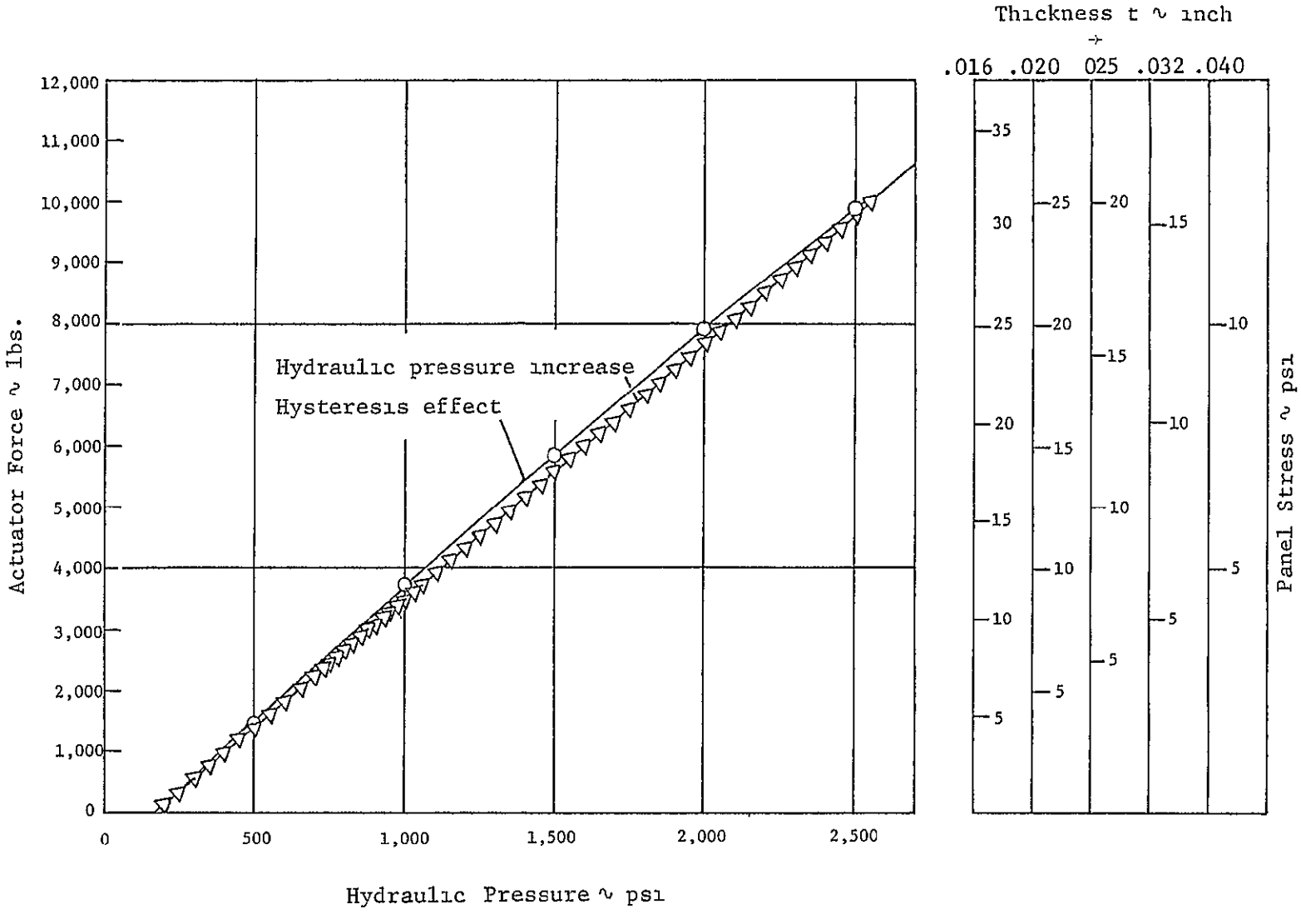

Figure 6.3· Relation Between Actuator Force, Hydraulic Pressure and Panel Stress for Panels of Various Thicknesses in Vertical Direction

6.2 Initial Test Results

Tests have been conducted using a .032" thick test panel under various uniaxial stress condtions: 0 - (2,500) - 12,500 psi. Referring to the calibration graph shown in Figure 6.3, these panel stresses correspond with the hydraulic pressures shown in Table 6 1

Table 6.1 Hydraulic Pressures Corresponding to In-Plane Panel Stresses of a .032" Thick Aluminum Panel.

Panel Stress ~ psi	Hydraulic Pressure ~ psi
unknown	0
0	165
2,500	560
5,000	940
7,500	1,320
10,000	1,700
12,500	2,080

A cross plot of the noise reduction graphs for the panel stresses above is shown in Figure 6.4 for frequencies below and above the fundamental resonance frequency, the stiffness and mass region respectively.

In the stiffness region the noise reduction increases with the in-plane panel stresses for a constant frequency. Increasing the panel stress from 0 to 5000 psi gave an increase of 22 dB in noise reduction at a frequency of 40 Hz. The next 5000 psi increase in panel stress

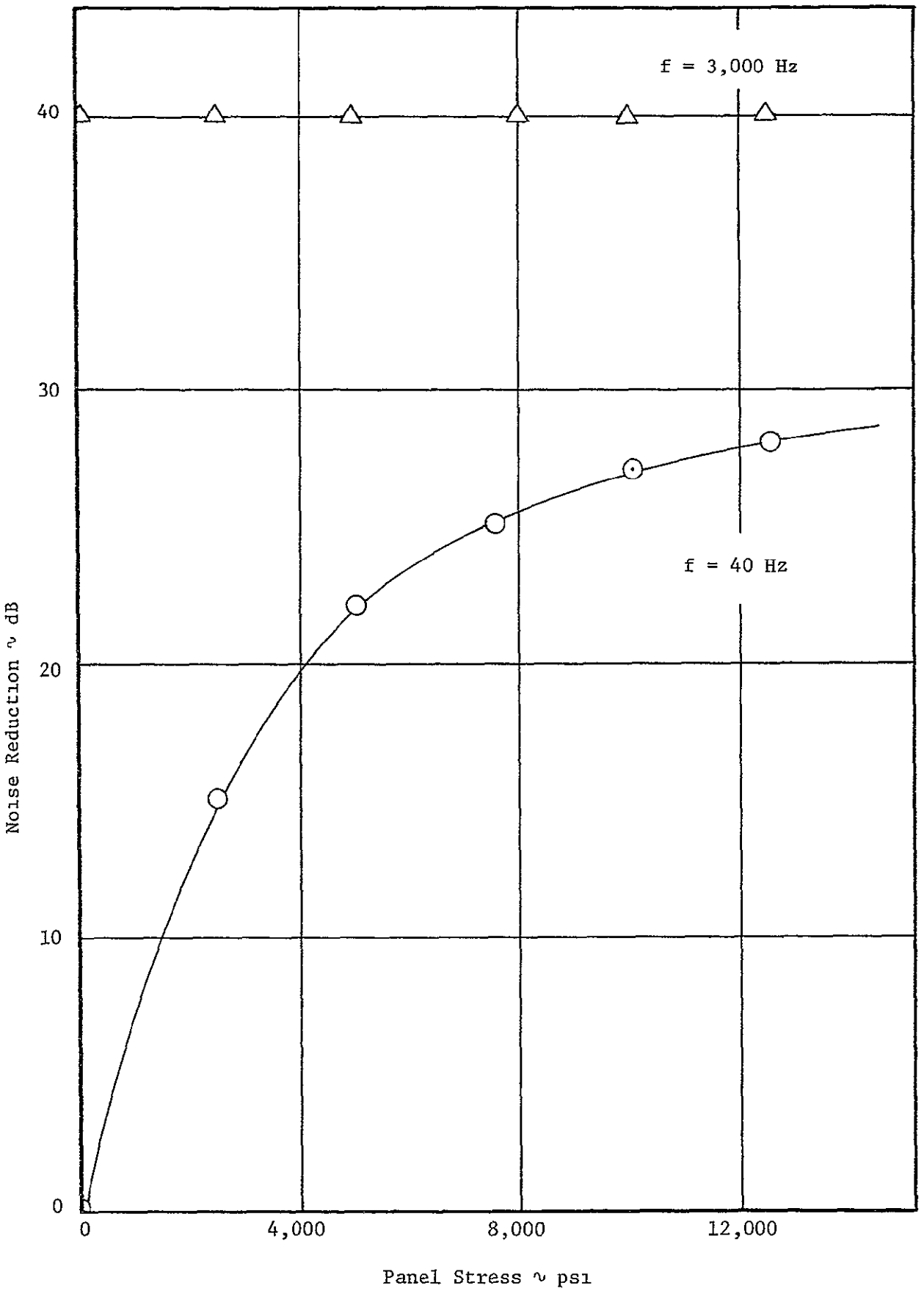

Figure 6 4 Noise Reduction Versus Panel Stress for a .032" Thick Aluminum Panel for Frequencies Above and Below the Fundamental Resonance Frequency

(5000 - 10,000 psi) also gave an increase in noise reduction, yet considerably less: 5 dB increase at a frequency of 40 Hz. It can be concluded that in-plane panel stresses stiffen the panel, which will increase the noise reduction in the region below the fundamental resonance frequency. The increase is considerable for the first 5000 psi panel stress. Hereafter, the noise reduction improvement is less.

In the mass region, where panel noise reduction characteristics are determined by mass, the noise reduction of the test panel does not change at all as function of in-plane stresses. It is concluded that applying stresses to a panel has no beneficial effects on the noise reduction characteristics above the fundamental resonance frequency.

Because the noise reduction increases in the stiffness region and stays the same in the mass region, the fundamental resonance frequency will shift to higher frequencies with the application of in-plane panel stresses (Figure 6.5).

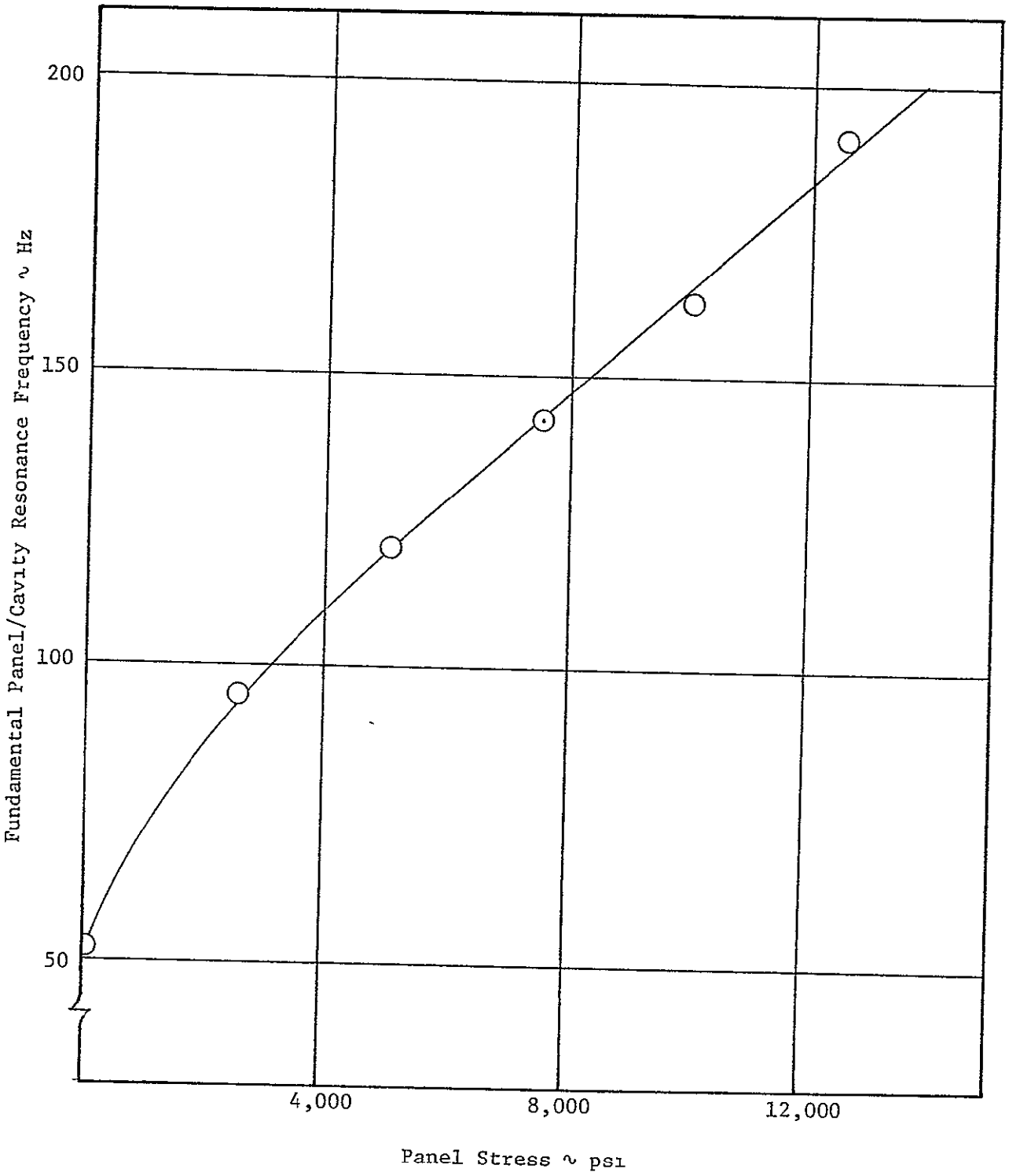

Figure 6 5 The Fundamental Panel/Cavity Resonance Frequency as Function of Panel Stress for a 032" Thick Aluminum Panel

CHAPTER 7

CONCLUSIONS AND RECOMMENDATIONS

- The theoretical analysis for panels hit by a plane wave under an oblique angle of sound incidence predicted the experimental results reasonably well.
- Theoretical panel and cavity modes have been analyzed, but they are not identified in the noise reduction curves.
- Resonance frequencies, critical frequencies and ring frequencies have been calculated for various configurations.
- Increasing the angle of sound incidence results in a lower noise reduction over the whole frequency region of interest (20 Hz - 5000 Hz).
- Riveted flat aluminum panels have a higher noise reduction than bonded panels in the stiffness-controlled frequency region.
- In the low-frequency region the bonded curved panels give better noise reduction characteristics than do the riveted panels.
- In the high-frequency region, different edge conditions do not change the noise reduction of a panel, if the total mass does not alter.
- Curving a flat aluminum panel (from R = ∞ to R = 20") greatly increases its noise reduction in the low frequency region. However, increasing the curvature of a curved panel (from R = 20" to R = 10") decreases the noise reduction.
- In-plane stresses stiffen the flat panel, which will increase the noise reduction in the stiffness-controlled region. The increase is considerable for the first 5000 psi panel stress. Hereafter, the noise reduction improvement reduces.

- A thorough investigation is recommended to identify and separate the panel and cavity modes in the test results obtained in the KU-FRL acoustic test facility.
- Also recommended is the researching of applications in which the beneficial test results can be expressed.

REFERENCES

1. Koval, Leslie R., "Effect of Air Flow, Panel Curvature, and Internal Pressurization on Field-Incidence Transmission Loss," Journal Acoustic Soc. Am., Vol. 59, No. 6, June 1978.

2. Kinsler, Lawrence E. and Frey, Austin R., Fundamentals of Acoustics, John Wiley & Sons, Inc., New York, 1962.

3. Barton, C. Kearney and Daniels, Edward F., "Noise Transmission Through Flat Rectangular Panels Into a Closed Cavity," NASA Technical Paper 1321, National Technical Information Service, Springfield, Virginia 22161, December 1978.

4. Beranek, Leo L., Noise and Vibration Control, McGraw-Hill Book Co., New York 1971.

5. Grosveld, Ferd and Van Aken, Jan, "Investigation of the Characteristics of an Acoustic Panel Test Facility," KU-FRL-317-9, Progress Report for NASA Grant NSG 1301, University of Kansas, Lawrence, Kansas, September 1978.

6. Getline, G. L., "Low-Frequency Noise Reduction of Lightweight Airframe Structures," NASA-CR-145104, Technical Report for Contract NAS1-13910, General Dynamics Convair Division, San Diego, California, August 1976.

APPENDIX A

SEPARATION OF THE REAL AND IMAGINARY PARTS OF THE FIBERGLASS IMPEDANCE Z_ℓ

Equation (35) gives for the fiberglass impedance Z_ℓ:

$$Z_\ell = \frac{\rho_f}{\sqrt{P_f}} \left(1 - i \frac{R_f}{\rho_f \omega}\right)^{1/2} \coth \left[i \frac{\omega \sqrt{P_f}}{c_f} \left(1 - i \frac{R_f}{\rho_f \omega}\right)^{1/2} h\right] \qquad (35)$$

Assuming $a = \frac{\rho_f}{\sqrt{P_f}}$ (a.1); $b = \frac{R_f}{\rho_f \omega}$ (a.2); and $d = \frac{h\omega\sqrt{P_f}}{c_f}$ (a.3),

Z_ℓ becomes: $Z_\ell = a\,(1 - i\,b)^{1/2} \coth \{i\,d\,(1 - i\,b)^{1/2}\}$ (a 4)

For $\coth \{i\,d\,(1 - i\,b)^{1/2}\}$ can be written:

$$\coth \{i\,d\,(1 - i\,b)^{1/2}\} = \coth \{n + i\,m\} \qquad (a.5)$$

where: $n = d \left\{\frac{-1 + (1 + b^2)^{1/2}}{2}\right\}^{1/2}$ (a.6)

and $m = d \left\{\frac{1 + (1 + b^2)^{1/2}}{2}\right\}^{1/2}$ (a.7)

Further evaluation of Equation (a.5) leads to

$$\coth \{n + im\} = \frac{e^{2(n+im)} + 1}{e^{2(n+im)} - 1} \qquad (a.8)$$

$$= \frac{e^{2n}(\cos 2m + i \sin 2m) + 1}{e^{2n}(\cos 2m + i \sin 2m) - 1} \qquad (a.9)$$

or: $$\coth \{n + im\} = \frac{e^{4n} - 1 - 2ie^{2n} \sin 2m}{\{(e^{2n}\cos 2m - 1)^2 - (e^{2n}\sin 2m)^2\}} \qquad (a.10)$$

Writing for

$$e^{4n} - 1 = p \qquad (a.11)$$

$$2e^{2n} \sin 2m = q \qquad (a.12)$$

and $$\{(e^{2n} \cos 2m - 1)^2 - (e^{2n} \sin 2m)^2\} = r \qquad (a.13)$$

Equation (a.5) becomes:

$$\coth \{id\ (1 - ib)^{1/2}\} = \frac{p - iq}{r} \qquad (a.14)$$

Substituting Equation (a.14) in (a.4), Z_ℓ can be written as:

$$Z_\ell = \left(\frac{am}{d} - \frac{ian}{d}\right)\left(\frac{p - iq}{r}\right) \qquad (a.15)$$

or

$$Z_\ell = \frac{a}{rd}(pm - qn) - i\left\{\frac{a}{rd}(qm + pn)\right\} \qquad (a.16)$$

CRINC